Connecting signaling mechanisms for symbiotic associations: From mosses to legumes

by

Zachary Paul Keyser

A dissertation submitted in partial fulfillment of

the requirements for the degree of

Doctor of Philosophy

(Plant Breeding and Plant Genetics)

at the

UNIVERSITY OF WISCONSIN-MADISON

2021

Date of final oral examination: 06/28/2021

The dissertation is approved by the following members of the Final Oral Committee:

Jean-Michel Ané, Professor, Agronomy and Bacteriology
Andrew Bent, Professor, Plant Pathology
Michael Havey, Professor Emeritus, Horticulture
Marisa Otegui, Professor, Botany
Michael Sussman, Professor, Biochemistry

Dedication

In loving memory of my father, Kevin R. Keyser (1962-2011)

Acknowledgements

I would be remiss if I did not thank the countless people who have helped make this feat possible. Without their support and assistance throughout my academic journey, I would not be where I am today. First, a very special thank you to my incredible wife, Kathryn Keyser, who has accompanied me along every step of the way, even on my worst days. I can honestly say I would not be accomplishing this goal without her. I am forever grateful for her undying encouragement and always believing in me. For what she has done for me, she deserves the greatest award imaginable.

I want to thank my mother, Sheila Schmidt, and late father, Kevin Keyser, for raising me to be the man I am and instilling me with a hard work ethic and perseverance. They have always supported me in everything I have done and encouraged me to do what I love. I am indebted to them for providing me the countless opportunities throughout my life which have gotten me here.

In addition, I would like to thank my brother, Jesse. His weekly video calls always helped to get my mind off work and to keep me uplifted. His ability to help me keep a positive attitude kept me going despite the numerous obstacles encountered during my research.

I would like to thank my in-laws, Ann, Gary, and Sara for their unconditional support and encouragement throughout my graduate studies. Their frequent visits not only gave me something to look forward to, but an excuse to give my mind a break from my research. Without the technological help of my father-in-law, who saved all of my files from a near dead hard drive, writing this dissertation would have seemed impossible.

While it goes without saying, I would like to also thank my graduate advisor, Dr. Jean-Michel Ané. I came to the University of Wisconsin - Madison with hopes of working with him and was fortunate enough to have him as a mentor. I am extremely grateful for the opportunity he provided me to work on research which I am passionate about. He has been a great example to me as to what a scientific research should be, and his guidance and constant push have been instrumental in my development.

I would also like to thank numerous others who served as mentors to me during my graduate studies. Dr. Andrew Bent, Dr. Michael Havey, Dr. Marisa Otegui, and Dr. Michael Sussman were all kind enough to serve on my graduate advisory committee. I thank each of them for their unique scientific viewpoints. I appreciate their constructive criticism, thought-provoking questions, and recommendations which have greatly impacted my research and my development. I also thank my career mentor, Huachun Larue, for her generosity with her time answering all my questions, helping address my weaknesses, and always pushing me to step out of my comfort zone.

Throughout my time in Madison, my lab mates, past and present, deserve a major thanks for their companionship, sympathetic ear, and general advice. Each made every day of work enjoyable, and I will always cherish their friendships. In particular I would like to thank Dhileepkumar Jayaraman and Shane Bernard for their research advice and helping make my integration into the lab smooth, as well as Dr. Anthony Bortolazzo, Dr. Thomas Irving, and Dr. Christina Arther for their research and editing contributions. I would also like to thank my undergraduate mentees who were a great help in my daily lab tasks and helped teach me how be a strong leader and team member.

Lastly, I would like to thank the USDA Hatch for my funding and the UW-Madison Plant Breeding and Plant Genetics program for allowing me continue my education complete this research.

Table of Contents

List of abbreviations

amiRNA = artificial micro RNA

AM = arbuscular mycorrhizal

BLAST = Basic local alignment search tool

bp = base pair

CDS = coding sequence

CRISPR = clustered regularly interspaced short palindromic repeats

CSP = common symbiosis pathway

DNA = deoxyribonucleic acid

ER = endoplasmic reticulum

FST= flanking sequence tags

GUS = beta-glucuronidase

gRNA = guide RNA

HMG-CoA = 3-hydroxy-3-methylglutaryl-CoA

HMGR = 3-hydroxy-3-methylglutaryl-CoA reductase

JCVI = J. Craig Venter Institute

kb = kilobase

LYK = Lysin motif kinase

LYR = Lysin motif kinase-related

LysM =Lysin motif

MVA = mevalonate

MEP= methylerythritol phosphate

PCR = polymerase chain reaction

qRT-PCR = quantitative reverse transcription PCR

RLK = receptor-like kinase

RN = Root nodule

RNA = ribonucleic acid

sgRNA = synthetic guide RNA (contains scaffold sequence)

Tnt1 = transposable element of tobacco type 1

tRNA = transfer RNA

Abstract

Root nodule symbiosis and arbuscular mycorrhizal symbiosis serve as the two most agriculturally beneficial plant-microbe interactions due to their ability to aid their host plants in nutrient acquisition. Decades long research into these interactions has elucidated the biological steps and molecular components required for their development in extensive detail. The signaling mechanisms involved in both symbioses share extreme similarity, and are collectively referred to as the common symbiosis pathway. It's likely that root nodule symbiosis arose from co-opting signaling mechanisms used in arbuscular mycorrhizal symbiosis. Our continued understanding of these symbiotic signaling mechanisms will provide us the greatest opportunity for engineering root nodule symbiosis into non-host plants.

This research is broadly focused on improving our knowledge of the common symbiosis pathway by identifying signaling mechanisms required for symbiotic associations and their connections with other cellular and biological functions. *CCaMK* and *IPD3* are essential for forming root nodule and arbuscular mycorrhizal symbiosis through their activity at the nuclear level in the common symbiosis pathway. Their presence is strongly correlated with the ability to form these associations, yet non-host mosses retain these genes. Here we show CCaMK and IPD3 in *Physcomitrium patens* maintain numerous molecular features for symbiotic signaling. Additionally, we revealed a biological role for PpCCaMK and PpIPD3 in inducing abscisic acid accumulation and brood cell formation, implicating them in stress response signaling.

Transducing the microbial signal detected at the plasma membrane to the nuclear envelope is essential for inducing changes required for symbiosis, but the

signaling mechanism is unclear. HMGRs convert HMG-CoA into mevalonate as part of the mevalonate pathway, and a single HMGR has been identified to serve in root nodule symbiosis and symbiotic signaling. We identified and characterized two *hmgr* mutants with nodulation defects, showing the involvement of multiple HMGRs, specifically HMGR1 and HMGR2c, in late stages of nodule development. We also show continued mevalonate pathway signaling for the production of an isoprenoid product used in prenylation is necessary for symbiotic signaling. Lastly, we provide a link between HMGRs and phospholipases in symbiotic signaling by demonstrating phospholipase activity occurs downstream of HMGR activity in the common symbiosis pathway.

Chapter 1 – Introduction: Improving agricultural sustainability through understanding beneficial plant-microbe interactions

1.1 – Essential plant nutrient acquisition

Plants require adequate levels of 17 essential nutrients for healthy growth and development, consisting of the macronutrients; carbon, hydrogen, oxygen, nitrogen, phosphorus, potassium, sulfur, calcium, and magnesium, and the micronutrients; boron, chlorine, copper, iron, manganese, molybdenum, nickel, and zinc. Plants acquire these macronutrients and micronutrients from either the air, water, or soil. Deficiencies in any of these nutrients causes deleterious effects on plant health, and in turn, plant yield (Mahler, 2004). The most agriculturally relevant of these deficiencies are of the three primary soil macronutrients; nitrogen, phosphorus, and potassium. Limitations in these three nutrients and/or water are the primary reasons for not reaching at least 75% of the attainable yield (Mueller et al., 2012). Due to the widespread occurrence of these deficiencies, fertilizers composed of nitrogen, phosphorus, and potassium are heavily applied to agricultural fields along with extensive irrigation. Using these management practices can increase agricultural productivity by up to 70% (Mueller et al., 2012).

Nitrogen is of particular importance for plant growth as it is incorporated into the fundamental building blocks of life: nucleic and amino acids and other essential plant molecules like chlorophyll (Taiz and Zeiger, 2010). Dinitrogen gas makes up the majority (78%) of the air, and organic nitrogen compounds are present throughout the soil. However, nitrogen deficiency is highly prevalent as plants cannot take up these abundant forms of nitrogen (Francis et al., 2007). Nitrate and ammonia, the plant-available forms of nitrogen, are much less plentiful (Mahler, 2004).

1.2 – Nitrogen fertilizers

Work by Fritz Haber and Carl Bosch made the application of nitrogen to agricultural fields feasible on a large scale through the chemical processing of atmospheric nitrogen, now termed the Haber-Bosch process. Biologically unavailable N_2 gas from the air is fixed into plant-accessible ammonia under high temperature and pressure, with the reaction "$2N_2 + 3H_2 \rightleftharpoons 2NH_3$." Following this process, ammonia is often further converted into other nitrogen compounds, such as urea, ammonium nitrate, and ammonium phosphate (EPA, 2009). Of the total fixed ammonia consumed in the U.S., agriculture uses approximately 88% in the form of fertilizer, totaling over 13,000,000 tons (Apodaca, 2017; USGS National Minerals Information Center, 2020).

While the use of nitrogen fertilizer has been touted as a solution for meeting our crop production requirements for decades, the production and application of nitrogen fertilizers generate several negative environmental impacts. Natural gas is used both as a hydrogen source and energy source for the Haber-Bosch process (IFA, 2009).Together, it is estimated to require 35 thousand ft^3 of natural gas per ton of ammonia produced (Kermeli et al., 2017). This equates to the release of 2-3 tons of CO_2 per ton of ammonia, or 14.6 million tons of CO_2 per year in the United States (Bicer et al., 2017; EPA, 2009).

The application of nitrogen fertilizers also negatively affects our water bodies. Nutrients applied to farm fields are not taken up by crops instantaneously. Less than 50% of applied nitrogen makes its way into corn, leaving the remaining nitrogen to leach out of the soil into rivers, lakes, oceans, and groundwater during periods of heavy rain or irrigation (Robertson and Vitousek, 2009). While there is no clear consensus for the

major driver of the formation of harmful algal blooms, increasing evidence points to high nitrogen and phosphorus levels having a significant role in this process. Nitrogen levels specifically can be correlated with the timing of blooms and are shown to trigger the growth of specific harmful algae and the production of dangerous cytotoxins (Davis et al., 2015; Gobler et al., 2016). This can create unsafe water conditions, decrease drinking water quality, and create dead zones killing wildlife (Huisman et al., 2018).

With the continued pressure for increased yield to keep up with the growing population and the negative impacts of fertilizer use, it is essential to identify more sustainable methods for providing high nutrient levels, especially nitrogen. Natural aid in acquiring various limiting nutrients and water exist in some crops through interactions with beneficial microbes. Improving these interactions and finding ways to transfer the ability to associate with beneficial microbes into a broader range of crops would be one way to help decrease our reliance on fertilizer use.

1.3 – Root nodule symbiosis

Biological nitrogen fixation is the primary source of naturally bioavailable soil nitrogen for plants. Microbes, referred to as diazotrophs, produce the enzyme nitrogenase, which can reduce atmospheric N_2 to ammonia. These nitrogen-fixing microbes can either be free-living or symbiotic bacteria. In terms of efficiency, symbiotic bacterial nitrogen fixation produces considerably more nitrogen than free-living diazotrophs (Arbestain et al., 2008). The most studied beneficial associations between plants and nitrogen-fixing bacteria are root nodule (RN) symbioses, so-called as it leads to the production of a new lateral root organ termed a nodule. This symbiosis only occurs in some lineages of land plants from within the nitrogen-fixing root nodule clade

(Fabales, Fagales, Cucurbitales, and Rosales) (Kistner and Parniske, 2002). The most prevalent and well-studied root nodule symbiosis occurs between legume plants and Gram-negative diazotrophs from 18 different genera, collectively referred to as rhizobia (Lindström and Mousavi, 2020). Also included are the interactions between actinorhizal plants and actinobacteria *Frankia and* between rhizobia and *Parasponia spp* (Den Camp et al., 2012; Griesmann et al., 2018).

For our purpose, we will focus on legume rhizobia symbiosis in the models *Medicago truncatula* and *Lotus japonicus* when discussing root nodule symbiosis. Broadly speaking, nodule formation and rhizobia colonization begin with the reciprocal detection of the symbiotic partners and attachment of rhizobia to the root hair surface. The root hair entraps the rhizobia by curling around the bacterial microcolony. The bacteria inside the curled root hair enter inside the root hair through the invagination of the cell membrane, creating an infection thread. Rhizobia grow and divide while moving through the infection thread, penetrating through the epidermal and cortical cell layers. Meanwhile, a *de novo* nodule meristem is initiated in the root cortex, followed by subsequent cortical cell divisions creating the nodule primordium. The infection thread enters into the developing nodule and branches throughout. In most cases, individual rhizobia bud off from the infection thread and are endocytosed into nodule cells surrounded by the plant membrane, creating the symbiosome, which eventually differentiates into a nitrogen-fixing bacteroid (Jones et al., 2007; Oldroyd, 2013). A fully developed nodule provides a conducive environment for nitrogen fixation by the rhizobia contained inside. Leghemoglobin produced by the host plant sequesters oxygen, creating an oxygen-depleted environment in the nodule. Along with the nodule inner

cortex, which serves as an oxygen diffusion barrier, the microaerobic conditions allow for sufficient respiration while protecting the nitrogenase from damage. This metabolically expensive nitrogen-fixation process receives its energy from the plant in the form of malate, which ultimately allows for efficient nitrogenase activity and the supply of nitrogen to the host plant (Lindström and Mousavi, 2020).

1.4 – Arbuscular mycorrhizal symbiosis

Another intracellular, beneficial plant-microbe interaction serving extensive agronomic benefits is the arbuscular mycorrhizal (AM) symbiosis. Unlike the RN symbiosis, AM symbiosis has a wide host range, with greater than 70% of land plants capable of this interaction. The fungal partners participating in this symbiosis are monophyletic obligate symbionts of the phylum Glomeromycotina. The initiation of symbiosis between these organisms begins with mutual detection via chemicals released into the rhizosphere. Fungal spores germinate, and the growing hyphae branch until they reach a nearby plant root. Once attached to the root surface, the fungus forms a hyphopodium, a cell penetration apparatus, and uses it to enter into the root epidermal cells. With guidance from the host plant, the hyphae travel through the apoplast to the cortex. Through the invagination of the plant cell membrane, the fungus enters into the cortical cells and repeatedly branches throughout (Si and Parniske, 2008). These highly branched fungal structures are referred to as arbuscules and serve as high-surface-area interfaces between the two organisms to facilitate nutrient exchange.

The AM symbiosis provides the host plant with increased access to nutrients and water through the large hyphal network. The mycelial network absorbs water,

phosphorus, ammonium, nitrate, and numerous metal ions in areas unexplored by the roots with less energy. Through the peri-arbuscular interface, the fungus transports excess nutrients to the host plant. The plant host, in return, provides up to 20% of photoassimilates to the fungus for continued growth through the transfer of sugars and lipids (Wang et al., 2017). A reciprocal exchange for carbon controls the levels of nitrogen and phosphorus transferred, and *vice versa*. The mutualistic regulation of transport allows for “fair trade” and the continuation of associations between equally beneficial partners (Fellbaum et al., 2011; Kiers et al., 2012).

1.5 – Molecular cross-talk between symbiotic partners in the rhizosphere

Soil microbes may be pathogenic or beneficial, thus it is essential for plants to distinguish between them. The first step in the association with either rhizobia or AM fungi is the mutual recognition of the symbiotic partners through chemicals released into the soil. Plants release root exudates, both passively and in response to stimuli. Root exudates contain a wide variety of chemicals, many of which are carbon-based organic molecules. These compounds are released from different zones of the root system and can alter the neighboring soil environment. They can serve roles in nutrient uptake, detoxification, and plant defense, to name a few (Badri and Vivanco, 2009).

The importance of root exudates in the initiation of AM symbiosis was identified through the finding that chemicals released by host plants stimulate spore germination and hyphal branching, while those of non-host plants do not (Borghetto et al., 1993; Branzanti and Gianinazzi, 1989). The compound responsible for hyphal branching was isolated from root exudates, analyzed, and revealed to be a sesquiterpene strigolactone, 5-deoxy-strigol, in *Lotus japonicus*. 5-deoxy-strigol and other natural and

synthetic strigolactones were all shown to induce the same hyphal branching response as root exudates at low concentrations (Akiyama et al., 2005). Volatile compounds released by the roots are also involved in initiating arbuscular mycorrhizal interactions, and increased CO_2 levels stimulate germination and increased hyphal growth (Bécard and Fortin, 1988). In some cases, specific flavonoids released into the rhizosphere by host plants also promote the germination of nearby arbuscular mycorrhizal fungi spores (Tsait and Phillips, 1991). Together, combinations of chemical signals exuded by plant roots aid AM fungi in finding their plant host.

As with AM symbiosis, root exudates produced by legumes are essential for RN symbiosis. Rhizobia exhibit chemotaxis toward their legume host differently from that of other microbes to plants (Currier and Strobel, 1976). The main chemicals driving rhizobia motility to the host plant are flavonoids, organic acids, and amino acids (Compton and Scharf, 2021). Increased concentrations of certain flavonoids promote the motility of rhizobium, such as *Rhizobium leguminosarum* biovar *phaseoli* in response to apigenin and luteolin (Aguilar et al., 1988). In other rhizobia, such as *Bradyrhizobium japonicum* USDA 110, organic acids and amino acids are the major chemoattractants (Barbour et al., 1991). Additionally, the presence of flavonoid compounds produced by legumes promote the growth and multiplication of rhizobia near the host plant (Hartwig et al., 1991)

In both RN symbiosis and AM symbiosis, the primary microbially produced signals are chitin-based molecules made up of multiple β-(1,4) *N*-acetyl glucosamine units. These signaling compounds produced by rhizobia all contain a long-chain fatty acid linked to their non-reducing end and are therefore referred to as lipo-

chitooligosaccharides (LCOs). LCOs are required by most rhizobia to initiate infection and nodule organogenesis (Dénarié et al., 1996). Arbuscular mycorrhizal fungi also produce LCOs as signaling molecules and versions without lipid modifications, referred to as chitooligosaccharides (COs) (Genre et al., 2013; Maillet et al., 2011). These microbial signals are active at extremely low concentrations as applications of LCOs in the 10^{-14} M range induce symbiotic responses in legumes (Sun et al., 2015). Depending on the microbial partner, these compounds vary in the number of *N*-acetyl glucosamine units and functional group modifications on the different subunits. Commonly, symbiotic LCOs/COs consist of 3-5 *N*-acetyl glucosamine subunits with acetyl, methyl, fucosyl, or sulfate decorations. Differences in the substitutions on the chitin backbone convey specificity between the microbial partner and the plant host. This is particularly true for legume-rhizobia symbiosis as many rhizobia only associate with specific or very limited numbers of legumes. However, due to the broad host range of arbuscular mycorrhizal symbiosis, the substitutions play less of a role in specificity in this symbiosis (Dénarié et al., 1996; Lerouge et al., 1990; Maillet et al., 2011; Si and Parniske, 2008). Arbuscular mycorrhizal fungi continually produce COs and LCOs and release them into the environment (Sun et al., 2015). However, in rhizobia, the production of LCOs is regulated by the detection of flavonoids produced by nearby legumes (Dénarié et al., 1996; Perret et al., 2000). In both cases, these signals serve in partner recognition and initiate changes in the host plant for the allowance of the symbiotic association (Oldroyd, 2013).

1.6 – Common symbiosis pathway

In addition to the similarities between the signaling molecules produced by the microbial partners in RN symbiosis and AM symbiosis, these symbioses share extreme similarity in the subcellular signaling pathway for forming the symbiotic relationships. Genetic studies in model legumes first identified many signaling components necessary for RN symbiosis. Later research in AM symbiosis identified that the same components were also essential for the association with arbuscular mycorrhizal fungi. Due to the abundance of shared mechanisms, this signal transduction pathway is collectively known as the "common symbiosis pathway" (CSP) (Catoira et al., 2000; Riely et al., 2004).

Perception of symbiotic signaling molecules. Initiation of the CSP begins with the detection of COs/LCOs by the host plant. Since our research is carried out in the model legume *M. truncatula*, which forms both AM and RN symbiosis, the molecular components will be referred to as their names in this species. The receptors responsible for detecting and binding the microbial signals are pairs of lysin motif (LysM) receptor-like kinases (RLKs) located at the plasma membrane surface. The receptor complex consists of one functional-kinase containing "LYK-type" receptor-like kinase and one non-functional kinase containing "LYR-type" receptor-like kinase which interact and form a heterodimer *in planta* (Moling et al., 2014). The primary RLKs which bind LCOs and serve in RN symbiosis are Lysin Motif Receptor-Like Kinase3 (LYK3) and Nod Factor Perception (NFP) (**Figure 1**). Individual mutants in these two receptors are defective in nodulation. *M. truncatula nfp* mutants are affected in all nodulation related responses, including the earliest known changes, whereas *lyk3* mutants are impared only at later

stages, such as infection. This suggests a mechanism involving an ‘early receptor’ (NFP) and a more stringent ‘entry receptor’ (LYK3) for complete association with an acceptable microbial partner (Amor et al., 2003; Arrighi, 2006; Limpens et al., 2003; Radutoiu et al., 2003; Smit et al., 2007). While LYK3 and NFP also detect mycorrhizal LCOs, the main RLKs that bind COs for AM symbiosis are CERK1 and LYR4 (Bozsoki et al., 2017; Feng et al., 2019; Gibelin-Viala et al., 2019). LysM RLKs are distinguished by their LysM motifs, which recognize and bind *N*-acetyl glucosamine units, which compose peptidoglycan and chitin (Buist et al., 2008). Amino acid variations in the three LysM motif sequences in symbiotic RLKs determine LCOs decoration specificity to select microbial partners (Bensmihen et al., 2011; Broghammer et al., 2012; Radutoiu et al., 2007). The LYK RLK shows autophosphorylation ability and the ability to transphosphorylate its LYR RLK partner, supporting a scenario where binding of LCOs to RLKs triggers phosphorylation activity and stimulation of downstream (Broghammer et al., 2012; Madsen et al., 2011).

Signal convergence through shared co-receptor. While not directly implicated in LCO/CO detection, a leucine-rich repeat-containing RLK, Does Not Make Infections 2/Nodulation Receptor Kinase (DMI2/NORK), is also required for signal transduction following signal detection by LYK3 and NFP (**Figure 1**). Unlike with the LysM receptors, which differ between AM and RN symbiosis, DMI2/NORK is shared between both symbioses. *dmi2/nork* mutants are unable to form associations with either rhizobia and arbuscular mycorrhizal fungi, as well as early symbiotic response phenotypes. However, these mutants respond to symbiotic signals with root hair deformations (Catoira et al., 2000; Stracke et al., 2002). This co-receptor interacts with the two symbiotic LysM RLKs

(Antolín-Llovera et al., 2014). The interaction between these receptors may serve to activate DMI2/NORK for signal transduction. The overexpression of DMI2/NORK, or its kinase domain alone, is capable of inducing the formation of spontaneous nodules and symbiotic genes in the absence of a microbial partner or their symbiotic signals (Ried et al., 2014; Saha et al., 2014). The turnover of DMI2/NORK is decreased in the presence of a rhizobial partner, stabilizing it and increasing its abundance. During symbiosis, DMI2/NORK is thus present at higher levels, allowing for increased activity (Pan et al., 2018).

Cytoplasmic signaling mechanisms. DMI2/NORK additionally interacts with 3-hydroxy-3-methylglutaryl coenzyme a reductase1 (HMGR1) (Kevei et al., 2007). This interaction suggests a possible mechanism in which DMI2/NORK activity stimulates HMGR1 to continue signaling from the plasma membrane to the nuclear envelope (**Figure 1**). HMGR activity is indeed important in this role, as pharmacological inhibition or RNAi knockdown of HMGR1 expression reduces both nodulation and colonization by AM fungi, indicating a conserved role for both symbioses (Kevei et al., 2007). Linking HMGR in the signal transduction process, numerous early symbiotic responses are also reduced in HMGR1 RNAi knockdown plants (Venkateshwaran et al., 2015). Additionally, the application of mevalonate, the product of HMGR activity, induces symbiotic responses in the absence of microbial symbiotic signals (Venkateshwaran et al., 2015). This direct role of mevalonate in triggering symbiotic responses suggests HMGR and the production of mevalonate may transduce symbiotic signaling from DMI2/NORK.

While not directly linked to DMI2/NORK, other signaling mechanisms serve roles in symbiotic signaling downstream of symbiotic receptors. Heterotrimeric G-proteins

serve as the most prevalent signaling mechanism, regulating countless cellular processes through GTP-binding and the subsequent binding of individual heterotrimeric G-protein signaling components to effector proteins (Koelle, 2006). Studies using chemical agonists and antagonists of G-protein signaling implicated this signaling mechanism in symbiotic signal transduction. Pertussis toxin, a G-protein antagonist, inhibits the induction of a symbiotic marker gene in response to LCOs. Inversely, G-protein agonists, such as mastaparan, induce symbiotic marker gene expression and the symbiosis-specific response of nuclear calcium spiking (Pingret et al., 1998; Sun et al., 2007).

Phospholipases similarly serve in signal transduction for diverse responses in plants. Activated phospholipases catalyze reactions converting membrane lipids into signaling messengers for modulating cellular processes (Takáč et al., 2019) Specifically, phospholipase C (PLC) and phospholipase D (PLD) are implicated in symbiotic signal transduction. Rhizobial LCOs quickly induce the formation of PLC and PLD-derived products, such as inositol triphosphate, diacylglycerol, and phosphatidic acid, connecting their activity to symbiosis-related responses. The inhibition of PLC with chemical antagonists suppresses symbiotic marker gene expression and root hair deformations (Den Hartog et al., 2001; Pingret et al., 1998). Similarly, the inhibition of PLD-derived phosphatidic acid formation also decreases root hair deformations in response to LCOs (Den Hartog et al., 2001).

Nuclear calcium-spiking. Following the activation of RLKs at the plasma membrane, nuclear calcium spiking occurs, defined as repeated oscillations of high and low calcium concentration in the nucleus minutes after detecting symbiotic signaling

molecules (Ehrhardt et al., 1996; Kosuta et al., 2008; Sieberer et al., 2009). No evidence currently exists for the secondary messenger responsible for triggering this response; however, it is reasonable to hypothesize that it is derived from the above-mentioned signaling mechanisms. Numerous ion transporters at the nuclear envelope have been identified that work together to generate and maintain nuclear calcium oscillations. The ion channel Does not Make Infections 1 (DMI1) in *M. truncatula* was the first nuclear-localized cation channel identified to serve in the common symbiosis pathway. *M. truncatula dmi1* mutants are defective in forming associations with rhizobia and arbuscular mycorrhizal fungi and early symbiotic responses (Ané et al., 2004; Catoira et al., 2000). Particularly, DMI1 is required for LCO-induced calcium spiking and likely functions in regulating calcium flux (Peiter et al., 2007; Wais et al., 2000). While initially believed to be a potassium channel, DMI1 is actually a calcium-regulated calcium channel in which calcium binding is required for calcium spiking and nodule development (Kim et al., 2019). Cyclic nucleotide-gated channels, CNGCs, also serve roles in calcium spiking and interact with DMI1 at the nuclear envelope. Mutants in three CNGC15s all show decreased interactions with rhizobia and AM fungi. They are defective in calcium spiking in response to symbiotic signaling molecules, specifically exhibiting decreased maintenance and irregular oscillations (Charpentier et al., 2016). Additionally, the nuclear membrane localized calcium ATPase, MCA8, serves as a calcium-pump in this process. As with the previously mentioned ion channels, mutants knocking down MCA8 expression show defects in symbiotic calcium spiking (Capoen et al., 2011). A mathematical model suggests that these nuclear-localized ion channels

work in concert, along with counter-ion channels, to generate and maintain the corresponding calcium oscillations in the nucleus (Granqvist et al., 2012).

Symbiotic gene induction. Continuing the CSP, Does not Make Infections 3 (DMI3) interprets this nuclear calcium flux. As with *dmi1* and *dmi2* mutants, *dmi3* mutants cannot symbiotically associate with rhizobia and arbuscular mycorrhizal fungi (Catoira et al., 2000). Unlike *dmi1/2* mutants, *dmi3* plants still exhibit normal nuclear calcium spiking. The blockage occurs at the stage of symbiotic gene expression, placing DMI3's role between calcium spiking and the induction of symbiosis-related genes (Wais et al., 2000). The DMI3 protein is a calcium-and-calmodulin-dependent protein kinase often referred to as CCaMK. DMI3/CCaMK is regulated by the binding of calcium and calmodulin at different specificities. The binding of calcium causes autophosphorylation of DMI3, decreasing its activity. However, higher calcium concentrations lead to the binding of calcium-bound calmodulin and increased transphosphorylation activity of DMI3 (Lévy et al., 2004; Miller et al., 2013)

DMI3 interacts with and phosphorylates the nuclear-localized Interacting Protein of DMI3 (IPD3) (Messinese et al., 2007; Yano et al., 2008). *ipd3* mutants are defective in both the formation of AM symbiosis and RN symbiosis, exhibited by blockage of symbiotic gene expression, reduced mycorrhization, and the abortion of infection threads. Interestingly, these mutants still form nodules, although uninfected and immature (Horváth et al., 2011; Yano et al., 2008). The identification of an IPD3-like protein, IPD3L, revealed partial redundancy between these two proteins. Double *ipd3/ipd3L* mutants exhibit more significant defects in symbiotic associations, as these plants are also incapable of nodule formation. Additionally, phosphomimetic mutants of

IPD3, in which two phosphorylation sites are converted from serine to aspartic acid, are sufficient to trigger spontaneous nodule formation, suggesting phosphorylation of IPD3 by DMI3 leads to activation of IPD3 (Jin et al., 2018).

Ultimately, the activity of the DMI3-IPD3 complex leads to the induction of symbiosis-related gene expression. Depending on the microbial partner, and their corresponding symbiotic signaling molecules, genes for AM symbiosis or RN symbiosis are induced. While how the plants decipher the specific microbial origin of the converged CSP signal is unclear, regulation of symbiotic association-related genes requires a complex transcription factor network. In both cases, IPD3 regulates the expression of other GRAS domain transcription factors by binding to their promoters, such as Nodule INception (NIN) and Reduced Arbuscular Mycorrhiza1 (RAM1) (Pimprikar et al., 2016; Singh et al., 2014). In RN symbiosis, Nodulation Signaling Pathway1 (NSP1) and NSP2 transcription factors are additionally recruited and activate subsequent transcription factors and genes necessary for nodulation, such as ERF Required for Nodulation (ERN) and Early Nodulin (ENOD) genes (Cerri et al., 2016; Hirsch et al., 2009; Oldroyd, 2013). For AM symbiosis, DELLA proteins work in complex with CCaMK and IPD3 to activate RAM1, which subsequently works with NSP2 to induce additional mycorrhization-related transcription factors (Oldroyd, 2013; Pimprikar et al., 2016). Activation of their targets leads to either the formation of nodules or mycorrhizal associations.

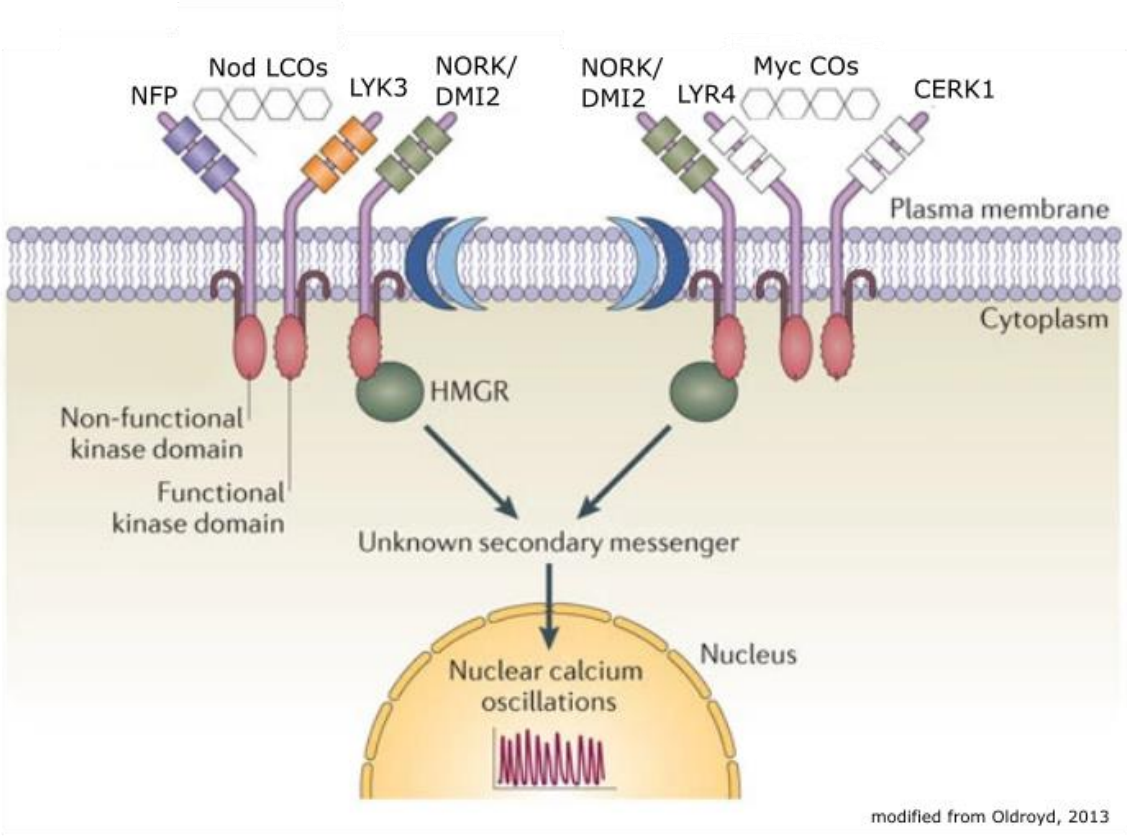

Figure 1: Common symbiosis pathway
Illustration of the *M. truncatula* core components involved in the common symbiosis pathway. The NFP and LYK3 receptor complex binds and detects LCOs produced by rhizobia. The LYR4 and CERK1 receptor complex binds and detects COs produced by AM fungi. Either signal is conveyed through the co-receptor, NORK/DMI2, by association with NFP and LYK3 or the predicted association with LYR4 and CERK1. HMGR1 interacts with NORK/DMI2 for the production of a secondary messenger(s) stemming from the mevalonate pathway. Calcium oscillations in the nucleus generated by the stimulation of nuclear ion channels ultimately lead to the induction of symbiotic gene expression.

1.7 – Conservation and evolution of the common symbiosis pathway

The similarities between the microbial molecules used in partner recognition and the signal transduction pathway activated by them between root nodule symbiosis and AM symbiosis point to a shared evolutionary history. Fossil evidence of arbuscular mycorrhizal-like symbioses dates back to over 400 million years to the Early Devonian

period (Remy et al., 1994). Corresponding to this, arbuscular mycorrhizal symbiosis has a vast host range. Over 70% of land plants form arbuscular mycorrhizal associations with Glomeromycotina fungi (Schwarzott et al., 2001). This includes members of the earliest diverging land plant lineages, such as liverworts and hornworts, as colonization by Glomeromycotina fungi with arbuscule-like structures can be observed in their thalli and rhizoids (Desiro et al., 2013; Field et al., 2015; Humphreys et al., 2010; Rimington et al., 2019). Supported by these findings, it is widely accepted that mycorrhizal associations were essential and responsible for the initial colonization of land by plants (Canada, 1975; Delaux and Schornack, 2021).

In contrast to AM symbiosis, RN symbiosis arose much more recently (De La Peña et al., 2018; Kistner and Parniske, 2002). Root nodule symbiosis is restricted to members of the Fabales, Fagales, Cucurbitales, and Rosales (FaFaCuRo). Not all members of the FaFaCuRo form nodules and associate with nitrogen-fixing bacteria, as closely related members of the same group differ in their ability to associate with nitrogen-fixing bacteria. Evolutionary studies predict a single gain of the nitrogen-fixing root nodule symbiosis in this monophyletic clade, followed by an estimated eight subsequent losses. Corresponding to this loss of function is the loss of multiple genes critical for root nodule symbiosis, most notably NIN and RPG (Griesmann et al., 2018).

As discussed earlier, RN symbiosis requires many of the same genes as AM symbiosis. The evolution of the root nodule symbiosis is therefore proposed to have co-opted many genes from AM symbiosis. Supporting this hypothesis is the presence of homologs of many genes critical for RN symbiosis in non-nodulating species, which can rescue nodulation defects in the corresponding legume mutants (Griesmann et al.,

2018; Oldroyd, 2013). Of the shared genes involved in forming both RN symbiosis and AM symbiosis, many of the genes are exclusive to symbiotic functions while others serve additional roles unrelated to symbiosis. In the cases of land plant lineages that do not form symbiotic relationships with AM fungi, this loss of function correlates with the concurrent absence of large gene sets with roles in forming symbiotic associations. The numerous genes that are lost are thought to be symbiotic-specific and do not serve other biological functions (Delaux et al., 2014). Two key genes strongly associated with being a host or non-host for AM and/or RN symbiosis are *CCaMK* and *IPD3*. However, although mosses cannot form these beneficial associations, they retain *CCaMK* and *IPD3* (Delaux et al., 2015; Wang et al., 2010). The biological reason for retaining these symbiotic-specific genes remains unclear and brings up questions regarding the selection pressure for maintaining them. Further investigation of the conservation of these genes and their biological functions in mosses could help identify mechanisms leading to transition from symbiotic host to non-host.

1.8 – HMGRs and their role in signaling

As noted earlier, an HMGR1 has been identified to play an important role in forming symbiotic associations. HMGRs are enzymes that catalyze the NADPH-dependent reduction of HMG-CoA into mevalonate (MVA). Eukaryotic (class I) HMGRs exhibit a highly conserved structure consisting of three domains; an N-terminal region, the linker, and a C-terminal region. The N-terminus contains 2 (in plants) to 8 (in animals) membrane-spanning helices and serves as a membrane anchor (Friesen and Rodwell, 2004; Stermer et al., 1994). This domain is responsible for the endoplasmic reticulum localization of eukaryotic HMGRs (Ferrero et al., 2015). The linker domain is a

short and flexible region that serves to connect the N-terminal domain to the C-terminal domain and may play a role in protein regulation (Friesen and Rodwell, 2004; Istvan and Deisenhofer, 2000; Stermer et al., 1994). The C-terminal domain of HMGRs is the catalytic region oriented toward the cytoplasm. This region is responsible for the enzymatic function of HMGR, as it contains the binding sites for both NADPH and HMG-CoA (Istvan and Deisenhofer, 2000; Li et al., 2014).

The generation of MVA through HMGR activity serves as the rate-limiting step of the mevalonate pathway. This pathway is a multi-enzyme process that is responsible for the synthesis of isoprenoids (Friesen and Rodwell, 2004). Isoprenoids are organic compounds composed of multiple five-carbon-containing isoprene units. New isoprenoids continue to be discovered yearly, leading to the characterization of tens of thousands of diverse isoprenoids so far (Holstein and Hohl, 2004; Sacchettini and Poulter, 1997). All forms of life produce isoprenoids, but the majority of them are synthesized by plants (Holstein and Hohl, 2004; Pulido et al., 2012; Tarkowská and Strnad, 2018). The large diversity of isoprenoids in plants may be due to the lineage containing multiple HMGR-coding genes, unlike most eukaryotes which contain a single *HMGR* (Friesen and Rodwell, 2004; Li et al., 2014).

Following the activity of HMGR, mevalonate is phosphorylated twice and decarboxylated by mevalonate kinase, phosphomevalonate kinase, and phosphomevalonate decarboxylase to generate isopentenyl pyrophosphate (IPP). Through the activity of isopentenyl pyrophosphate isomerase, the reconfiguration of IPP creates its isomer dimethylallyl pyrophosphate (DMAPP). Together, IPP and DMAPP serve as the two isoprenoid precursors from which all isoprenoids are derived (Pulido et

al., 2012). The condensation of these two compounds by geranyl pyrophosphate synthase in plants, or farnesyl pyrophosphate in animals, produces geranyl pyrophosphate (GPP). From GPP, the addition of another IPP through the subsequent activity of farnesyl pyrophosphate synthase creates farnesyl pyrophosphate (FPP). Finally, the subsequent addition of another IPP to FPP by geranylgeranyl pyrophosphate synthase produces geranylgeranyl pyrophosphate (GGPP) (Holstein and Hohl, 2004). The repeated condensation of isoprene units leads to the formation of increasingly larger isoprenoids, ranging from 10-carbon monoterpenes to over 40-carbons polyterpenes in 5-carbon increments. The various unique isoprenoids are then derived by subsequent modifications, such as cyclization and side-chain substitutions (Tarkowská and Strnad, 2018).

The most well-recognized isoprenoid is the sterol cholesterol, known for its effect on heart health in humans (Friesen and Rodwell, 2004). Its importance has led to the identification of numerous inhibitors of mevalonate pathway enzymes for medicinal purposes, which can elucidate the importance of this pathway in plants (Tobert, 2003). Other isoprenoids serve other diverse roles, exemplified by those identified in plants. Many plant hormones are products of the mevalonate pathway, such as DMAPP derived cytokinins, FPP-derived brassinosteroids, and GGPP derived gibberellins (Tarkowská and Strnad, 2018). Other isoprenoids are antimicrobials, such as numerous FPP-derived sesquiterpenes and GGPP derived diterpenes (Holstein and Hohl, 2004). FPP and GGPP can also directly participate in cell signaling. The addition of these compounds to proteins is referred to as prenylation and is known to modify protein activity by altering their localization (Hála and Žárský, 2019). These limited examples

illustrate the importance of the mevalonate pathway in plant growth, development, reproduction, and reproduction. Additional isoprenoids serve in membrane structure, photosynthesis, cell signaling, and more metabolic activities (Holstein and Hohl, 2004; Tarkowská and Strnad, 2018).

The identification and characterization of *hmgr* mutants in plants exemplifies the broad range of isoprenoid functions and the essentiality of the mevalonate pathway. *Arabidopsis thaliana* mutants in one of the two *HMGR* genes, *hmg1,* exhibit male sterility, stunting, and early-senescence compared to wild-type (Suzuki et al., 2004). At a subcellular level, HMGRs are implicated in endoplasmic reticulum morphology. The same *hmg1* mutant exhibits an abundance of ER body aggregates at the nuclear envelope (Ferrero et al., 2015).

With such wide-serving roles, HMGRs and the other members of the mevalonate pathway require extensive regulation. Often described as one of the most regulated enzymes, HMGRs are regulated through transcription, translation, and post-translational mechanisms (Friesen and Rodwell, 2004; Stermer et al., 1994). A wide variety of biotic and abiotic stimuli can trigger these changes. Baseline HMGR activity strongly varies with tissue age and rate of cell division. HMGR activity is exceptionally high in buds, emerging fruits, growing roots, and germinating seeds. In response to ethylene, wounding, and pathogens, HMGR activity is regulated by increased transcript abundance. Post-translationally, HMGR proteins can be controlled by phosphorylation, calcium concentrations, and degradation. Specifically, phosphorylation reduces HMGR activity while phosphatases activate HMGRs (Stermer et al., 1994). Depending on the species, plant HMGR activity is increased in the presence of calmodulin and calcium or

calcium alone in a reversible manner. Furthermore, HMGRs contain a PEST motif associated with high turnover rates and their activity can be altered by inhibiting cysteine proteases. As plants contain multiple HMGRs, this allows for differential regulation of particular HMGRs based on the incoming signal (Stermer et al., 1994). Certain stimuli cause more than 200-fold changes in HMGR activity (Friesen and Rodwell, 2004). Additionally, modifications of HMGRs through a truncation to just the catalytic domain alters its regulation, illustrating the regulatory functions of the N-terminal and/or linker domains (Dale et al., 1995). This autoactive HMGR can serve as an important tool for further understanding new roles of HMGR regulation in other processes.

1.9 – Investigation into symbiotic signaling mechanism connections

Rigorous genetic studies revealed numerous molecular components essential for RN and AM symbiosis, many of which are involved in both processes. Research findings illustrate a shared subcellular signaling pathway used for the associations with both microbial partners, but a complete picture of the pathway remains unclear. Further investigations into the signaling components and the evolutionary history for developing such beneficial associations are instrumental for uncovering what distinguishes AM host plants from RN host plants.

The presence of *CCaMK* and *IPD3* in the non-symbiotic moss, *Physcomitrium patens*, is intriguing as these genes are often lost along with the ability to form AM associations. We hypothesize that the maintenance of these symbiotic genes is for an alternate biological purpose, possibly in fungal interactions. The research in **chapter 2** aims to characterize the molecular and biological functions of the *P. patens CCaMK* and

IPD3 homologs. We identify partial conservation of the *P. patens* CCaMK-IPD3 signaling complex in their molecular features for symbiotic signaling. We also report that the activities of CCaMK and IPD3 stimulate brood cell formation and ABA accumulation in *P. patens*, similar to drought stress responses, but these components are not necessary for drought stress signaling.

The previous discovery of the involvement of an HMGR in the formation of symbiotic associations opens up many questions regarding the role of HMGRs in nodulation and symbiotic signaling. We hypothesize that multiple HMGRs serve functions in developing symbiotic associations in legumes, and their activity is necessary for continued signal transduction in the cytoplasm. In **chapter 3** we aimed to identify the individual HMGRs which are involved in nodulation. Our methods uncovered the requirement for multiple HMGRs, namely HMGR1 and HMGR2c, in the development of RN symbiosis in *M. truncatula*. Also described here are the methods used in our attempts to knockdown and knockout multiple HMGRs to address questions regarding functional redundancy. Furthermore, our work in **chapter 4** aims to determine the mechanism-of-action of HMGRs in symbiotic signaling and the subsequent signaling steps. Through biochemical inhibition assays, we uncovered farnesyl pyrophosphate synthase activity and protein prenylation are required for symbiotic signaling. Additionally, we place the role of phospholipase activity downstream of HMGRs in the common symbiosis pathway. Our findings indicate the use of a signaling mechanism in which HMGR activity, and the continuation of the mevalonate pathway through farnesyl pyrophosphate synthase activity, leads to the production of prenyl groups, unknown

proteins are prenylated, and their activity leads to activation of PLC and PLD for the transduction of symbiotic signals detected at the plasma membrane.

1.10 – References

Aguilar, J.M.M., Ashby, A.M., Richards, A.J.M., Loake, G.J., Watson, M.D., Shaw, C.H., 1988. Chemotaxis of Rhizobium leguminosarum biovar phaseoli towards flavonoid inducers of the symbiotic nodulation genes 132, 2741–2746.

Akiyama, K., Matsuzaki, K., Hayashi, H., 2005. Plant sesquiterpenes induce hyphal branching in arbuscular mycorrhizal fungi 435, 824–827. https://doi.org/10.1038/nature03608

Amor, B. Ben, Shaw, S.L., Oldroyd, G.E.D., Maillet, F., Penmetsa, R.V., Cook, D., Long, S.R., Dénarié, J., Gough, C., 2003. The NFP locus of Medicago truncatula controls an early step of Nod factor signal transduction upstream of a rapid calcium flux and root hair deformation. Plant J. 34, 495–506. https://doi.org/10.1046/j.1365-313X.2003.01743.x

Ané, J.-M., Kiss, G.B., Riely, B.K., Penmetsa, R.V., Oldroyd, G.E.D., Ayax, C., Lévy, J., Debellé, F., Baek, J.-M., Kaló, P., Rosenberg, C., Roe, B.A., Long, S.R., Dénarié, J., Cook, D.R., 2004. Medicago truncatula DMI1 required for bacterial and fungal symbioses in legumes. Science 303, 1364–1367. https://doi.org/10.1126/science.1092986

Antolín-Llovera, M., Ried, M.K., Parniske, M., 2014. Cleavage of the symbiosis receptor-like kinase ectodomain promotes complex formation with nod factor receptor 5. Curr. Biol. 24, 422–427. https://doi.org/10.1016/j.cub.2013.12.053

Apodaca, L.E., 2017. 2017 Minerals Yearbook. U.S. Geol. Surv. 77.1-77.5.

Arbestain, M.C., Macías, F., Chesworth, W., Chesworth, Ward, Spaargaren, O., Semoka, J., 2008. Nitrogen Cycle. pp. 491–494. https://doi.org/10.1007/978-1-4020-3995-9_381

Arrighi, J.-F., 2006. The Medicago truncatula Lysine Motif-Receptor-Like Kinase Gene Family Includes NFP and New Nodule-Expressed Genes. Plant Physiol. 142, 265–279. https://doi.org/10.1104/pp.106.084657

Badri, D. V, Vivanco, J.M., 2009. Regulation and function of root exudates. Plant, cell and envir. 32, 666–681. https://doi.org/10.1111/j.1365-3040.2009.01926.x

Barbour, W.M., Hattermann, D.R., Stacey, G., 1991. Chemotaxis of Bradyrhizobium japonicum to soybean exudates. Appl. Environ. Microbiol. 57, 2635–2639. https://doi.org/10.1128/aem.57.9.2635-2639.1991

Bécard, G., Fortin, J.A., 1988. Early events of vesicular arbuscular mycorrhiza formation on Ri T-DNA transformed roots. New Phytol 108, 211–218.

Bensmihen, S., de Billy, F., Gough, C., 2011. Contribution of NFP LysM domains to the recognition of Nod factors during the Medicago truncatula/Sinorhizobium meliloti symbiosis. PLoS One 6, 11. https://doi.org/10.1371/journal.pone.0026114

Bicer, Y., Dincer, I., Vezina, G., Raso, F., 2017. Impact Assessment and Environmental Evaluation of Various Ammonia Production Processes. Environ. Manage. 59, 842–855. https://doi.org/10.1007/s00267-017-0831-6

Giovannetti, M., Sbrana, C., Avio, L., Citernesi, S., Logi, C., 1993. Differential hyphal morphogenesis in arbuscular mycorrhizal fungi during pre infection stages. New Physol. 125, 587–593.

Bozsoki, Z., Cheng, J., Feng, F., Gysel, K., Vinther, M., Andersen, K.R., Oldroyd, G., Blaise, M., Radutoiu, S., Stougaard, J., 2017. Receptor-mediated chitin perception in legume roots is functionally separable from Nod factor perception. Proc. Natl. Acad. Sci. U. S. A. 114, E8118–E8127. https://doi.org/10.1073/pnas.1706795114

Branzanti, B., Gianinazzi-perason, V., Gianinazzi, S., 1989. In Vitro Enhancement of Spore Germination and Early Hyphal Growth of a Vesicular-Arbuscular Mycorrhizal Fungus by Host Root Exudates and Plant Flavonoids. Symbiosis 7, 243–255.

Broghammer, A., Krusell, L., Blaise, M., Sauer, J., Sullivan, J.T., Maolanon, N., Vinther, M., Lorentzen, A., Madsen, E.B., Jensen, K.J., Roepstorff, P., Thirup, S., Ronson, C.W., Thygesen, M.B., Stougaard, J., 2012. Legume receptors perceive the rhizobial lipochitin oligosaccharide signal molecules by direct binding. Proc. Natl. Acad. Sci. U. S. A. 109, 13859–13864. https://doi.org/10.1073/pnas.1205171109

Buist, G., Steen, A., Kok, J., Kuipers, O.P., 2008. LysM, a widely distributed protein motif for binding to (peptido)glycans. Mol. Microbiol. 68, 838–847. https://doi.org/10.1111/j.1365-2958.2008.06211.x

Pirosynski, K.A., and Malloch, D.W. 1975. The origin of land plants:a matter of mycotrophism. Biosystems 6, 153-164.

Capoen, W., Sun, J., Wysham, D., Otegui, M.S., Venkateshwaran, M., Hirsch, S., Miwa, H., Downie, J.A., Morris, R.J., Ané, J.-M., Oldroyd, G.E.D., 2011. Nuclear membranes control symbiotic calcium signaling of legumes. Proc. Natl. Acad. Sci. U. S. A. 108, 14348-14353. https://doi.org/10.1073/pnas.1107912108

Catoira, R., Galera, C., de Billy, F., Penmetsa, R. V, Journet, E.P., Maillet, F., Rosenberg, C., Cook, D., Gough, C., Dénarié, J., 2000. Four genes of Medicago truncatula controlling components of a Nod factor transduction pathway. Plant Cell 12, 1647–1666. https://doi.org/10.1105/tpc.12.9.1647

Cerri, M.R., Frances, L., Kelner, A., Fournier, J., Middleton, P.H., Auriac, M.C., Mysore, K.S., Wen, J., Erard, M., Barker, D.G., Oldroyd, G.E., de Carvalho-Niebel, F., 2016. The symbiosis-related ERN transcription factors act in concert to coordinate rhizobial host root infection. Plant Physiol. 171, 1037–1054. https://doi.org/10.1104/pp.16.00230

Charpentier, M., Sun, J., Martins, T. V., Radhakrishnan, G. V., Findlay, K., Soumpourou, E., Thouin, J., Very, A.-A., Sanders, D., Morris, R.J., Oldroyd, G.E.D., 2016. Nuclear-localized cyclic nucleotide-gated channels mediate symbiotic calcium oscillations. Science 352, 1102–1105. https://doi.org/10.1126/science.aae0109

Compton, K.K., Scharf, B.E., 2021. Rhizobial Chemoattractants, the Taste and Preferences of Legume Symbionts. Front. Plant Sci. 12, 1–8. https://doi.org/10.3389/fpls.2021.686465

Currier, W.W., Strobel, G.A., 1976. Chemotaxis of Rhizobium to Plant Root Exudates.1 820–823.

Dale, S., Arro, M., Becerra, B., Morrice, N.G., Boronat, A., Hardie, D.G., Ferrer, A., 1995. Bacterial expression of the catalytic domain of 3-Hydroxy-3-Methylglutaryl-CoA Reductase (isoform HMGR1) from Arabidopsis thaliana, and its inactivation by

phosphorylation at Ser577 by Brassica oleracea 3-Hydroxy-3-Methylglutaryl-CoA Reductase Kinase. Eur. J. Biochem. 233, 506–513. https://doi.org/10.1111/j.1432-1033.1995.506_2.x

Davis, T.W., Bullerjahn, G.S., Tuttle, T., McKay, R.M., Watson, S.B., 2015. Effects of increasing nitrogen and phosphorus concentrations on phytoplankton community growth and toxicity during planktothrix blooms in sandusky bay, lake erie. Environ. Sci. Technol. 49, 7197–7207. https://doi.org/10.1021/acs.est.5b00799

De La Peña, T.C., Fedorova, E., Pueyo, J.J., Mercedes Lucas, M., 2018. The symbiosome: Legume and rhizobia co-evolution toward a nitrogen-fixing organelle? Front. Plant Sci. 8, 1–26. https://doi.org/10.3389/fpls.2017.02229

Delaux, P.M., Radhakrishnan, G. V., Jayaraman, D., Cheema, J., Malbreil, M., Volkening, J.D., Sekimoto, H., Nishiyama, T., Melkonian, M., Pokorny, L., Rothfels, C.J., Sederoff, H.W., Stevenson, D.W., Surek, B., Zhang, Y., Sussman, M.R., Dunand, C., Morris, R.J., Roux, C., Wong, G.K.S., Oldroyd, G.E.D., Ane, J.M., 2015. Algal ancestor of land plants was preadapted for symbiosis. Proc. Natl. Acad. Sci. U. S. A. 112, 13390–13395. https://doi.org/10.1073/pnas.1515426112

Delaux, P.M., Schornack, S., 2021. Plant evolution driven by interactions with symbiotic and pathogenic microbes. Science. 371, 796. https://doi.org/10.1126/science.aba6605

Delaux, P.M., Varala, K., Edger, P.P., Coruzzi, G.M., Pires, J.C., Ané, J.M., 2014. Comparative Phylogenomics Uncovers the Impact of Symbiotic Associations on Host Genome Evolution. PLoS Genet. 10, 7. https://doi.org/10.1371/journal.pgen.1004487

Den Camp, R.H.M.O., Polone, E., Fedorova, E., Roelofsen, W., Squartini, A., Den Camp, H.J.M.O., Bisseling, T., Geurts, R., 2012. Nonlegume Parasponia andersonii deploys a broad rhizobium host range strategy resulting in largely variable symbiotic effectiveness. Mol. Plant-Microbe Interact. 25, 954–963. https://doi.org/10.1094/MPMI-11-11-0304

Den Hartog, M., Musgrave, A., Munnik, T., 2001. Nod factor-induced phosphatidic acid and diacylglycerol pyrophosphate formation: A role for phospholipase C and D in root hair deformation. Plant J. 25, 55–65. https://doi.org/10.1046/j.1365-313X.2001.00931.x

Dénarié, J., Debellé, F., Promé, J.C., 1996. Rhizobium lipo-chitooligosaccharide nodulation factors: Signaling molecules mediating recognition and morphogenesis. Annu. Rev. Biochem. 65, 503–535. https://doi.org/10.1146/annurev.bi.65.070196.002443

Desiro, A., Duckett, J.G., Pressel, S., Villarreal, J.C., Bidartondo, M.I., 2013. Fungal symbioses in hornworts: a chequered history. Proc R Soc B. 280, 20130297. http://dx.doi.org/10/1098/rspb.2013.0207

Ehrhardt, D.W., Wais, R.J., Long, S.R., 1996. Calcium spiking in plant root hairs responding to Rhizobium nodulation signals. Cell 85, 673–681.

EPA, 2009. Technical support document for the ammonia production sector: Proposed rule for mandatory reporting of greenhouse gases. Office of AIr and Radiation. U.S. Environmental Protection Agency. 1–22.

Fellbaum, C.R., Gachomo, E.W., Beesetty, Y., Choudhari, S., Strahan, G.D., Pfeffer, P.E., 2011. Carbon availability triggers fungal nitrogen uptake and transport in

arbuscular mycorrhizal symbiosis. PNAS. 109, 7, 2666-2671 https://doi.org/10.1073/pnas.1118650109/-/DCSupplemental.www.pnas.org/cgi/doi/10.1073/pnas.1118650109

Feng, F., Sun, J., Radhakrishnan, G. V., Lee, T., Bozsóki, Z., Fort, S., Gavrin, A., Gysel, K., Thygesen, M.B., Andersen, K.R., Radutoiu, S., Stougaard, J., Oldroyd, G.E.D., 2019. A combination of chitooligosaccharide and lipochitooligosaccharide recognition promotes arbuscular mycorrhizal associations in Medicago truncatula. Nat. Commun. 10. https://doi.org/10.1038/s41467-019-12999-5

Ferrero, S., Grados-Torrez, R.E., Leivar, P., Antolín-Llovera, M., López-Iglesias, C., Cortadellas, N., Ferrer, J.C., Campos, N., 2015. Proliferation and Morphogenesis of the Endoplasmic Reticulum Driven by the Membrane Domain of 3-Hydroxy-3-Methylglutaryl Coenzyme A Reductase in Plant Cells. Plant Physiol. 168, 899–914. https://doi.org/10.1104/pp.15.00597

Field, K.J., Rimington, W.R., Bidartondo, M.I., Allinson, K.E., Beerling, D.J., Cameron, D.D., Duckett, J.G., Leake, J.R., Pressel, S., 2015. First evidence of mutualism between ancient plant lineages (Haplomitriopsida liverworts) and Mucoromycotina fungi and its response to simulated Palaeozoic changes in atmospheric CO2. New Phytol. 205, 743–756. https://doi.org/10.1111/nph.13024

Francis, C.A., Beman, J.M., Kuypers, M.M.M., 2007. New processes and players in the nitrogen cycle: The microbial ecology of anaerobic and archaeal ammonia oxidation. ISME J. 1, 19–27. https://doi.org/10.1038/ismej.2007.8

Friesen, J.A., Rodwell, V.W., 2004. The 3-hydroxy-3-methylglutaryl coenzyme-A (HMG-CoA) reductases. Genome Biol. 5, 248. https://doi.org/10.1186/gb-2004-5-11-248

Genre, A., Chabaud, M., Balzergue, C., Puech-Pagès, V., Novero, M., Rey, T., Fournier, J., Rochange, S., Bécard, G., Bonfante, P., Barker, D.G., 2013. Short-chain chitin oligomers from arbuscular mycorrhizal fungi trigger nuclear Ca2+ spiking in Medicago truncatula roots and their production is enhanced by strigolactone. New Phytol. 198, 190–202. https://doi.org/10.1111/nph.12146

Gibelin-Viala, C., Amblard, E., Puech-Pages, V., Bonhomme, M., Garcia, M., Bascaules-Bedin, A., Fliegmann, J., Wen, J., Mysore, K.S., le Signor, C., Jacquet, C., Gough, C., 2019. The Medicago truncatula LysM receptor-like kinase LYK9 plays a dual role in immunity and the arbuscular mycorrhizal symbiosis. New Phytol. 223, 1516–1529. https://doi.org/10.1111/nph.15891

Gobler, C.J., Burkholder, J.A.M., Davis, T.W., Harke, M.J., Johengen, T., Stow, C.A., Van de Waal, D.B., 2016. The dual role of nitrogen supply in controlling the growth and toxicity of cyanobacterial blooms. Harmful Algae 54, 87–97. https://doi.org/10.1016/j.hal.2016.01.010

Granqvist, E., Wysham, D., Hazledine, S., Kozlowski, W., Sun, J., Charpentier, M., Martins, T.V., Haleux, P., Tsaneva-Atanasova, K., Downie, J.A., Oldroyd, G.E.D., Morris, R.J., 2012. Buffering capacity Explains signal variation in symbiotic calcium oscillations. Plant Physiol. 160, 2300–2310. https://doi.org/10.1104/pp.112.205682

Griesmann, M., Chang, Y., Liu, X., Song, Y., Haberer, G., Crook, M.B., Billault-Penneteau, B., Lauressergues, D., Keller, J., Imanishi, L., Roswanjaya, Y.P., Kohlen, W., Pujic, P., Battenberg, K., Alloisio, N., Liang, Y., Hilhorst, H., Salgado, M.G., Hocher, V., Gherbi, H., Svistoonoff, S., Doyle, J.J., He, S., Xu, Y., Xu, S., Qu, J., Gao, Q., Fang, X., Fu, Y., Normand, P., Berry, A.M., Wall, L.G., Ané, J.M.,

Pawlowski, K., Xu, X., Yang, H., Spannagl, M., Mayer, K.F.X., Wong, G.K.S., Parniske, M., Delaux, P.M., Cheng, S., 2018. Phylogenomics reveals multiple losses of nitrogen-fixing root nodule symbiosis. Science. 361. https://doi.org/10.1126/science.aat1743

Hála, M., Žárský, V., 2019. Protein prenylation in plant stress responses. Molecules 24, 1–14. https://doi.org/10.3390/molecules24213906

Hartwig, U.A., Joseph, C.M., Phillips, D.A., 1991. Flavonoids Released Naturally from Alfalfa Seeds Enhance Growth Rate of Rhizobium meliloti. Plant Physiol. 1021, 797–803.

Hirsch, S., Kim, J., Muñoz, A., Heckmann, A.B., Downie, J.A., Oldroyd, G.E.D., 2009. GRAS Proteins Form a DNA Binding Complex to Induce Gene Expression during Nodulation Signaling in Medicago truncatulaw. Plant Cell 21, 545–557. https://doi.org/10.1105/tpc.108.064501

Holstein, S.A., Hohl, R.J., 2004. Isoprenoids : Remarkable Diversity of Form and Function. Lipids. 39, 293–309.

Horváth, B., Yeun, L.H., Domonkos, Á., Halász, G., Gobbato, E., Ayaydin, F., Miró, K., Hirsch, S., Sun, J., Tadege, M., Ratet, P., Mysore, K.S., Ané, J.-M., Oldroyd, G.E.D., Kaló, P., 2011. Medicago truncatula IPD3 is a member of the common symbiotic signaling pathway required for rhizobial and mycorrhizal symbioses. Mol. Plant-Microbe Interact. 24, 1345–1358. https://doi.org/10.1094/mpmi-01-11-0015

Huisman, J., Codd, G.A., Paerl, H.W., Ibelings, B.W., Verspagen, J.M.H., Visser, P.M., 2018. Cyanobacterial blooms. Nat. Rev. Microbiol. 16, 471–483. https://doi.org/10.1038/s41579-018-0040-1

Humphreys, C.P., Franks, P.J., Rees, M., Bidartondo, M.I., Leake, J.R., Beerling, D.J., 2010. Mutualistic mycorrhiza-like symbiosis in the most ancient group of land plants. Nat. Commun. 1. https://doi.org/10.1038/ncomms1105

IFA, 2009. Energy Efficiency and CO2 Emissions in Ammonia Production. Production 4.

Istvan, E.S., Deisenhofer, J., 2000. The structure of the catalytic portion of human HMG-CoA reductase. Biochim. Biophys. Acta - Mol. Cell Biol. Lipids 1529, 9–18. https://doi.org/10.1016/S1388-1981(00)00134-7

Jin, Y., Chen, Z., Yang, J., Mysore, K.S., Wen, J., Huang, J., Yu, N., Wang, E., 2018. IPD3 and IPD3L function redundantly in rhizobial and mycorrhizal symbioses. Front. Plant Sci. 9, 1–12. https://doi.org/10.3389/fpls.2018.00267

Jones, K.M., Kobayashi, H., Davies, B.W., Taga, M.E., Walker, G.C., 2007. How rhizobial symbionts invade plants: the Sinorhizobium-Medicago model. Nat. Rev. Microbiol. 5, 619–33. https://doi.org/10.1038/nrmicro1705

Kermeli, K., Worrel, E., Graus, W., Mariëlle Corsten, 2017. Energy Efficiency and Cost Saving Opportunities for Ammonia and Nitrogenous Fertilizer Production: An ENERGY STAR® Guide for Energy & Plant Managers 1–430.

Kevei, Z., Lougnon, G., Mergaert, P., Horváth, B., Kereszt, A., Jayaraman, D., Zaman, N., Marcel, F., Regulski, K., Kiss, G.B., Kondorosi, A., Endre, G., Kondorosi, E., Ané, J.-M., Horváth, G. V, Horvath, G. V, 2007. 3-hydroxy-3-methylglutaryl coenzyme A reductase1 interacts with NORK and is crucial for nodulation in Medicago truncatula. Plant Cell 19, 3974–3989. https://doi.org/10.1105/tpc.107.053975

Kiers, E.T., Kiers, E.T., Duhamel, M., Beesetty, Y., Mensah, J.A., Franken, O.,

Verbruggen, E., Fellbaum, C.R., Kowalchuk, G.A., Hart, M.M., Bago, A., Palmer, T.M., West, S.A., Vandenkoornhuyse, P., Jansa, J., Bücking, H., 2012. Reciprocal Rewards Stabilize Cooperation in the Mycorrhizal Symbiosis. Science 33, 880, 10–13. https://doi.org/10.1126/science.1208473

Kim, S., Zeng, W., Bernard, S., Liao, J., Ane, J., Jiang, Y., Venkateshwaran, M., 2019. Ca2+-regulated Ca2+ channels with an RCK gating ring control plant symbiotic associations. Nat. Commun. 10, 1–12. https://doi.org/10.1038/s41467-019-11698-5

Kistner, C., Parniske, M., 2002. Evolution of signal transduction in intracellular symbiosis. Trends Plant Sci. 7, 511–518. https://doi.org/10.1016/S1360-1385(02)02356-7

Koelle, M.R., 2006. Heterotrimeric G Protein Signaling: Getting inside the Cell. Cell 126, 25–27. https://doi.org/10.1016/j.cell.2006.06.026

Kosuta, S., Hazledine, S., Sun, J., Miwa, H., Morris, R.J., Downie, J.A., Oldroyd, G.E.D., 2008. Differential and chaotic calcium signatures in the symbiosis signaling pathway of legumes. Proc. Natl. Acad. Sci. U. S. A. 105, 9823–9828. https://doi.org/10.1073/pnas.0803499105

Lerouge, P., Roche, P., Faucher, C., Maillet, F., Truchet, G., Promé, J.C., Dénarié, J., 1990. Symbiotic host-specificity of Rhizobium meliloti is determined by a sulphated and acylated glucosamine oligosaccharide signal. Nature 344, 781–784. https://doi.org/10.1038/344781a0

Lévy, J., Bres, C., Geurts, R., Chalhoub, B., Kulikova, O., Duc, G., Journet, E.-P., Ané, J.-M., Lauber, E., Bisseling, T., Dénarié, J., Rosenberg, C., Debellé, F., 2004. A Putative Ca 2 and Calmodulin- Dependent Protein Kinase Required. Science 303, 1361–4.

Li, W., Liu, W., Wei, H., He, Q., Chen, J., Zhang, B., Zhu, S., 2014. Species-specific expansion and molecular evolution of the 3-hydroxy-3-methylglutaryl coenzyme A reductase (HMGR) gene family in plants. PLoS One 9, 1–10. https://doi.org/10.1371/journal.pone.0094172

Limpens, E., Franken, C., Smit, P., Willemse, J., Bisseling, T., Geurts, R., 2003. LysM Domain Receptor Kinases Regulating Rhizobial Nod Factor-Induced Infection. Science 302, 630–633. https://doi.org/10.1126/science.1090074

Lindström, K., Mousavi, S.A., 2020. Effectiveness of nitrogen fixation in rhizobia. Microb. Biotechnol. 13, 1314–1335. https://doi.org/10.1111/1751-7915.13517

Madsen, E.B., Antolín-Llovera, M., Grossmann, C., Ye, J., Vieweg, S., Broghammer, A., Krusell, L., Radutoiu, S., Jensen, O.N., Stougaard, J., Parniske, M., 2011. Autophosphorylation is essential for the in vivo function of the Lotus japonicus Nod factor receptor 1 and receptor-mediated signalling in cooperation with Nod factor receptor 5. Plant J. 65, 404–417. https://doi.org/10.1111/j.1365-313X.2010.04431.x

Mahler, R.L., 2004. Nutrients Plants Require. University of Idaho. CIS 1124 20–23.

Maillet, F., Poinsot, V., André, O., Puech-Pagès, V., Haouy, A., Gueunier, M., Cromer, L., Giraudet, D., Formey, D., Niebel, A., Martinez, E.A., Driguez, H., Bécard, G., Dénarié, J., 2011. Fungal lipochitooligosaccharide symbiotic signals in arbuscular mycorrhiza. Nature 469, 58–63. https://doi.org/10.1038/nature09622

Messinese, E., Mun, J.-H.H., Yeun, L.H., Jayaraman, D., Rougé, P., Barre, A., Lougnon, G., Schornack, S., Bono, J.-J., Cook, D.R., Ané, J.-M., Rouge, P., 2007. A novel nuclear protein interacts with the symbiotic DMI3 calcium- and calmodulin-

dependent protein kinase of Medicago truncatula. Mol. Plant-Microbe Interact. 20, 912–921. https://doi.org/10.1094/MPMI-20-8-0912

Miller, J.B., Pratap, A., Miyahara, A., Zhou, L., Bornemann, S., Morris, R.J., Oldroyd, G.E.D., 2013. Calcium/calmodulin-dependent protein kinase is negatively and positively regulated by calcium, providing a mechanism for decoding calcium responses during symbiosis signaling. Plant Cell 25, 5053–5066. https://doi.org/10.1105/tpc.113.116921

Moling, S., Pietraszewska-Bogiel, A., Postma, M., Fedorova, E.E., Hink, M.A., Limpens, E., Gadella, T.W.J., Bisseling, T., 2014. Nod Factor Receptors Form Heteromeric Complexes and Are Essential for Intracellular Infection in Medicago Nodules. Plant Cell 26, 4188-4199. https://doi.org/10.1105/tpc.114.129502

Mueller, N.D., Gerber, J.S., Johnston, M., Ray, D.K., Ramankutty, N., Foley, J.A., 2012. Closing yield gaps through nutrient and water management. Nature 490, 254–257. https://doi.org/10.1038/nature11420

Oldroyd, G.E.D., 2013. Speak, friend, and enter: Signalling systems that promote beneficial symbiotic associations in plants. Nat. Rev. Microbiol. 11, 252–263. https://doi.org/10.1038/nrmicro2990

Pan, H., Stonoha-Arther, C., Wang, D., 2018. Medicago plants control nodulation by regulating proteolysis of the receptor-like kinase DMI2. Plant Physiol. 177, 792–802. https://doi.org/10.1104/pp.17.01542

Peiter, E., Sun, J., Heckmann, A.B., Venkateshwaran, M., Riely, B.K., Otegui, M.S., Edwards, A., Freshour, G., Hahn, M.G., Cook, D.R., Sanders, D., Oldroyd, G.E.D., Downie, J.A., Ané, J.M., 2007. The Medicago truncatula DMI1 protein modulates cytosolic calcium signaling. Plant Physiol. 145, 192–203. https://doi.org/10.1104/pp.107.097261

Perret, X., Staehelin, C., Broughton, W.J., 2000. Molecular Basis of Symbiotic Promiscuity. Microbiol. Mol. Biol. Rev. 64, 180–201. https://doi.org/10.1128/mmbr.64.1.180-201.2000

Pimprikar, P., Carbonnel, S., Paries, M., Katzer, K., Klingl, V., Bohmer, M.J., Karl, L., Floss, D.S., Harrison, M.J., Parniske, M., Gutjahr, C., 2016. A CCaMK-CYCLOPS-DELLA complex activates transcription of RAM1 to regulate arbuscule branching. Curr. Biol. 26, 987–998. https://doi.org/10.1016/j.cub.2016.01.069

Pingret, J.L., Journet, E.P., Barker, D.G., 1998. Rhizobium Nod factor signaling. Evidence for a G protein-mediated transduction mechanism. Plant Cell 10, 659–672.

Pulido, P., Perello, C., Rodriguez-Concepcion, M., 2012. New insights into plant Isoprenoid metabolism. Mol. Plant 5, 964–967. https://doi.org/10.1093/mp/sss088

Radutoiu, S., Madsen, L.H., Madsen, E.B., Felle, H.H., Umehara, Y., Grønlund, M., Sato, S., Nakamura, Y., Tabata, S., Sandal, N., Stougaard, J., Gronlund, M., Sato, S., Nakamura, Y., Tabata, S., Sandal, N., Stougaard, J., 2003. Plant recognition of symbiotic bacteria requires two LysM receptor-like kinases. Nature 425, 585–592. https://doi.org/10.1038/nature02039

Radutoiu, S., Madsen, L.H., Madsen, E.B., Jurkiewicz, A., Fukai, E., Quistgaard, E.M.H., Albrektsen, A.S., James, E.K., Thirup, S., Stougaard, J., 2007. LysM domains mediate lipochitin-oligosaccharide recognition and Nfr genes extend the symbiotic host range. EMBO J. 26, 3923–3935.

https://doi.org/10.1038/sj.emboj.7601826
Remy, W., Taylor, T.N., Hass, H., Kerp, H., 1994. Four hundred-million-year-old vesicular arbuscular mycorrhizae. Proc Natl Acad Sci U S A 91, 11841–11843. https://doi.org/10.1073/pnas.91.25.11841
Ried, M.K., Antolín-Llovera, M., Parniske, M., 2014. Spontaneous symbiotic reprogramming of plant roots triggered by receptor-like kinases. Elife 3, 1–17. https://doi.org/10.7554/eLife.03891
Riely, B.K., Ané, J.M., Penmetsa, R.V., Cook, D.R., 2004. Genetic and genomic analysis in model legumes bring Nod-factor signaling to center stage. Curr. Opin. Plant Biol. 7, 408–413. https://doi.org/10.1016/j.pbi.2004.04.005
Rimington, W.R., Pressel, S., Duckett, J.G., Field, K.J., Bidartondo, M.I., 2019. Evolution and networks in ancient and widespread symbioses between Mucoromycotina and liverworts. Mycorrhiza 29, 551–565. https://doi.org/10.1007/s00572-019-00918-x
Robertson, G.P., Vitousek, P.M., 2009. Nitrogen in agriculture: Balancing the cost of an essential resource. Annu. Rev. Environ. Resour. 34, 97–125. https://doi.org/10.1146/annurev.environ.032108.105046
Sacchettini, J.C., Poulter, C.D., 1997. Creating Isoprenoid Diversity. Science 277, 1788-1789.
Saha, S., Dutta, A., Bhattacharya, A., DasGupta, M., 2014. Intracellular catalytic domain of symbiosis receptor kinase hyperactivates spontaneous nodulation in absence of rhizobia. Plant Physiol. 166, 1699–1708. https://doi.org/10.1104/pp.114.250084
Schwarzott, D., Walker, C., Schubler, A., 2001. A new fungal phylum , the Glomeromycota : phylogeny and evolution. Mycol. Res. 105, 1413–1421.
Si, S., Parniske, M., 2008. E b Arbuscular mycorrhiza : the mother of plant root endosymbioses 6, 763–775. https://doi.org/10.1038/nrmicro1987
Sieberer, B.J., Chabaud, M., Timmers, A.C., Monin, A., Fournier, J., Barker, D.G., 2009. A nuclear-targeted cameleon demonstrates intranuclear Ca2+ spiking in Medicago truncatula root hairs in response to rhizobial nodulation factors. Plant Physiol. 151, 1197–1206. https://doi.org/10.1104/pp.109.142851
Singh, S., Katzer, K., Lambert, J., Cerri, M., Parniske, M., 2014. CYCLOPS, A DNA-binding transcriptional activator, orchestrates symbiotic root nodule development. Cell Host Microbe 15, 139–152. https://doi.org/10.1016/j.chom.2014.01.011
Smit, P., Limpens, E., Geurts, R., Fedorova, E., Dolgikh, E., Gough, C., Bisseling, T., 2007. Medicago LYK3, an Entry Receptor in Rhizobial Nodulation Factor Signaling. Plant Physiol. 145, 183–191. https://doi.org/10.1104/pp.107.100495
Stermer, B. a, Bianchini, G.M., Korth, K.L., 1994. Regulation of HMG-CoA reductase activity in plants. J. Lipid Res. 35, 1133–40.
Stracke, S., Kistner, C., Yoshida, S., Mulder, L., Sato, S., Kaneko, T., Tabata, S., Sandal, N., 2002. A plant receptor-like kinase required for both bacterial and fungal symbiosis. Nature 417, 959–962.
Sun, J., Miller, J.B., Granqvist, A.E.U., Wiley-Kalil, A., Gobbato, E., Maillet, F., Cottaz, S., Samain, E., Venkateshwaran, M., Fort, S., Morris, R.J., Ané, J.-M., Dénarié, J., Oldroyd, G.E.D., 2015. Activation of Symbiosis Signaling by Arbuscular Mycorrhizal Fungi in Legumes and Rice. Plant Cell 27, 823-838 https://doi.org/10.1105/tpc.114.131326

Sun, J., Miwa, H., Downie, J.A., Oldroyd, G.E.D., 2007. Mastoparan activates calcium spiking analogous to Nod factor-induced responses in Medicago truncatula root hair cells. Plant Physiol. 144, 695–702. https://doi.org/10.1104/pp.106.093294

Suzuki, M., Kamide, Y., Nagata, N., Seki, H., Ohyama, K., Kato, H., 2004. Loss of function of 3-hydroxy-3-methylglutaryl coenzyme A reductase 1 (HMG1) in Arabidopsis leads to dwarfng , early senescence and male sterility , and reduced sterol levels. Plant J. 1, 750–761. https://doi.org/10.1111/j.1365-313X.2003.02003.x

Taiz, L., Zeiger, E., 2010. Plant Physiology. Sinauer Associates, Inc., Sunderland, pp. 107–118.

Takáč, T., Novák, D., Šamaj, J., 2019. Recent advances in the cellular and developmental biology of phospholipases in plants. Front. Plant Sci. 10. https://doi.org/10.3389/fpls.2019.00362

Tarkowská, D., Strnad, M., 2018. Isoprenoid-derived plant signaling molecules: biosynthesis and biological importance. Planta 247, 1051–1066. https://doi.org/10.1007/s00425-018-2878-x

Tobert, J.A., 2003. Lovastatin and beyond: The history of the HMG-CoA reductase inhibitors. Nat. Rev. Drug Discov. 2, 517–526. https://doi.org/10.1038/nrd1112

Tsait, S.I.U.M., Phillips, D.A., 1991. Flavonoids released naturally from alfalfa promote development of symbiotic glomus spores in vitro. App. Envir. Micro. 57, 1485–1488.

USGS National Minerals Information Center, 2020. Nitrogen Statistics and Information, U.S. Geological Survey, Mineral Commodity Summaries.

Venkateshwaran, M., Jayaraman, D., Chabaud, M., Genre, A., Balloon, A.J., Maeda, J., Forshey, K.L., den Os, D., Kwiecien, N.W., Coon, J.J., Barker, D.G., Ané, J.-M., 2015. A role for the mevalonate pathway in early plant symbiotic signaling. PNAS 112. https://doi.org/10.1073/pnas.1413762112

Wais, R.J., Galera, C., Oldroyd, G.E.D., Catoira, R., Penmetsa, R. V, Cook, D., Gough, C., Denarié, J., Long, S.R., Dénarié, J., 2000. Genetic analysis of calcium spiking responses in nodulation mutants of Medicago truncatula. Proc Natl Acad Sci U S A 97, 13407–13412. https://doi.org/10.1073/pnas.230439797

Wang, B., Yeun, L.H., Xue, J.Y., Liu, Y., Ané, J.M., Qiu, Y.L., 2010. Presence of three mycorrhizal genes in the common ancestor of land plants suggests a key role of mycorrhizas in the colonization of land by plants. New Phytol. 186, 514–525. https://doi.org/10.1111/j.1469-8137.2009.03137.x

Wang, W., Shi, J., Xie, Q., Jiang, Y., Yu, N., Wang, E., 2017. Nutrient Exchange and Regulation in Arbuscular Mycorrhizal Symbiosis. Mol. Plant 10, 1147–1158. https://doi.org/10.1016/j.molp.2017.07.012

Yano, K., Yoshida, S., Müller, J., Singh, S., Banba, M., Vickers, K., Markmann, K., Mu, J., White, C., Schuller, B., Sato, S., Asamizu, E., Tabata, S., Murooka, Y., Perry, J., Wang, T.L., Kawaguchi, M., Imaizumi-Anraku, H., Hayashi, M., Parniske, M., Muller, J., 2008. CYCLOPS, a mediator of symbiotic intracellular accommodation. Proc. Natl. Acad. Sci. 105, 20540–20545.

Chapter 2 – Conserved components of the common symbiosis pathway regulate ABA levels and stress-associated developmental reprogramming in Physcomitrium. (MANUSCRIPT IN SECOND ROUND OF REVIEWS WITH iSCIENCE)

Thomas J. Kleist[1,2,3,*,#,§], Anthony Bortolazzo[4,5*], Zachary P. Keyser[5,6], Adele M. Perera[1], Thomas B. Irving[5], Muthusubramanian Venkateshwaran[6,7], Fatiha Atanjaoui[3], Ren-Jie Tang[1], Heather N. Cartwright[2], Michael L. Christianson[1], Peggy G. Lemaux[1], Sheng Luan[1], and Jean-Michel Ané[5,6,#]

[1] Department of Plant & Microbial Biology, University of California-Berkeley, Berkeley, CA 94720, USA
[2] Department of Plant Biology, Carnegie Institute for Science, Stanford, CA 94305, USA
[3] Institute for Molecular Physiology, Department of Biology, Heinrich Heine University, Düsseldorf 40225, Germany (current affiliation)
[4] Laboratory of Genetics, University of Wisconsin-Madison, Madison, WI 53706, USA
[5] Department of Bacteriology, University of Wisconsin-Madison, Madison, WI 53706, USA
[6] Department of Agronomy, University of Wisconsin-Madison, Madison, WI 53706, USA
[7] School of Agriculture, University of Wisconsin-Platteville, Platteville, WI 53818, USA (current affiliation)

* These authors contributed equally to this work.

[#] Corresponding Authors: Thomas J. Kleist, Phone: +49 211 81-14826, Email: kleistt@hhu.de, Jean-Michel Ané, Phone: 608-262-6457, Email: jeanmichel.ane@wisc.edu

Zachary Keyser's (ZK) contributions to Chapter 2 manuscript

ZK validated the ability of PpCCaMK modifications to generate a form that is constitutively active. This included all cloning work for the construction of the necessary plasmid constructs, *Agrobacterium rhizogenes* transformations, *Medicago truncatula* transformation methods, histochemical staining, and microscopy for phenotyping and imaging. ZK performed *M. truncatula* mutant rescue experiments for determining the symbiotic functional conservation of *Physcomitrium* IPD3, For this experiment, ZK designed and cloned the genetic elements necessary for the constructs used, transformed *A. rhizogenes,* generated mutant roots with *M. trunctula* transformations, histochemically stained roots, and imaged and phenotyped the symbiotic responses of the plants. For all experiments performed by ZK, ZK performed the data analysis. In regards to manuscript preparation, ZK wrote a substantial portion of the manuscript, consisting of the results, methods, and discussion on topics pertaining to experiments performed by ZK, edited multiple iterations of the manuscript and illustrated figures S5 and S6.

2.1 – Abstract

Symbioses between angiosperms and rhizobia or arbuscular mycorrhizal fungi are controlled through a conserved signaling pathway. Microbe-derived, chitin-based elicitors activate plant cell-surface receptors and trigger oscillatory nuclear calcium signals, decoded by a calcium/calmodulin-dependent protein kinase (CCaMK) and its target transcription factor Interacting Protein of DMI3 (IPD3). Genes encoding CCaMK and IPD3 have been lost in multiple non-mycorrhizal plant lineages yet retained among non-mycorrhizal mosses. Here, we demonstrated that the moss *Physcomitrium patens*

is equipped with a bona fide CCaMK that can functionally complement a *Medicago truncatula* loss-of-function mutant. Conservation of regulatory phosphosites allowed us to generate predicted hyperactive forms of *Physcomitrium patens* CCaMK and IPD3. Expression of synthetically activated CCaMK or IPD3 in *Physcomitrium patens* led to abscisic acid (ABA) accumulation and ectopic development of brood cells, which are asexual propagules that facilitate escape from local abiotic stresses. We, therefore, propose a functional role for *Physcomitrium patens* CCaMK-IPD3 in stress-associated developmental reprogramming.

2.2 – Introduction

During their early evolution, plants faced numerous challenges in the shift from freshwater to terrestrial environments. These problems included decreased water availability, the sparsity of nutrients, and increased ultraviolet radiation levels. The shared ancestor of extant land plants evolved several strategies to surmount these stressors. For example, arbuscular mycorrhizal fungi (AMF) and AMF-like interactions with fungal mutualists likely aided early land plants in acquiring water and nutrients (Bonfante and Genre, 2008; Pirozynski and Malloch, 1975; Read et al., 2000). Arbuscular mycorrhizae are controlled infections of plant roots by fungi of the Glomeromycotina (Parniske, 2008; Spatafora et al., 2016). The establishment of intracellular arbuscules within cortical root cells enables the fungus to provide the plant host with greater access to resources such as phosphate, nitrogen, potassium, and water in exchange for host photosynthates (Garcia et al., 2017; Parniske, 2008; Smith and Read, 2010).

Endomycorrhizal, AMF-like interactions occur in early-diverging plant lineages, including some liverworts. Moreover, fossil samples provide evidence for ancient AMF-like associations. Endophytic structures with a striking similarity to arbuscules are present in the Early Devonian fossil record of the Rhynie chert (Remy et al., 1994; Strullu-Derrien et al., 2014, 2015). Fossilized fungal spores with similar morphology to extant AMF have been found in the Ordovician (Redecker et al., 2000). The broad phylogenetic distribution of AMF and AMF-like host lineages among land plants and the available fossil evidence point towards establishing plant-fungal symbioses early in land plant evolution (Wang & Qiu, 2006). Mosses are one of the earliest diverging and most diverse lineages of extant land plants. Whereas numerous pathogenic, saprotrophic, and commensal fungal interactions have been described in mosses (Davey and Currah, 2006), no convincing evidence has been published to date for *bona fide* mutualistic interactions among mosses and AMF with the possible exception of *Takakia*, which is distantly related to other extant mosses (Newton *et al.*, 2000; Liu *et al.*, 2019). A few reports describing observations of AMF within moss samples (e.g., Rabatin, 1980; Carleton & Read, 1991) were likely due to misinterpretation of fungal growth present in senescent or dead plant tissues.

Perception and accommodation of AMF are achieved through a conserved signal transduction pathway in plants, often referred to as the “common symbiosis pathway” (Delaux et al., 2013; Oldroyd, 2013). AM fungi exude chitooligosaccharides and lipo-chitooligosaccharides (LCOs) into the rhizosphere. LysM-receptor-like kinases (RLKs) at the plasma membrane of plant cells directly bind to these chitin-derived molecules and are required for colonization (Maillet et al., 2011; Brohammer et al., 2012;

Fliegmann et al., 2013; Buendia et al., 2015; Sun et al., 2015). Activation of RLKs upon ligand binding ultimately leads to repetitive oscillations of calcium concentrations, often referred to as “calcium spikes”, in plant nuclei (Ané et al., 2004; Capoen et al., 2011). These oscillatory calcium signals are decoded by a calcium/calmodulin-dependent protein kinase (CCaMK, also known as DOESN’T MAKE INFECTIONS 3 or DMI3 in *Medicago truncatula*) (J. Levy et al. 2004; Miller et al., 2013). Activated CCaMK phosphorylates the transcription factor Interacting Protein of DMI3 (IPD3, also known as CYCLOPS in *Lotus japonicus*) at two serine residues required for infection (Chen et al., 2008; Horváth et al., 2011; Messinese et al., 2007; Singh et al., 2014). CCaMK and IPD3 initiate transcriptional cascades required for developmental reprogramming and AMF colonization by working in concert with numerous GRAS transcription factors (Gobbato et al., 2012; Xue et al., 2015). Endosymbiotic interactions with nitrogen-fixing rhizobial bacteria arose roughly 90 million years ago in select land plant lineages, most notably the “nitrogen-fixing clade” of the Rosids (Doyle, 2011). Similar to AMF, rhizobia communicate with their host-plant in the rhizosphere through LCO exudates. Indeed, many of the core symbiosis signaling components are also required for rhizobial colonization of legume roots and nitrogen fixation (Venkateshwaran et al., 2013).

Nearly all AMF-host plants that have been studied possess the full complement of this core signaling pathway, from angiosperms to liverworts (Delaux et al., 2015; Wang et al., 2010). In several instances, plant lineages that have lost the ability to host AMF have also lost several symbiosis pathway genes. This correlation is exemplified by the Brassicaceae in which many species, including the model plant *Arabidopsis thaliana* (Figure 1A, Supplemental Table 1), are unable to host AMF and have concomitantly lost

many of the core common signaling components (Delaux et al., 2014; Garcia et al., 2015). The retention of symbiosis signaling genes in non-mycorrhizal mosses, including the model organism *Physcomitrium patens* (Physcomitrium), provides a striking counter-example (Delaux et al., 2015; Wang et al., 2010). Given that mosses have retained the vertically inherited symbiosis signaling pathway yet cannot form AMF or AMF-like interactions, we pursued an investigation of the biochemical properties and physiological function(s) of these proteins in mosses using Physcomitrium as a model.

CCaMK and *IPD3* are two of the genes whose presence or absence most strongly correlates with AMF host compatibility or incompatibility, respectively, in studied plant lineages (Delaux et al., 2014; Garcia et al., 2015; Wang et al., 2010). Moreover, genetic studies in legumes have elucidated mutational strategies to produce gain-of-function variants of either of these two proteins that can auto-activate root nodule development in the absence of symbionts or symbiont-derived signals, a phenomenon termed spontaneous nodulation. Expression of a constitutively active CCaMK, lacking the C-terminal autoinhibitory domain, in *Medicago truncatula* (Medicago) or *Lotus japonicus* (Lotus) is sufficient to cause the development of root nodules in the absence of rhizobia or rhizobial exudates (Gleason et al., 2006; Tirichine et al., 2006). Spontaneous nodule development can also be achieved by substituting an aspartate for a threonine residue in the kinase auto-activation loop of Medicago CCaMK. In Lotus, nuclear-localized and constitutively active CCaMK induced the partial development of the pre-penetration apparatus, a structure that facilitates hyphal entry of AMF into host roots (Genre et al., 2008; Takeda et al., 2012). A pair of phosphomimetic substitutions in the IPD3 ortholog, CYCLOPS, in Lotus is likewise sufficient to induce the

development of root nodules (Singh et al., 2014). These legume gain-of-function mutants revealed the pivotal role of the CCaMK-IPD3 module in this signaling pathway. We hypothesized that similar molecular genetic manipulations in Physcomitrium might lead to phenotypes that could provide clues to the possible biological relevance of these genes in mosses.

In this study, we investigated the evolutionary conservation, biochemical activities, and physiological function(s) of the two CCaMK and sole IPD3 homologs present in the Physcomitrium genome. We cloned the coding sequence of each homolog from cDNA. We used yeast two-hybrid and biochemical assays to demonstrate that one of two CCaMKs and the sole IPD3 homolog from Physcomitrium have retained many of the biochemical properties required for CCaMK and IPD3 functionality in angiosperms. We further demonstrated that the Physcomitrium CCaMK, which shared biochemical properties with angiosperm CCaMKs, could restore both nodulation and mycorrhization when expressed in a Medicago *ccamk-1* mutant background defective for both symbioses. Additionally, Physcomitrium IPD3 is capable of partially restoring nodulation defects in Medicago *ipd3-1* mutants. Transgenic expression of modified forms of CCaMK and IPD3 predicted to show constitutive activation in Physcomitrium (but not the unmodified forms driven by the same promoter) promoted ectopic development of brood cells, a well-characterized developmental program of mosses in response to drought or osmotic stress. Brood cell development was accompanied by changes in abiotic stress-responsive *LEA* gene transcript levels and elevated amounts of abscisic acid (ABA). Whereas activation of PpCCaMK or PpIPD3 promoted brood cell development, genetic deletion of either the *CCaMK* or *IPD3* loci from Physcomitrium

was insufficient to block brood cell development in response to osmotic stress treatment, suggesting other pathways exist for activation of brood cell development. Our results collectively indicate that the Physcomitrium CCaMK-IPD3 signaling module has retained many of the biochemical properties that typify these components in symbiont host plants and that the CCaMK-IPD3 module regulates ABA levels and associated developmental reprogramming to promote escape from adverse environmental conditions.

2.3 – Results

Conservation of the CCaMK-IPD3 Signaling Module in Physcomitrium

Homologs of CCaMK encoded in the *Physcomitrium patens* genome sequence version 3.3 were identified by BLAST (Altschul *et al.*, 1990) of the predicted proteome using Medicago CCaMK/DMI3 (MtCCaMK, Medtr8g043970) and Lotus CCaMK (LjCCaMK, Lj3g3v1739280) as queries. The top five hits were used for reciprocal BLAST against the predicted Medicago or Lotus proteomes (**Supplemental Figure 1A, B**). The two most significant BLAST hits in Physcomitrium, *Pp3c21_15330* (E-value = 0, hereafter PpCCaMK) and *Pp3c19_20580* ($E = 6 \times 10^{-171}$, hereafter PpCCaMKb), each returned MtCCaMK or LjCCaMK as the top reciprocal BLAST hit with highly significant E-values ($E \leq 6 \times 10^{-176}$). The top reciprocal BLAST hits for other loci were identified as calcium-dependent protein kinases (CDPKs), which lack the distinctive CaM-binding site found in CCaMKs. Thus, it appears that up to two loci in the Physcomitrium genome may encode functional CCaMKs. Full-length coding sequences (CDS) were cloned from each locus to validate inferred gene models. Amino acid sequences were aligned using MUSCLE (Edgar, 2004), and the resulting sequence alignment corroborated that the

protein kinase domain, auto-activation loop, predicted CaM-binding site, and three calcium-binding EF-hand domains were each conserved in candidate PpCCaMKs (**Supplemental Figure 1C**). Closer inspection of the auto-activation loop, which is required for MtCCaMK function, revealed that PpCCaMK and PpCCaMKb each have a serine residue at the position orthologous to the auto-phosphorylated threonine residue (T271) in MtCCaMK (**Figure 1B**), which suggests that PpCCaMK and/or PpCCaMKb may likewise be subject to regulatory autophosphorylation.

To identify potential IPD3 homologs encoded in the Physcomitrium genome, we employed a similar strategy. The protein sequences of Medicago IPD3 (MtIPD3, Medtr5g026850) or Lotus IPD3/CYCLOPS (LjIPD3, Lj2g3v1549600) were used as queries; and, in each search, only a single locus (*Pp3c23_22500V3*) yielded a significant E-value ($E = 1 \times 10^{-21}$ or $E = 1 \times 10^{-22}$, respectively). Results of reciprocal BLAST searches of the predicted proteomes of Medicago or Lotus corroborated that *Pp3c23_22500V3* is the sole Physcomitrium locus encoding an IPD3 homolog ($E < 1 \times 10^{-16}$, **Supplemental Figure 2A, B**). Cloning and sequencing of Physcomitrium *IPD3* from total gametophyte RNA revealed that the most abundant transcript spliceform was annotated as *Pp3c23_22500V3.2* (or *Pp3c23_22500V3.5*, which differ only in untranslated regions). The inferred full-length PpIPD3 protein sequence was aligned to MtIPD3, LjIPD3, and a recently identified paralog of MtIPD3 from Medicago named IPD3L (Jin *et al.*, 2018). The multiple sequence alignment revealed that each of the functionally important regions described for Medicago or Lotus IPD3, including CCaMK-targeted phospho-motifs and a C-terminal coiled-coil domain, are also present in PpIPD3 (**Supplemental Figure 2C**). In particular, two sequence motifs surrounding

CCaMK-targeted phosphosites necessary and sufficient for activation of LjIPD3 are strongly conserved in PpIPD3 (**Figure 1C**), suggesting that CCaMK-mediated phosphoregulation of IPD3 may be conserved in Physcomitrium.

If the identified CCaMK and IPD3 homologs constitute a functional signaling module in Physcomitrium, then the respective genes should be co-expressed in the same cell types. To determine and compare the relative expression patterns of *PpCCaMK*, *PpCCaMKb*, and *PpIPD3*, we mined their expression profiles from two Physcomitrium transcriptome atlas studies (Frank and Scanlon, 2015; Ortiz-Ramírez et al., 2016). Data from both studies confirmed that *PpCCaMK*, *PpCCaMKb*, and *PpIPD3* show strongly overlapping expression patterns. Each is expressed in protonema, which we had expected based on our ability to clone each CDS from protonemal cDNA. Moreover, *PpCCaMK* showed greater transcript abundance than *PpCCaMKb* in all tested tissues (**Supplemental Figure 3**). Physical interaction between CCaMK and IPD3 has been demonstrated in multiple legume models (Messinese et al., 2007; Yano et al., 2008). We tested whether PpCCaMK or PpCCaMKb could interact with PpIPD3 in yeast two-hybrid (Y2H) assays. PpIPD3 was fused to the GAL4 split-transcription factor activation domain (AD) and tested in pairwise combination with PpCCaMK or PpCCaMKb fused to the GAL4 DNA-binding domain (BD). Co-transformation of PpIPD3-AD with PpCCaMK-BD caused robust growth on selective media, indicative of strong interaction. However, no growth or evidence for interaction was detected between PpIPD3-AD and PpCCaMKb-BD (**Figure 1D**). The lower expression levels of *PpCCaMKb* compared to *PpCCaMK*, along with the apparent inability of its gene

product to bind PpIPD3, suggest that *PpCCaMKb* may encode a non-functional protein or function in a different context.

Legume CCaMKs have been characterized biochemically, and their autophosphorylation activity is known to be stimulated by elevated levels of calcium and inhibited by calmodulin (CaM) in the presence of high calcium levels (e.g., *Miller et al.*, 2013). Based on the conservation of the autoactivation loop shown in Figure 1B, we predicted that PpCCaMK and/or PpCCaMKb would lead to similar activities *in vitro*. To test if either Physcomitrium CCaMK homolog showed calcium/CaM-dependent protein kinase activity, we purified recombinant PpCCaMK and PpCCaMKb, along with positive and negative controls, and assayed autophosphorylation activity using radiolabeled adenosine triphosphate. Autophosphorylation of purified PpCCaMK was detectable and enhanced in buffer containing free calcium ions compared to the EGTA control (**Figure 1E**). The autophosphorylation of PpCCaMK was attenuated in the presence of calcium and calmodulin, as described for Medicago CCaMK (Miller et al., 2013). No detectable kinase activity was observed for PpCCaMKb under the same conditions. These results demonstrated that PpCCaMK has retained similar calcium- and calmodulin-regulated kinase activity and suggested that PpCCaMKb may not be enzymatically active. To further assess whether PpCCaMK and/or PpCCaMKb are *bona fide* CCaMKs, we tested whether either could bind calmodulin (CaM) *in vitro*. Biotin-labeled CaM was applied to immobilized recombinant PpCCaMK and PpCCaMKb and detected by chemiluminescence to check for binding (**Figure 1F**). PpCCaMK showed similar CaM-binding activity levels to MtCCaMK, the positive control; however, PpCCaMKb showed nearly undetectable CaM-binding activity under the same conditions. Thus, consistent

with gene expression and Y2H data, biochemical data supported a model wherein PpCCaMK, but not PpCCaMKb, comprises a functional signaling module with PpIPD3. Given the presence of this symbiosis signaling module in Physcomitrium, co-culture of wild-type moss with the model mycorrhizal fungus *Rhizophagus irregularis* was attempted. Still, no evidence of intracellular infection was obtained after six months of co-culture (**Supplemental Figure 4**), consistent with the prevailing interpretation that Physcomitrium is not an AMF host plant.

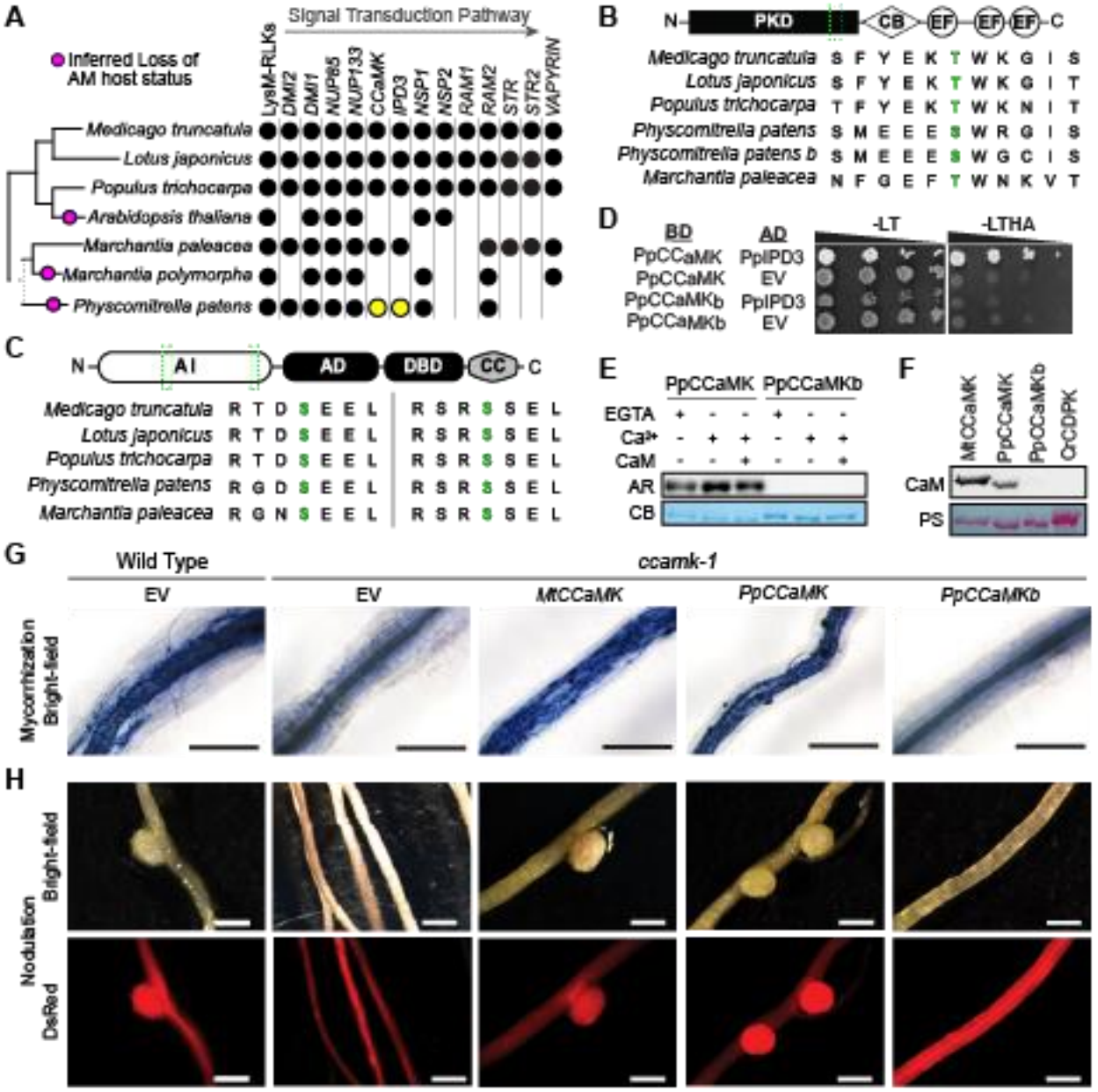

<u>Figure 1:</u> Functional conservation of CCaMK and IPD3 in Physcomitrium.
(**A**) Species cladogram (left) showing the presence or absence of symbiotic signaling genes in corresponding lineages (right). Physcomitrium *CCaMK* and *IPD3* are highlighted in yellow. See **Supplemental Table 1** for details. (**B**) Domain architecture diagram of CCaMK and multiple sequence alignment of the region (green) surrounding the regulatory autophosphorylation site (green). CB: CaM-binding domain, PKD: protein-kinase domain, EF: EF-hand. (**C**) Domain architecture diagram of IPD3 and multiple sequence alignments of regions (green) surrounding two regulatory phospho-sites (green) that are necessary and sufficient for activation of LjIPD3/CYCLOPS. AI: autoinhibitory domain, AD: activation domain, DBD: DNA-binding domain, CC: coiled-coil. (**D**) PpCCaMK interacted with PpIPD3 in yeast two-hybrid assay, whereas

PpCCaMKb or empty vector (EV) controls did not. The left panel shows growth on control (-LT) media; the right panel shows growth on the test (-LTHA) media to screen for physical interactions. AD: activating-domain, BD: DNA-binding-domain. (**E**) Kinase assays using purified recombinant proteins showed that PpCCaMK but not PpCCaMKb exhibited kinase activity and that kinase activity is responsive to calcium (Ca^{2+}) and CaM. AR: autoradiogram, CB: Coomassie Brilliant Blue stain. (**F**) Calmodulin-binding assays show that PpCCaMK or positive control (MtCCaMK) binds calmodulin, whereas PpCCaMKb or negative control from *Chlamydomonas reinhardtii* (CrCDPK) does not. PS: Ponceau S staining (**G**) *PpCCaMK* rescues the arbuscular mycorrhizal defects of the *Medicago truncatula ccamk-1* mutant. Roots transformed with *MtCCaMK* or *PpCCaMK* developed intracellular hyphae, arbuscules, and vesicles after inoculation with *Rhizophagus irregularis*. (**H**) *PpCCaMK* rescues the nodulation defects of the *Medicago truncatula ccamk-1* mutant. Roots transformed with *MtCCaMK* or *PpCCaMK* developed root nodules after inoculation with *Sinorhizobium meliloti*.
Black scale bars = 500 µm. White scale bars = 2 mm.

Heterologous expression of synthetically activated PpCCaMK stimulates symbiotic signaling in *Medicago.*

Deleting the C-terminal autoinhibitory domains in Medicago or Lotus CCaMK leads to autoactivation of the common symbiosis pathway and spontaneous nodule formation (Gleason et al., 2006). We investigated whether an equivalent deletion of the *PpCCaMK* C-terminus could promote spontaneous activation of the common symbiosis pathway by heterologous expression of native or modified PpCCaMK in Medicago roots. *M. truncatula* plants carrying the *pENOD11::GUS* reporter were transformed with constructs expressing *MtCCaMK*, *PpCCaMK*, or just the kinase domain of these proteins (*MtCCaMK*^{K} and *PpCCaMK*^{K}, respectively). Plants transformed with a vector control either treated or untreated with *S. meliloti* LCOs were used as positive and negative controls, respectively. Roots expressing *MtCCaMK* and *PpCCaMK* did not exhibit any detectable *ENOD11* expression (**Supplemental Figure 5A**). In contrast, roots expressing *MtCCaMK*^{K} and *PpCCaMK*^{K} not only expressed *ENOD11* strongly but also carried spontaneous nodules (**Supplemental Figure 5B**), indicating that

PpCCaMK is functionally capable of activating the symbiosis signaling pathway in Medicago.

Complementation of symbiosis-defective phenotypes of Medicago *ccamk* loss-of-function mutants by heterologous expression of *PpCCaMK*

To further interrogate the functionality of PpCCaMK or PpCCaMKb *in vivo*, within the functional context of the symbiotic signaling pathway, we tested their ability to rescue the symbiotic phenotypes of Medicago *ccamk-1* mutants, which are defective for both nodulation and mycorrhization. 'Hairy root' genetic transformations mediated by *Agrobacterium rhizogenes* were used to introduce expression vectors containing the CDS from *MtCCaMK* (positive control), *PpCCaMK*, *PpCCaMKb*, or the empty vector (EV) negative control into roots of Medicago *ccamk-1* plants. A red fluorescent protein (RFP) visual marker was used to confirm that transformations were successful. To test for AMF colonization, transformed roots were inoculated with *Rhizophagus irregularis* and grown in co-culture for six weeks. Trypan blue staining was used to visualize arbuscules and revealed that roots transformed with vectors containing PpCCaMK or MtCCaMK formed arbuscules indicative of colonization. In contrast, roots transformed with PpCCaMKb or the EV did not show any instances of arbuscule formation (**Figure 1G**). To test for the ability to nodulate, transformed roots were inoculated with *Sinorhizobium meliloti* and co-cultured for two weeks. Whereas roots transformed with the EV or *PpCCaMKb* did not form any nodules, roots transformed with *PpCCaMK* formed nodules similarly to roots transformed with *MtCCaMK* (**Figure 1H**). These data corroborate the conservation of key functional features of CCaMK between legumes

and mosses and demonstrate that PpCCaMK can decode symbiotic signals when expressed heterologously in legumes.

Partial rescue of symbiosis-defective phenotypes of Medicago *ipd3* loss-of-function mutants through complementation with *PpIPD3*

To determine the extent to which *PpIPD3* can functionally substitute for *MtIPD3*, we assessed the ability of heterologously expressed *PpIPD3* to rescue the symbiotic defects of the *M. truncatula ipd3-1* mutant. Roots of the *ipd3-1* mutant were transformed with vectors driving transgenic expression of *MtIPD3* or *PpIPD3* or with an empty vector (EV) for a negative control. Roots of wild-type plants transformed with the empty vector were used as a positive control. All constructs also contained a tdTomato fluorescent reporter for the confirmation of transformation. In each case, roots were inoculated with the *Sinorhizobium meliloti* multi-reporter strain CL304 expressing a construct carrying both *hemA::lacZ* and *PnifH::GUS* (Lang et al., 2018). As expected, based on the findings of Horváth et al. (2011), roots of the *Mtipd3-1* mutants transformed with the EV control developed nodules, however, few nodules were infected by rhizobia, and none of these nodules showed detectable expression of *nifH*, in contrast to wild-type plants transformed with the same EV. Nodules produced on the *Mtipd3-1* mutants transformed with *MtIPD3* were similar to those on wild-type plants transformed with the EV, indicating a rescue of the symbiotic phenotype (**Supplemental Figure 6**). In contrast, the transformation of the *Mtipd3-1* mutant roots with *PpIPD3* only partially rescued the symbiotic defects with many colonized nodules observed, but none containing rhizobia showing expression of *nifH* (**Supplemental Figure 6**). These findings indicate that

PpIPD3 contains some of the molecular features necessary for coordinating nodule infection but not necessarily for establishing mutually beneficial symbiosis.

Developmental reprogramming and brood cell formation associated with synthetic activation of CCaMK-IPD3 in Physcomitrium

Previous studies in legumes have shown that mutated forms of CCaMK or IPD3 are sufficient to cause striking gain-of-function phenotypes: the development of nodules or the pre-penetration apparatus in the absence of rhizobial or mycorrhizal symbionts (Gleason et al., 2006; Singh et al., 2014; Takeda et al., 2012; Tirichine et al., 2006). We introduced equivalent amino acid substitutions or deletions into PpCCaMK or PpIPD3 to engineer predicted gain-of-function variants. Native or modified forms (hereafter referred to as PpCCaMK^{K}, PpCCaMK^{D}, and PpIPD3^{DD}) were transgenically expressed in *Physcomitrium* under the control of a maize ubiquitin (ZmUBI1) promoter (**Supplemental Table 2**). Expression of unmodified PpIPD3 in this manner did not cause any noticeable effects on the development or morphology of protonemata or gametophores under standard axenic growth conditions, as these lines closely resembled wild-type *Physcomitrium* or empty vector (EV) controls (**Figure 2A, B, Supplemental Figure 7A**). Under identical conditions, lines expressing the predicted constitutively active variant, PpIPD3^{DD}, driven by the same promoter, developed branched chains of slowly growing, nearly isodiametric cells with dense chloroplasts and prominent cell wall thickenings (**Figure 2C**, **Supplemental Figure 7B, C**). These features are diagnostic of brood cells, which are stress-resistant asexual propagules found in mosses (Correns, 1899; Duckett and Ligrone, 1992; Pressel and Duckett, 2010; Schnepf and Reinhard, 1997). Lines expressing PpIPD3^{DD} failed to form normal

chloronema or caulonema and did not develop gametophores (**Supplemental Figure 7D**). Transformants expressing unmodified PpCCaMK displayed typical protonemal morphology and were able to develop gametophores, albeit with reduced frequency and size (**Figure 2D**). Brood cell formation was not observed in lines expressing unmodified PpCCaMK under standard growth conditions. Transformants expressing a phosphomimetic variant, PpCCaMK^{D}, developed mixed populations of phenotypically normal protonema and brood cells under standard growth conditions (**Figure 2E**, **Supplemental Figure 7E**). Gametophores were rarely observed and, if present, were stunted and malformed (**Supplemental Figure 7F**). Lines expressing PpCCaMK^{K} showed similar but more severe phenotypes as compared to PpCCaMK^{D} expressing lines, with frequent brood cell development and scarce instances of gametophore formation (**Figure 2F**). Quantitative analysis of protonemal cell dimensions revealed highly statistically significant differences in cell length and width for lines expressing gain-of-function forms of PpCCaMK or PpIPD3 compared to untransformed lines or lines expressing the native form of PpCCaMK or PpIPD3 (**Supplemental Figure 8**). Expression of native IPD3 or gain-of-function PpIPD3^{DD} tagged with Green Fluorescent Protein (GFP) using the same vector demonstrated that protein product is present in either case, retains preferential localization to nucleus, and does not form aggregates or show other obvious signs of gross overexpression (**Supplemental Figure 9**). The developmental phenotypes that we observed in CCaMK and IPD3 gain-of-function lines, particularly the constitutive development of brood cells, which generally only occurs in response to stress, led us to hypothesize that the Physcomitrium CCaMK-IPD3 module

functions in developmental reprogramming to mediate resistance to or escape from stress conditions.

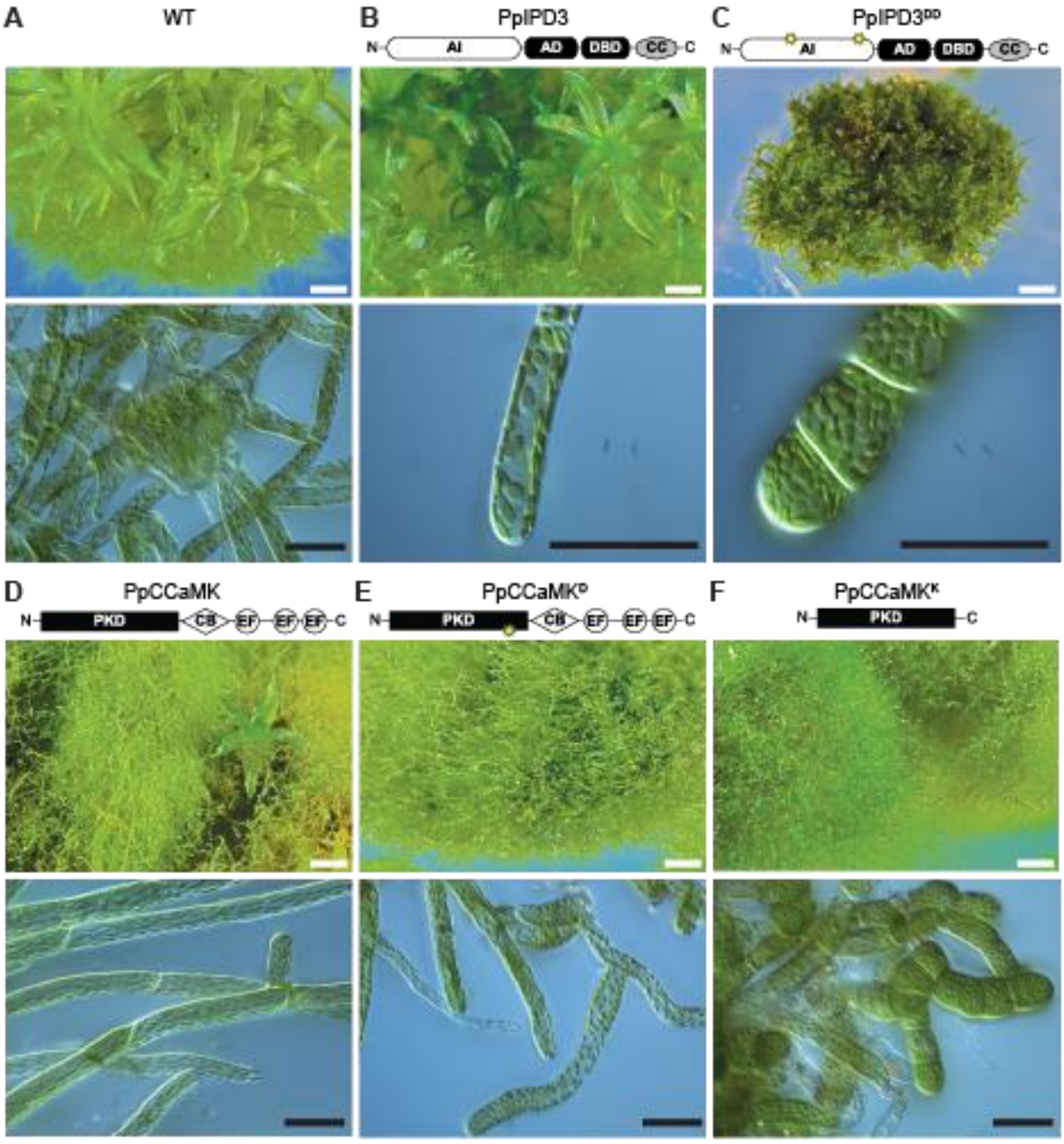

<u>Figure 2:</u> Ectopic development of brood cells in Physcomitrium expressing synthetically activated, engineered forms of PpCCaMK or PpIPD3.

(**A**) Example of protonema and gametophores in wild-type Physcomitrium under standard *in vitro* growth conditions. (**B**) Lines transformed with unmodified PpIPD3 driven by a *Zea mays UBIQUITIN1* (ZmUBI1) promoter did not display abnormal gametophore or protonemal morphology. (**C**) Lines transformed with a modified *PpIPD3* (*PpIPD3*^{DD}) carrying two phosphomimetic substitutions in the autoinhibitory domain, driven by the same promoter, constitutively formed brood cells and failed to develop gametophores. (**D**) Lines transformed with the native form of *PpCCaMK* developed excess protonema and fewer gametophores compared to WT controls, but protonemal morphology was not strongly affected. (**E**) Lines transformed with a modified *PpCCaMK* containing a phosphomimetic substitution in the regulatory domain (*PpCCaMK*^{D}) typically did not develop any gametophores, and gametophores that did develop were stunted (see **Supplemental Figure 7B**). Brood cells were commonly found among protonema under unstressed conditions (see **Supplemental Figure 7B-C**) (**F**) Lines transformed with a modified *PpCCaMK* with the C-terminal regulatory region deleted (*PpCCaMK*^{K}) constitutively developed brood cells under standard growth conditions. Constructs were driven by the same promoter. Samples were grown in BCDAT medium under the same conditions. Images are representatives of 4-week- (top) or 2-week-old (bottom) subcultured lines. White scale bars = 500 µm. Black scale bars = 50 µm.

Elevated levels of ABA and *LATE EMBRYOGENESIS ABUNDANT* transcripts in Physcomitrium expressing synthetically activated forms of CCaMK or IPD3

The stress-associated phytohormone abscisic acid (ABA) has long been linked to the induction of brood cells (Bopp, 2000; Schnepf and Reinhard, 1997). As expected, treatment of wild-type protonema with ABA phenocopied the gain-of-function effects of PpCCaMK^{K} or PpIPD3^{DD} and stimulated the development of brood cells (**Figure 3A**). Quantitative RT-PCR was used to test whether stress-associated, ABA-inducible marker genes were likewise upregulated in CCaMK-IPD3 gain-of-function lines. We selected two previously described marker genes, *LEA3-1* and *LEA3-2*, which encode LATE EMBRYOGENESIS ABUNDANT (LEA) proteins (Shinde et al., 2012, 2013) and confirmed that transcript levels were elevated in wild-type protonemata treated with exogenously supplied ABA (**Figure 3B**). Initially characterized in seeds, LEA proteins serve as osmoprotective molecules and are thought to confer abiotic stress resistance in brood cells, thereby enhancing their dispersal ability (**Figure 3C**). Transgenic lines

that constitutively form brood cells accumulated elevated levels of *LEA3-1* and *LEA3-2* under standard growth conditions (i.e., in the absence of any stress agent) relative to wild type (**Figure 3D**). Transcript levels were more abundant in gain-of-function lines compared to lines expressing unmodified PpCCaMK or PpIPD3. For example, expression of PpCCaMK^{K} was associated with significantly higher levels of *LEA3-1* transcript compared to lines expressing native PpCCaMK from the same promoter ($p < .05$). As observed for developmental phenotypes, expression of PpIPD3^{DD} had the most substantial effect on *LEA* transcript abundance, and the accumulation of *LEA3-1* and *LEA3-2* transcripts was significantly higher in lines expressing PpIPD3^{DD} compared to lines expressing PpIPD3 ($p < .01$), providing further evidence for a functional link between activation of the Physcomitrium CCaMK-IPD3 module and ABA signaling.

The observed phenotypic similarities between ABA-treated wild-type Physcomitrium and PpCCaMK-IPD3 gain-of-function lines may, in theory, be caused by an increase in ABA accumulation, an increase in ABA sensitivity, activation of a different pathway with similar effects, or a combination of these scenarios. To further investigate the mechanism whereby the CCaMK-IPD3 module elicited these responses, we quantified ABA levels in tissues overexpressing IPD3^{DD} compared to wild type by ELISA (enzyme-linked immunosorbent assays). Three independently transformed lines were analyzed. All three IPD3^{DD} lines contained significantly higher ABA levels than wild type (**Figure 3E**), suggesting that the ABA-like responses we observed are likely due, at least in part, to increased ABA accumulation.

<u>Figure 3:</u> Phenotypic comparison of Physcomitrium CCaMK-IPD3 gain-of-function lines to ABA-treated WT protonema.

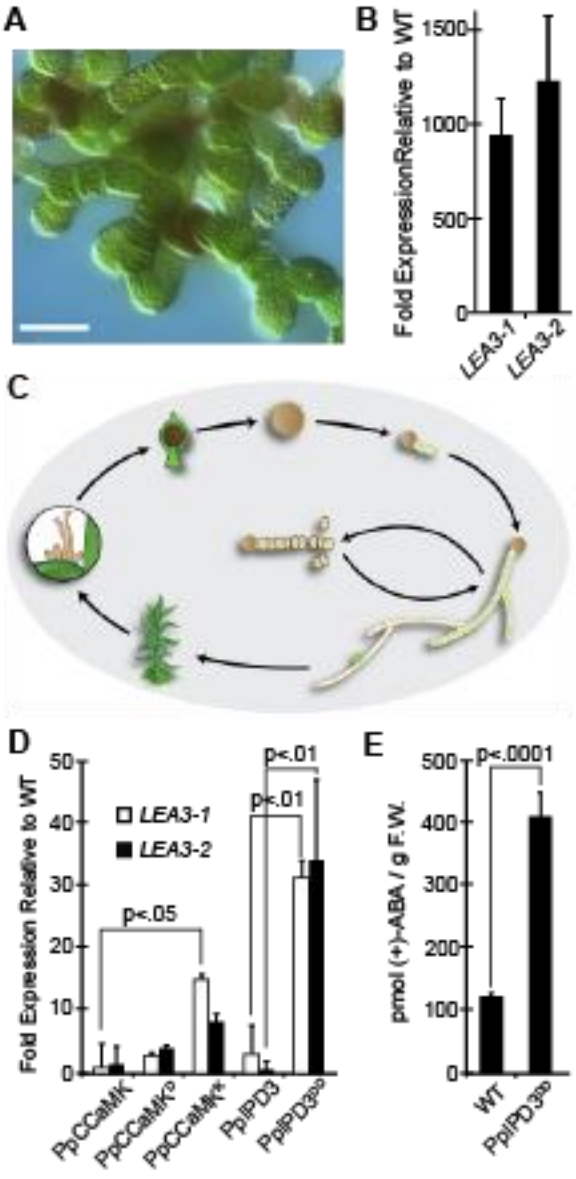

(**A**) WT protonema developed brood cells under unstressed conditions in BCDAT growth medium within two weeks of treatment with 100 µM ABA. Scale bar = 50 µm. (**B**) Quantitative reverse transcription PCR (RT-qPCR) demonstrated that WT protonemal tissues treated with ABA contain elevated transcript levels for the ABA response marker genes *LEA3-1* and *LEA3-2*. Error bars indicate the standard error of the mean (SEM) among treatments. (**C**) Illustrated life cycle of Physcomitrium. Spores (top) germinate and give rise to chloronema, which give rise to caulonema and gametophores. Gametangia develop in leaf axils of gametophores, and motile sperm swim through the environment to achieve fertilization. The mature zygote forms a spore capsule. From germination until fertilization, the moss is dependent on locally available water. Under stress conditions (e.g., drought), brood cells serve as stress-resistant 'vegetative spores' that fragment to facilitate dispersal. Brood cells germinate upon relief from stress; the life cycle resumes with the development of chloronema. (**D**) RT-qPCR analyses indicated that activation of the CCaMK-IPD3 signaling module is associated with elevated transcript levels for the ABA response marker genes *LEA3-1* and *LEA3-2*. Error bars indicate SEM among biological replicates. Results were statistically evaluated using the Tukey honestly significant difference (HSD) test. The p-values that yielded statistical significance below a threshold of .05 are annotated. (**E**) Enzyme-linked immunosorbent assays (ELISAs) revealed substantially elevated levels of (+)-ABA in protonemal tissues of lines expressing PpIPD3^{DD} compared to wild-type controls under standard in vitro growth conditions. A minimum of two independently transformed lines were tested. Error bars indicate SEM among three biological replicates. The p-value was obtained using a two-sample Student's t-test.

Brood cell formation in Physcomitrium *ccamk* and *ipd3* loss-of-function mutants

To investigate if the CCaMK-IPD3 module is required to develop brood cells, we assayed responses to stress treatments in deletion lines lacking either the *CCaMK* or *IPD3* genomic locus. Each locus was deleted by homologous recombination with antibiotic selective markers. Disruption of the respective locus was confirmed by PCR genotyping using genomic DNA and by RT-PCR (**Supplemental Figure 10**). These lines displayed stereotypical protonemal and gametophore morphology when grown under standard conditions (**Figure 4A, B**). When treated with ABA or hyperosmotic media supplemented with mannitol, multiple independently generated *ccamk* and *ipd3* knockout lines responded similarly to wild-type controls by developing brood cells, which do not develop in wild-type moss under standard laboratory growth conditions (**Figure 4B**). These results suggest that, while sufficient to stimulate ABA accumulation and brood cell formation, the CCaMK-IPD3 module is not required for brood cell development in response to ABA or osmotic stress treatments. We did not observe any noticeable differences in levels of brood cell formation between mutant and wild-type on both treatments, indicating that genetic perturbation of the CCaMK-IPD3 module does not substantially alter the sensitivity of Physcomitrium to ABA. These data imply functional redundancy in stress-induced developmental programming. Our results are collectively consistent with the hypothesis that the CCaMK-IPD3 module operates in the context of a broader signaling network that mediates stress-responsive developmental reprogramming in Physcomitrium (**Figure 4C**).

Figure 4: Neither CCaMK nor IPD3 is required for brood cell formation under ABA treatment or osmotic stress conditions.

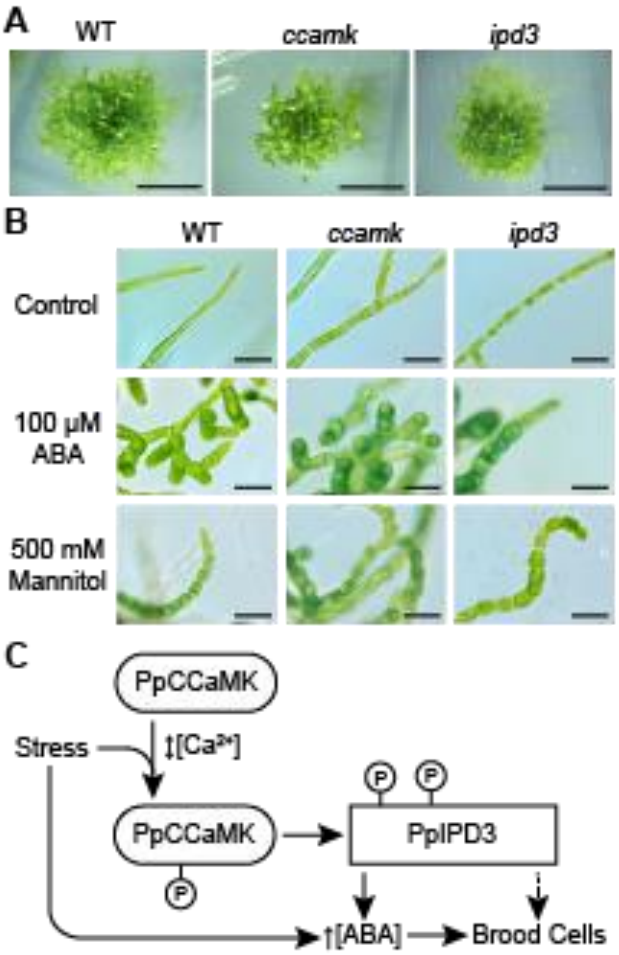

(**A**) Physcomitrium *ccamk* and *ipd3* deletion mutants did not show any obvious phenotypic aberrations relative to WT under standard *in vitro* growth conditions in the BCDAT medium. Scale bar = 500 mm (**B**) Physcomitrium *ccamk* and *ipd3* deletion mutants were able to develop brood cells when 100 µM ABA was added to BCDAT medium under standard growth conditions or when hyperosmotic stress was applied by addition of 500 mM mannitol to the growth medium. Treatments were performed for two weeks before images were taken. Two independently generated deletion mutant lines each were tested for *IPD3* and *CCaMK*. Scale bar = 50 µm. (**C**) Diagram showing a hypothetical model for PpCCaMK-IPD3 function during stress signaling in relation to ABA accumulation and brood cell formation. In this model, stress conditions provoke changes in nucleocytoplasmic Ca^{2+} levels, leading to activation of PpCCaMK. Trans-phosphorylation of PpIPD3 renders it active and leads to elevated levels of ABA and the development of brood cells. The ability of *ccamk* and *ipd3* deletion lines to develop brood cells in response to tested stress treatments indicates that there are likely other pathways that trigger stress-induced ABA accumulation. The dotted line indicates uncertainty whether or not PpIPD3 acts exclusively through ABA signaling to promote brood cell development.

2.4 – Methods

Bioinformatic analyses. To identify CCaMK and IPD3 homologs encoded in the Physcomitrium genome, the full-length protein sequences of CCaMK and IPD3 from *Lotus japonicus* (LjCCaMK, UniProt: A0AAR7, loci: Lj3g3v1739280; LjIPD3, UniProt: A9XMT3, locus ID: Lj2g3v1549600) and *Medicago truncatula* (MtCCaMK, UniProt: Q6RET7, locus ID: Medtr8g043970; MtIPD3, UniProt: A7TUE1, locus ID:

Medtr5g026850) were retrieved from UniProt and used as BLASTp queries against the predicted *Physcomitrium patens* version 3.3 predicted proteome (Lang *et al.*, 2018) using Phytozome 12 (https://phytozome.jgi.doe.gov/pz/portal.html). The BLOSUM62 scoring matrix was used. E-value thresholds were set to -1 for CCaMK searches and $1x10^{4}$ for IPD3 searches. Other parameters followed default settings. Data were downloaded and analyzed from December 11 to 17, 2019. The top five hits were used as queries for reciprocal BLASTp searches against either the *Lotus japonicus* MG20 v3.0 protein database (https://lotus.au.dk/blast/#database-protein) using default settings or the *Medicago truncatula* Mt4.0 predicted proteome, accessed through Phytozome 12 and performed using default settings (Tang *et al.*, 2014; Mun *et al.*, 2016). For each reciprocal BLASTp search, the top hit was displayed. Multiple sequence alignments were made using MUSCLE (Edgar, 2004) version 3.8.425 plugin for Geneious Prime under default settings and were annotated manually or using the InterProScan feature in Geneious Prime (Biomatters). Accession numbers for putative orthologs referred to in Figure 1A can be found in **Supplemental Table 1**.

***Biological material and growth conditions*.** For moss growth and phenotypic assays, *Physcomitrium patens*, ecotype Gransden 2004, was used (Rensing *et al.*, 2008). Tissue was grown on BCD medium supplemented with 5 mM diammonium tartrate (BCDAT medium), pH 6.0, supplemented with 0.8% high gel strength agar (Sigma) or 1% Phytoblend (Caisson Labs). The medium was supplemented with (+/-)-abscisic acid (Sigma) or mannitol, as indicated. Moss cultures were grown in a growth chamber at 22°C under 50-100 µmol m^{-2} s^{-1} light with a 16-hour photoperiod. *Medicago*

truncatula mutant-rescue assays were performed as previously described (Delaux *et al.*, 2015).

Medicago mutant rescue and symbiotic phenotype screening. *Medicago truncatula* mutant-rescue assays were performed as previously described but were instead inoculated with the *S. meliloti* multi reporter strain CL304 (Lang *et al.*, 2018) for *ipd3-1* rescues (Delaux *et al.*, 2015). Following nodulation, we stained the roots with X-Gluc and magenta-X-gal following procedures in Schiessl et al. (2019) without tissue prefixation. *pENOD11::GUS* plants expressing different variations of *CCaMK* were stained 3 weeks post-transformation with GUS staining solution as done in Radhakrishnan *et al.* (2020). As controls, *pENOD11::GUS* plants with transgenic roots expressing an EV control vector were either subject to a 24-hour treatment of 10^{-8} M LCOs from *S. meliloti* (GM16390) or left untreated before GUS staining.

Co-culture of Physcomitrium and Rhizophagus irregularis. Three-week-old gametophores were collected from cellophane-overlaid Knop agar plates. Gametophores were transferred to half-strength Knop semi-liquid medium (0.15% Phytagel) in 24-well plates. In each well, 2 ml of semi-liquid Knop medium was poured, and approximately 50 spores of *R. irregularis* lRBV'95 were added. One gametophore was placed gently over the medium such that the rhizoids were immersed within the semi-liquid medium. This experimental setup was incubated at 25°C with a light intensity of 55 µmol m^{-2} s^{-1}, with a 16hr photoperiod, for six months. Starting from one month after co-culturing, AMF colonization was analyzed every week for up to six months using bright-field or confocal microscopy. Trypan blue staining of *R. irregularis* was performed as described (Koske and Gemma, 1989). For confocal microscopy, the

fungal hyphae were stained using Wheat Germ Agglutinin Alexa Fluor® 488 (Excitation: 488 nm; Emission: 520 nm), and the rhizoids and the gametophores were observed by chlorophyll autofluorescence (Excitation: 488 nm, Emission: 670 nm).

Plant transformations. Biolistic transformation of Physcomitrium protonema was carried out as previously described (Kleist *et al.*, 2017). Briefly, purified plasmid DNA was precipitated onto 1 µm spherical gold particles (Seashell Technologies), following manufacturer recommendations. Particles were delivered to protonemal cultures grown on cellophane-overlaid solid BCDAT medium; parameters for bombardment were identical to Kleist *et al.* (2017). Bombarded cultures were moved onto BCDAT medium supplemented with Hygromycin B (Thermo Fisher) 50 µg/mL concentration. The pANIC5A vector, which contains a free *Porites porites* red fluorescent protein (RFP) driven by a separate promoter (Mann *et al.*, 2012), was used for each construct. Colonies that survived antibiotic selection were embedded in solid BCDAT medium supplemented with 50 µg/mL Hygromycin B (Thermo Fisher), and lines that showed RFP fluorescence were selected for characterization. Transgenic lines were maintained by transfer to fresh BCDAT medium supplemented with 50 µg/mL Hygromycin B (Thermo Fisher). Phenotypic analyses were performed using cultures grown in BCDAT medium without antibiotic. Retention of transgenes was verified by checking RFP fluorescence.

Protoplasts were obtained from one-week-old protonemal cultures using 2% Driselase (Sigma, D8037) in an 8% mannitol solution for cell wall digestion. Protoplast transformations to produce *ccamk* or *ipd3* deletion mutants were performed as previously with minor modifications (Hohe *et al.*, 2004). Briefly, an 8% mannitol solution

was made using 1/10 BCDAT medium set to pH 5.8 to improve protoplast survival. Antibiotic selection was performed using 50 µg/mL Hygromycin B or 40 µg/mL G418. For *ipd3* deletion lines, stable transformants were identified by RFP fluorescence using a Zeiss Lumar epifluorescence stereoscope. *Medicago truncatula* root transformations were carried out using *Agrobacterium rhizogenes* strain MSU440, harboring either the pK7FWG2 binary vector (Delaux *et al.,* 2015) or GoldenGate Level 2 binary vector pAGM4673 for *ipd3-1* rescue assays.

Molecular cloning and plasmid construction. DNA and RNA were extracted from protonemal tissue following previously described protocols (Kleist *et al.*, 2014). The Quantitect (Qiagen) reverse transcription kit was used to synthesize cDNA for cloning and qPCR. PCR reactions were performed using Phusion (Thermo Fisher) or Primestar GXL DNA Polymerase (Clontech). The sequences of oligonucleotide primers used in this study are given in **Supplemental Table 3**. Single- and multi-site Gateway (Thermo Fisher) cloning reactions were performed per the manufacturer's recommendations. The coding sequences (CDSs) of *PpCCaMK, PpCCaMKb,* and *PpIPD3* were cloned into pDONR/Zeo and modified, as described, by site-directed mutagenesis using whole-plasmid amplification with anticomplementary primers followed by digestion with FastDigest *Dpn*I (Thermo Fisher). Assembly PCR was used to attach an eGFP tag and a polyglycine linker to the N-terminus of IPD3 or IPD3^{DD}.

Native or modified CDSs were subcloned into pANIC5A for plant expression (Mann et al., 2012), pVP16 for N-terminal fusion to maltose-binding protein (MBP), pK7FWG2 for expression in *Medicago truncatula* roots, and pGBT9-BS-GW (*PpCCaMK* and *PpCCaMKb*) or pGAD-GH-GW (*PpIPD3*) for yeast two-hybrid assays. Multisite

Gateway recombination was used to generate the deletion construct for *IPD3*. Approximately one kilobase region located at the N-terminal or C-terminal end of the gene was cloned into pENTRY attB1-attB4 or attB3-attB2 vectors. *Porites* sp. red fluorescent protein (RFP), driven by a *Panicum virgatum UBIQUITIN* promoter (Mann *et al.*, 2012), was cloned into a pENTRY attB4r-attB5r vector. An antibiotic resistance construct containing the *NPTII* gene driven by a cauliflower mosaic virus 35S promoter was cloned into a pENTRY attB5-attB3r vector. The four fragments were assembled by LR reaction using LR clonase plus enzyme (Thermo Fisher) using a Gateway-compatible destination vector with attL1 and attL2 sites. After sequence confirmation, the linear deletion construct was amplified by PCR using Primestar GXL DNA Polymerase (Takara). The PCR product was purified and concentrated to 1 µg/µL using the PureLink PCR purification kit (Invitrogen).

As proper rescue of *ipd3-1* requires the correct expression pattern for *MtIPD3*, we amplified the 1,233 bp region upstream of the *MtIPD3* start codon (*MtIPD3* promoter) and 442 bp region downstream of the *MtIPD3* stop codon (*MtIPD3* terminator) from Medicago genomic DNA and cloned them into GoldenGate level 0 acceptor plasmids (Horváth *et al.*, 2011). For *ipd3-1* rescue experiments, the *MtIPD3* or *PpIPD3* coding sequences were then cloned into level 1 GoldenGate cloning vectors along with the *MtIPD3* promoter and terminator sequences. For gain-of-function *CCaMK* experiments, the coding sequences of *MtCCaMK*, *MtCCaMK*^{K}, *PpCCaMK*, and *PpCCaMK*^{K} were combined with a cauliflower mosaic virus 35S promoter and terminator into GoldenGate level 1 vectors. The *IPD3* and *CCaMK* GoldenGate level 1 variants were then cloned into separate GoldenGate level 2 vectors, containing a

tdTomato fluorescent reporter. All GoldenGate cloning reactions were performed following the procedures in Binder et al. (2014).

Yeast two-hybrid assays. The coding sequences of *PpCCaMK*, *PpCCaMKb*, and *PpIPD3* were subcloned into pGAD-GH-GW or pGBT9-GW for yeast two-hybrid analysis. Vectors were co-transformed into *Saccharomyces cerevisiae* strain AH109 using the lithium acetate method. Interactions were assayed by growth on synthetic defined media lacking leucine and tryptophan (-LT) or lacking leucine, tryptophan, histidine, and adenine (-LTHA, MP Biomedicals) at 30° C, as previously described (Kleist *et al.*, 2014).

Protein expression and purification. Maltose-binding protein (MBP) fused to PpCCaMK, PpCCaMKb, and CrCDPK1 fusion constructs were transformed into *E. coli* strain Rosetta2, whereas the MBP-MtCCaMK fusion construct was transformed into *E. coli* strain B834-pRARE2 for protein expression. Protein expression and purification were carried out as previously described (Delaux *et al.*, 2015).

Kinase activity and calmodulin-binding assays. Kinase assays were performed as previously described with slight modifications (Miller *et al.*, 2013). 1 µg of MBP-PpCCaMK or MBP-PpCCaMKb protein was incubated in ATP-containing buffer (50 mM HEPES, pH 7.5, 1 mM DTT, 200 µM ATP, 5 µCi [g-^{32}P]ATP, and 10 mM $MgCl_2$). 20 µL reactions were incubated at 30°C for five minutes with 0.2 mM $CaCl_2$ (+Ca^{2+}) or 2.5 mM EGTA (+EGTA). Where stated, 0.5 µM bovine Calmodulin (Millipore) was added. Reactions were terminated by incubation at 95°C for 5 min. Subsequently, samples were separated on 10% SDS-PAGE gels before imaging. Radioactivity was quantified by Molecular Dynamics Storm® 860 phosphorimager (Sunnyvale, CA), and

data were analyzed using the Molecular Dynamics ImageQuant® software. Calmodulin-binding assays using recombinant CCaMKs were performed similarly to previous reports (e.g., Routray *et al.*, 2013) with slight modifications. Bovine brain calmodulin (EMD Millipore) was biotinylated using the ECL Protein Biotinylation Module (GE Healthcare Life Sciences). Proteins were immobilized on a polyvinylidene difluoride (PVDF) membrane followed by incubation in Tris-buffered saline, 0.1% Tween 20 (TBS-T) supplemented with 1 mM $CaCl_2$ and 3 µg/mL biotinylated calmodulin for one hour. Subsequently, the membrane was incubated in TBS-T supplemented with 1 : 6,000 streptavidin-horseradish peroxidase conjugate (GE Healthcare Life Sciences) for 1 hour. Bound calmodulin was detected using ECL Prime (GE Healthcare Life Sciences).

Extraction and quantification of ABA. ABA extraction and quantitation was done was previously described with slight modifications (Ondzighi-Assoume *et al.*, 2016). For each sample, 100 mg of starting tissue was used. Tissue was lyophilized, ground using 3 mm glass beads, and then ABA extracted using the referenced methanol-based method. The resulting aqueous ABA extracts were then quantitated using the Phytodetek ABA ELISA assay (Agdia).

Quantitative RT-PCR. Total mRNA was extracted from abscisic acid (ABA)-treated and untreated wild-type samples, as well as from gain-of-function lines. 3 µg RNA samples were reverse transcribed using the Quantitect Reverse Transcription kit (Qiagen), per manufacturer's recommendations, and the resulting 60 µL cDNA samples were diluted by the addition of 90 µL nuclease-free water. The iTaq Universal SYBR Green Supermix (Bio-Rad) was used for qPCR reactions following the manufacturer's recommendations, and reactions were run on a DNA Engine Opticon™ continuous

fluorescence detector. Ubiquitin-conjugating enzyme E2 (Pp1s34_302V6) was used throughout as a reference gene (Le Bail *et al.*, 2013). After baseline subtraction, results were analyzed using the ΔΔC(t) method, wherein fold change is taken as 2^[(reference gene – query gene)$_{\text{transgenic/treated line}}$ – (reference gene – query gene)$_{\text{wildtype/untreated line}}$]. For each line, 3 to 4 biological replicates were used, with a minimum of 2 technical replicates (i.e., each qPCR run was performed multiple times). Statistical tests are described below.

Statistical analyses. For quantitative measurements of ABA content, 7 biological replicates were analyzed for wild-type, and 3 biological replicates of three independently transformed lines were analyzed for IPD3^{DD}. Every biological replicate was tested in triplicate for the ABA ELISA. Data were analyzed and tested using a Student's T-Test using the R statistical programming language (R Core Team, 2014). For RT-qPCR analyses, samples were compared via one-way ANOVA analysis using R (R Core Team, 2014). Levene's Test confirmed equality of variance for both sets of data (Levene, 1960). The Tukey honest significant difference (HSD) was used for posthoc analysis of ANOVA results (Tukey, 1949), and the p-values that were reported were calculated using this method. For *ipd3-1* rescue experiments, each treatment was compared for differences in total nodule number per root, the number of colonized nodules per root, and the number of nodules containing rhizobia expressing nifH per root using R (R Core Team, 2014). The sample size per treatment varied from 16 roots to 44 roots. Levene's test determined equal variance for total nodule number between samples, but not for either number of colonized nodules or number of nifH expressing nodules (Levene, 1960). We then performed an ANOVA for the total number of nodules

and Kruskal-Wallace tests for both the number of colonized nodules and nifH expressing nodules. Dunn's test with a Benjamini-Hockberg p-value adjustment was performed for post hoc analysis of the Kruskal-Wallace results.

Microscopy, photography, and image processing. Differential interference contrast (DIC) micrographs were acquired using a Zeiss AxioImager M1 microscope with a 40X, 1.4 numerical aperture (NA) or 100X, 1.3 NA objective and a QImaging 5 MPix MicroPublisher color camera or an Olympus BX60 microscope using a 20X, 0.5 NA and an Olympus DP 72 color camera. Macrophotography images were acquired using a Canon EOS 6D 20.2 Megapixel CMOS Digital SLR camera equipped with a Canon MP-E 65 mm f/2.8 1-5x macro lens and Canon MT-24EX macro twin-light flash. Manually acquired z-stacks were focus-stacked using Helicon Focus (HeliconSoft). A Zeiss AxioZoom.V16 equipped with Plan NeoFluar Y 1x / 0.25 NA objective and Axiocam 305 color camera (Zeiss) was used for cell dimension measurements. Samples were taken from edges of approximately month-old cultures grown under standard conditions, as described above. Three independently transformed lines were analyzed per construct. Measurements were performed manually in Zen Blue software version 2.6 (Zeiss). Graphs were generated, and statistical analyses were performed using Origin Pro 2020.

Confocal fluorescence microscopy was performed using a Leica TCS SP8 equipped with a resonant scanner and white light laser (WLL). Scan speed was set to 8000 Hertz. A 20x / 0.70 NA multi-immersion objective was used with glycerine. Fluorescence images were collected in three-step sequences on HyD SMD detectors. RFP was detected at 575-625 nanometers (nm), and chlorophyll was detected from

650-750 nm under WLL excitation at 561 nm with a notch filter 488/561/633. eGFP was detected at 500-550 nm under WLL excitation at 488 nm with notch filter 488, and transmitted light was detected with a PMT. Calcofluor white was detected at 415-465 nm under 405 nm excitation. Samples were stained with 10 mg / mL calcofluor white/fluorescent brightener 28 (Sigma, F3543) for 30 minutes with gentle agitation and rinsed twice with sterile water before imaging. Subcellular localization images shown are average z-stack projections and were prepared using FIJI (Schindelin *et al.*, 2012).

Physcomitrium stress assays. Freshly blended protonema from either wild-type or *ipd3-1* lines were plated onto cellophane-overlaid BCDAT medium plates, supplemented with ABA or mannitol, at concentrations indicated. Stress treatments were grown under standard temperature and photoperiod conditions unless stated otherwise.

2.5 – Discussion

Evolution of the CCaMK-IPD3 Signaling Module Across Land Plant Evolution. Many of the critical components of the symbiosis pathway were present in the algal ancestors of land plants, indicating that they have been vertically inherited across land plants (Delaux et al., 2015). Across evolutionary time, spanning from the divergence of bryophytes to the emergence of angiosperms, AMF-like interactions have remained morphologically similar (Remy et al., 1994; Strullu-Derrien et al., 2014). In light of plant comparative genomics of AMF-host versus non-host lineages, the symbiosis pathway in the earliest land plants likely contributed to the recognition and intracellular infection of AMF, as the presence/absence of the symbiosis pathway is strongly correlated with host/non-host status, respectively (Delaux, 2017; Delaux et al.,

2014; Garcia et al., 2015; Kamel et al., 2016). Among embryophytes, the moss clade is a striking exception to this genomic signature. To date, there has been no demonstration of the mutualistic transfer of nutrients between mosses and AMF. On the contrary, endophytic fungal interactions described in mosses have appeared restricted to dead or senescing tissues (Pressel et al., 2010). This peculiarity piqued our interest in the conserved components of the common symbiosis pathway in mosses.

In the present study, we investigated the functional reason for retaining the CCaMK-IPD3 signaling module in non-mycorrhizal mosses, which stands in stark contrast to multiple independent losses of these genes in non-mycorrhizal angiosperm and liverwort lineages. Biochemical and mutant-rescue assays demonstrate that the biochemical activities of CCaMK and IPD3 are conserved broadly throughout land plants, which suggests that CCaMK may decode similar oscillatory calcium signals in bryophytes. The biochemical similarity of Physcomitrium CCaMK to homologs in angiosperms is consistent with a previously published *in vitro* comparison (Okada et al., 2003). We used a gain-of-function strategy in Physcomitrium to shed light on the physiological consequences of CCaMK-IPD3 activation. The developmental phenotypes observed in Physcomitrium cells expressing CCaMK and IPD3 carrying predicted gain-of-function mutations imply a functional link between the CCaMK-IPD3 module and ABA signaling in mosses. The heterologous expression of native and engineered forms of PpCCaMK or IPD3 in Medicago roots corroborated the predicted effects of gain-of-function mutations and demonstrated partial functional conservation with Medicago homologs. The most striking finding in this study is the developmental phenotype of $IPD3^{DD}$-expressing Physcomitrium lines: $IPD3^{DD}$ transgenics displayed prolific, nearly

constitutive formation of brood cells, mainly to the exclusion of other cell types. The effect does not appear to be attributable to transcript or protein abundance, as controls transformed with the same vectors differing only by two codon changes to introduce phosphomimetic substitutions putatively. The observation that gain-of-function lines expressing modified forms of CCaMK showed a less severe phenotype than lines expressing modified forms of IPD3 might simply reflect a signaling bottleneck of natively expressed IPD3 upon the activities of expressed CCaMK. Comparative genomics across green plants have shown that core ABA signaling components are conserved in bryophytes (Wang et al., 2015). Although ABA biosynthesis and downstream signal transduction have been studied in the context of Physcomitrium protonemal development (Komatsu et al., 2013; Schnepf and Reinhard, 1997; Shinde et al., 2012; Takezawa et al., 2015; Vesty et al., 2016; Yotsui et al., 2013), our data provide the first link between CCaMK-IPD3 and ABA signaling in Physcomitrium.

Calcium Signaling in Physcomitrium Protonemata. We propose a model wherein calcium-dependent activation of CCaMK and trans-phosphorylation of IPD3 in Physcomitrium leads to ABA accumulation and brood cell formation. The rescue of Medicago *ccamk-1* mutants by *PpCCaMK* seemingly suggests that PpCCaMK may be activated by similar oscillatory calcium signals, as seen in legumes in response to symbionts. Additionally, the observed partial rescue of the Medicago *ipd3-1* mutant indicates partial conservation of function between PpIPD3 and MtIPD3, with PpIPD3 likely retaining the ability to be activated by CCaMK and stimulate expression of some (but not all) known downstream transcription factors. Whereas calcium oscillations in growing protonemal tips have been well documented (e.g., Bascom et al., 2018),

nuclear calcium oscillations and potential elicitors have not been described in Physcomitrium. Hyperosmotic stress has been shown to elicit a pronounced transient elevation of cytosolic calcium levels. However, this response was neither oscillatory nor predominantly restricted to the nuclear region (Kleist et al., 2017). Recently, Galotto et al. (2020) reported that chitin can elicit oscillatory calcium signals, although these oscillations appear to occur primarily in the cytosol. Given these discrepancies and the abundance of predicted calcium-binding proteins encoded in the Physcomitrium genome, further work is needed to identify factors involved in the coding and decoding stress-induced calcium signals. The regular elicitation and development of brood cells in Physcomitrium *ccamk* or *ipd3* deletion lines in response to ABA or osmotic stress implies the existence of other signaling components capable of triggering brood cell formation in response to abiotic stressors. In addition to identifying putatively functionally redundant signaling components, other interesting topics for future work include whether parallel pathways are calcium-dependent or -independent and whether ABA hyperaccumulation, which we observed, is required for the developmental phenotypes of CCaMK-IPD3 gain-of-function lines.

Physiological Function of Brood Cells. The established physiological function of brood cells is to serve as stress-resistant asexual propagules that break away from parent plants and enable mosses to escape osmotic stress and dehydration. For this reason, they have also been referred to as ‘vegetative spores.’ The phenotypes of Physcomitrium CCaMK and IPD3 gain-of-function lines suggest that these components may also be linked to osmotic stress and dehydration responses. Because osmotic stress and dehydration are closely related to oxidative stress, it is worth noting that

CCaMK has been associated with oxidative stress responses in other plants. CCaMK expression is induced by ABA or oxidative stress in rice; CCaMK was also required for ABA-mediated antioxidant responses (Shi et al., 2012, 2014). Similarly, CCaMK has been reported to be activated by nitric oxide and required for ABA-mediated antioxidant activity in maize (Ma et al., 2012; Yan et al., 2015). In wheat (*Triticum aestivum*), CCaMK expression is modulated by ABA and osmotic stress, likely through the activity of numerous predicted ABA-response elements in its promoter region (Yang et al., 2011). In light of these observations, the CCaMK-IPD3 may play a role in abiotic stress acclimation in Physcomitrium and other plants. This possibility may explain its retention in non-mycorrhizal mosses.

The cell wall thickenings, lipid reserves, and enhanced dispersal ability of brood cells could conceivably be useful in evading pathogenesis, although this idea is presently unsubstantiated. Fungal pathogens, as well as oomycetes, have been shown to induce reactive oxygen species (ROS) production, cell-wall depositions (including callose depositions mediated in part through ABA signaling), and altered fatty acid metabolism (Oliver et al., 2009; de León, 2011; de León et al., 2015). There are also mechanistic links between pathogen perception and the symbiosis pathway in angiosperms. In rice, chitin-receptor *cerk1* mutants were impaired in both mycorrhizal and blast fungus infections (Miyata et al., 2014), and CERK1 is conserved as a chitin-induced immunity signaling receptor in Physcomitrium, possibly hinting at a further link between the common symbiosis pathway and immunity signaling (Bressendorff et al., 2016). These observations may warrant further investigation into the possibility that

brood cells and the CCaMK-IPD3 pathway could also serve a heretofore unnoticed function in moss acclimation to biotic stresses.

Summary. In summary, the activation of CCaMK or its downstream target transcriptional activator IPD3 in Physcomitrium induces ABA signaling and the constitutive formation of brood cells, which serve as asexual propagules that enable escape from abiotic stresses. Our observations are consistent with a model wherein PpCCaMK-IPD3 functions to decode stress-associated calcium signatures and developmental reprogramming. Further work is needed to identify upstream elicitors that lead to CCaMK activation and direct transcriptional targets of IPD3 in Physcomitrium. Further studies will also be necessary to determine precisely at which point nitrogen fixation is blocked in *Mtipd3-1* mutants rescued with *PpIPD3* and which functional features in *MtIPD3* are required for the development of fully functional nodules. Functional inquiries into CCaMK and IPD3 homologs in other early-diverging embryophytes such as the mycorrhizal host plant *Marchantia paleacea* and charophyte green algae are expected to complement these efforts and provide a fuller perspective of the evolutionary establishment of the molecular mechanisms underpinning the plant-microbe common symbiosis pathway.

Limitations of the Study. Here, we have shown that synthetic activation of CCaMK or its target transcription factor triggers ABA-associated developmental reprogramming and formation of asexual propagules termed brood cells. Notably, *ccamk* or *ipd3* knockout mutants are still able to form brood cells in response to stress or ABA treatments, which would be consistent with parallel or alternative signaling

processes; future work should target these putative components. Further mechanistic insight may be gleaned by testing whether expression of synthetically activated forms of CCaMK or IPD3 is sufficient to trigger brood cell formation in Physcomitrium mutants defective for ABA biosynthesis (e.g., Takezawa et al., 2014). Lastly, future work should build upon available tools for calcium imaging in Physcomitrium (e.g., Kleist et al., 2017) and focus particularly on calcium dynamics in the nucleus and perinuclear region, which are known to govern CCaMK function in angiosperms.

2.6 – Acknowledgements

The authors would like to thank Tony Chour, Min Su Park, Mitch Wanta, and Cali Lunowa for technical assistance and Prof. Brett Mishler (University of California, Berkeley) for helpful discussions. Some of the microscopy was performed at the Newcomb Imaging Center, Department of Botany, University of Wisconsin – Madison, or at the Biological Imaging Facility at the University of California, Berkeley. This work was supported in part by grants from the NSF to S.L. (grant # MCB-0723931 and # ISO-1339239). T.J.K. was funded in part by the NSF Graduate Research Fellowship Program (grant # DGE-1106400). This work was supported in part by the Vilas Faculty Young/Mid-Career Award to J.M.A. AB was funded through an NIH Training Grant to the Laboratory of Genetics (grant # 5T32GM007133-40) and by the NSF Graduate Research Fellowship Program (grant # DGE-1256259).

2.7 – Author Contributions

T.J.K., A.B., Z.P.K., R.-J.T., M.L.C., P.G.L., S.L., and J.-M.A. designed the research. T.J.K., A.B., Z.P.K., A.M.P., M.V., F.A., and H.N.C. performed the experiments. T.J.K., A.B., Z.P.K., T.B.I., M.V., R.-J.T., M.L.C., S.L., and J.-M.A analyzed the data. T.J.K, A.B., Z.P.K., and J.-M.A. wrote the paper with assistance and input from all authors.

2.8 – Supplementary Figures

A

			Reciprocal		
Locus ID	**E-Value**	**Description**	**Locus ID**	**Description**	**E-Value**
Pp3c21_15330V3	0	CCaMK	Medtr8g043970	CCaMK / DMI3	0
Pp3c19_20580V3	2×10^{-169}	CCaMKb	Medtr8g043970	CCaMK / DMI3	8×10^{-159}
Pp3c4_7390V3	3×10^{-71}	CDPK	Medtr5g089320	CDPK17-Like	0
Pp3c8_690V3	1×10^{-70}	CDPK	Medtr5g089320	CDPK17-Like	0
Pp3c3_37890V3	9×10^{-69}	MAPK-activated CDPK	Medtr8g099095	CDPK3-Like	0

B

			Reciprocal		
Locus ID	**E-Value**	**Description**	**Locus ID**	**Description**	**E-Value**
Pp3c21_15330V3	0	CCaMK	Lj3g3v1739280	CCaMK	0
Pp3c19_20580V3	6×10^{-171}	CCaMKb	Lj3g3v1739280	CCaMK	6×10^{-176}
Pp3c8_690V3	1×10^{-69}	CDPK	Lj4g3v3002290	CDPK3-Like	0
Pp3c9_21410V3	2×10^{-69}	CDPK	Lj4g3v3002290	CDPK3-Like	0
Pp3c4_7390V3	5×10^{-69}	CDPK	Lj4g3v3002290	CDPK3-Like	0

C

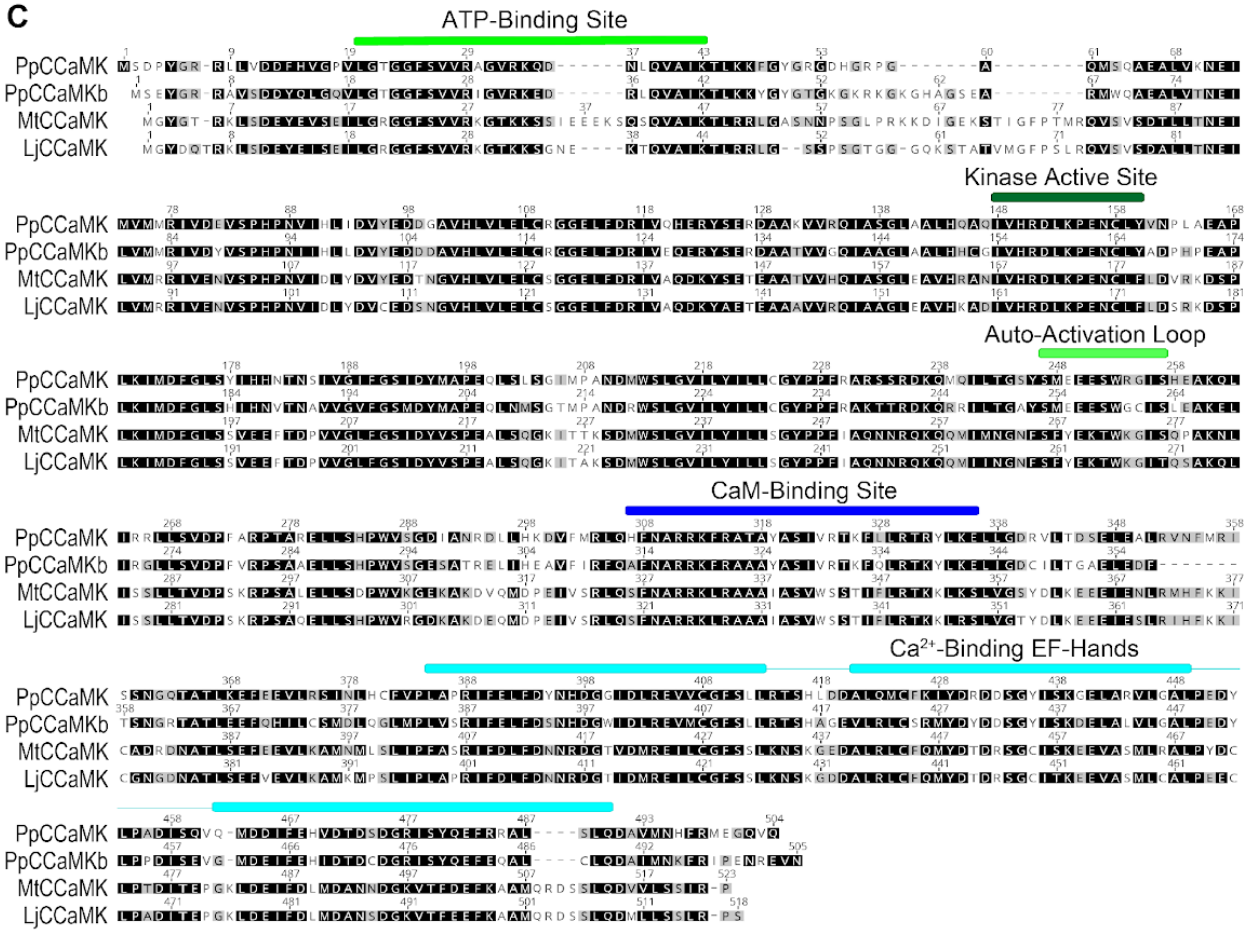

<u>Supplemental Figure 1</u>: Bioinformatic analysis of Physcomitrium CCaMK/CCaMKb compared to characterized homologs.

(A) Results of BLASTp search of Physcomitrium predicted proteome using Medicago CCaMK/DMI3 as query. Genomic locus ID, expectation (E)-values, and gene descriptions are provided. (Shaded) Reciprocal BLASTp with E-values for each

reciprocal best hit against the Medicago predicted proteome. CDPK: Ca2+-dependent protein kinase, MAPK: Mitogen-activated PK. (B) Results of BLASTp search of Physcomitrium predicted proteome using Lotus CCaMK as query, and reciprocal BLAST for each against the Lotus predicted proteome. Table format is identical to A. (C) Alignment of CCaMK protein sequences made using MUSCLE. Functional predictions are annotated above the alignment. Detailed descriptions are provided in Materials and Methods.

A

			Reciprocal		
Locus ID	**E-Value**	**Description**	**Locus ID**	**Description**	**E-Value**
Pp3c23_22500V3	1 x 10^{-21}	IPD3	Medtr5g026850	IPD3	1 x 10^{-16}
Pp3c24_11410V3	2	Galactan 1,3-β-Galactosidase	Medtr5g015460	Glycosyl Hydrolase	8 x 10^{-153}
Pp3c16_24380V3	3	CCHC-Type Zinc Finger Protein	Medtr8g468600	CCHC-Type Zinc Finger Protein	2 x 10^{-59}
Pp3c1_2420V3	20	Xyloglucan Endotransglycosylase	Medtr4g045853	Xyloglucan Endotransglycosylase	4 x 10^{-55}
Pp3c25_860V3	30	Alkaline Ceramidase-Related	Medtr1g096320	Alkaline Ceramidase-Related	2 x 10^{-170}

B

			Reciprocal		
Locus ID	**E-Value**	**Description**	**Locus ID**	**Description**	**E-Value**
Pp3c23_22500V3	1 x 10^{-22}	IPD3	Lj2g3v1549600	IPD3 / CYCLOPS	5 x 10^{-24}
Pp3c5_28790V3	4	Clathrin Assembly Protein	Lj4g3v1881980	ENTH/ANTH/VHS Family	3 x 10^{-6}
Pp3c24_11410V3	7	Galactan 1,3-β-Galactosidase	Lj2g3v1968430	Glycosyl Hydrolase	9 x 10^{-153}
Pp3c22_12090V3	10	Protein Kinase Superfamily	Lj4g3v0462390	Protein Kinase Superfamily	6 x 10^{-113}
Pp3c14_4840V3	10	Small Acidic Protein Family	Lj0g3v0243989	Arg/Ser-Rich Coiled Coil Protein	5 x 10^{-34}

C

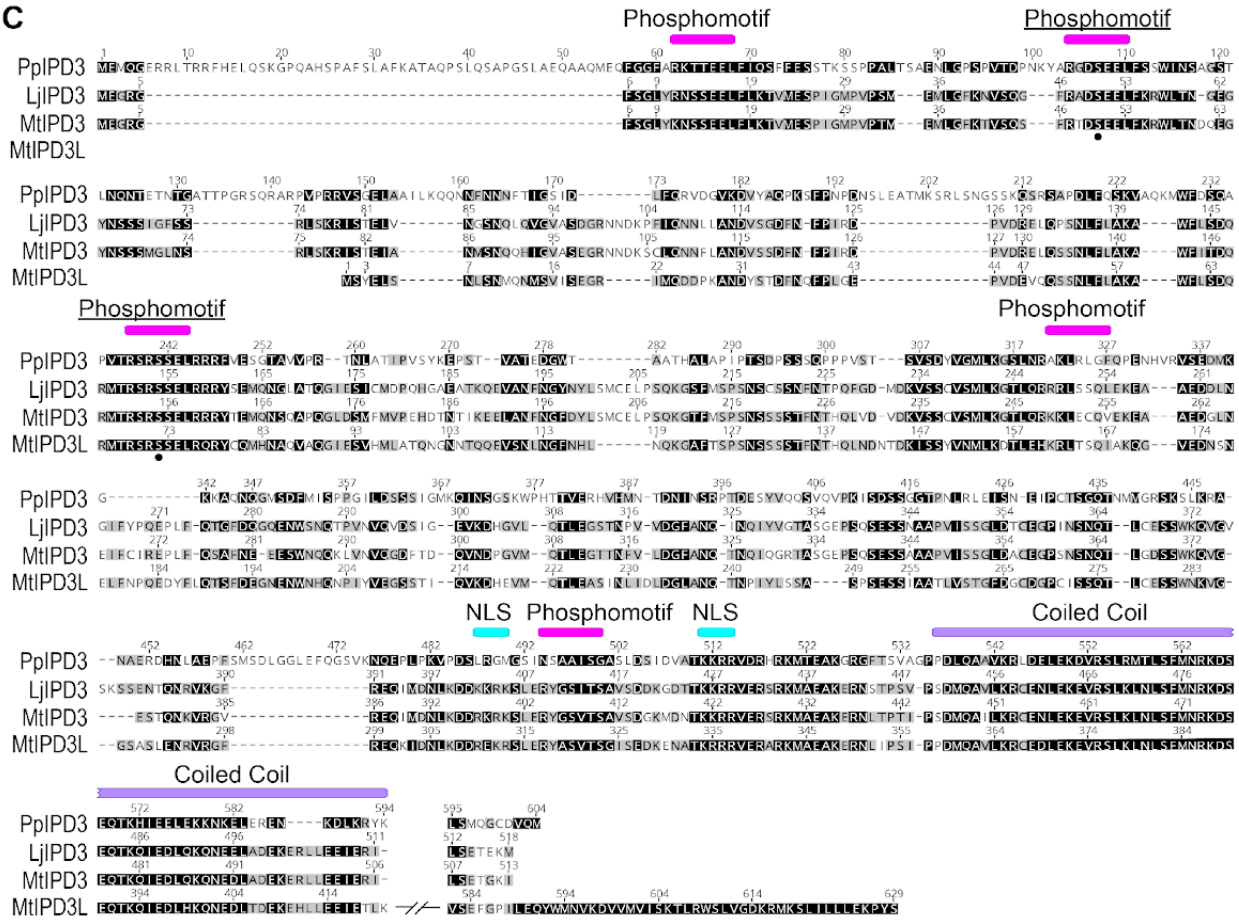

Supplemental Figure 2: Bioinformatic analysis of Physcomitrium IPD3 compared to characterized homologs.

(A) Results of BLASTp search of Physcomitrium predicted proteome using Medicago IPD3 as query. Genomic locus ID, expectation (E)-values, and gene descriptions are provided. (Shaded) Reciprocal BLASTp with E-values for each reciprocal best hit

against the Medicago predicted proteome. (B) Results of BLASTp search of Physcomitrium predicted proteome using Lotus IPD3/CYCLOPS as query, and reciprocal BLAST for each against the Lotus predicted proteome. Table format is identical to A. (C) Alignment of CCaMK protein sequences made using MUSCLE. Functional predictions are annotated above the alignment. Underlined phosphomotifs are critical for regulation of LjIPD3/CYCLOPS. NLS: Nuclear localization sequence. Detailed descriptions are provided in Materials and Methods.

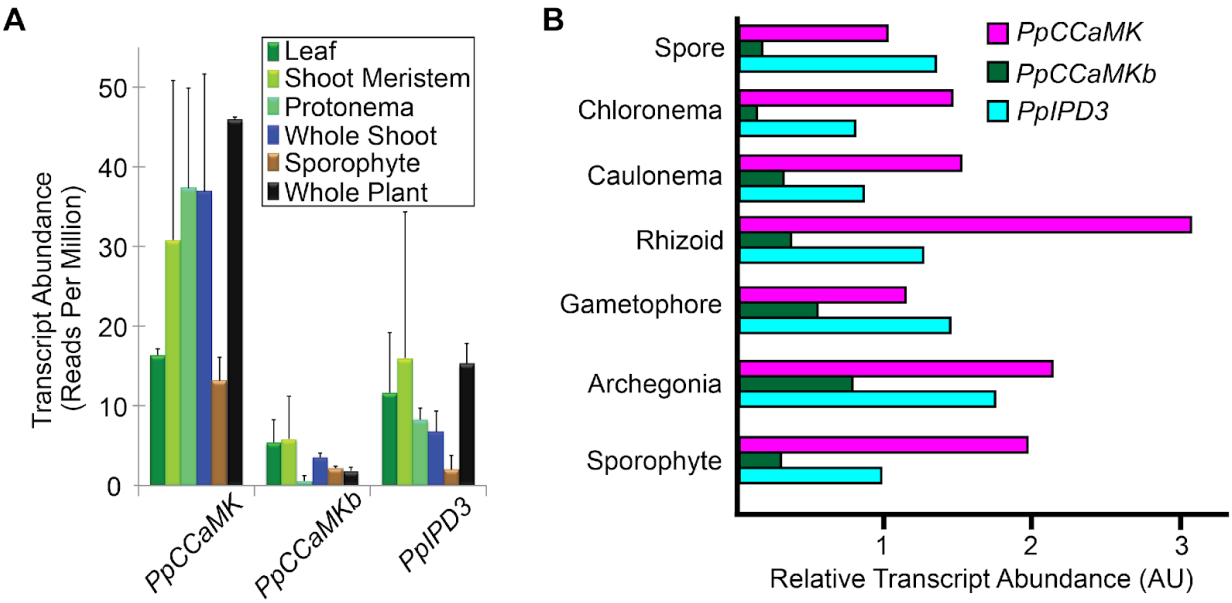

<u>Supplemental Figure 3:</u> Transcript abundance profiles for *PpCCaMK, PpCCaMKb*, and *PpIPD3*.

(A) Inferred transcript abundance, expressed in reads per million sequenced reads, for *PpIPD3, PpCCaMKb*, and *PpIPD3* across tissues sampled by laser-microdissection RNA-seq analysis (Frank and Scanlon, 2015). Error bars indicate standard error of the mean (SEM) among biological samples. (B) Inferred relative transcript abundance, expressed in arbitrary units (AU) for *PpIPD3*, *PpCCaMKb*, and *PpIPD3* from a published transcriptome atlas based on RNA-seq data (Ortiz-Ramírez et al., 2016).

<u>Supplemental Figure 4:</u> Co-culture of the arbuscular mycorrhizal fungus Rhizophagus irregularis with Physcomitrium.
(A) Bright-field micrograph showing Physcomitrium cells from a sample that was co-cultured with *Rhizophagus irregularis* for three months. Fungal hyphae were stained with trypan blue. No evidence for intracellular colonization was observed. (B) Bright-field micrograph showing Physcomitrium cells from a sample that was co-cultured with *Rhizophagus irregularis* for six months. Note that, despite extensive contact between fungal hyphae and Physcomitrium cells, no hyphal penetration was observed. (C) Confocal micrograph showing Physcomitrium cells from a sample that was co-cultured with *Rhizophagus irregularis* for three months. Chlorophyll autofluorescence (blue) and fungal hyphae stained with AlexaFluor 488 (green) conjugated to wheat germ agglutinin (WGA) are shown in pseudocolor. All scale bars = 100 µm.

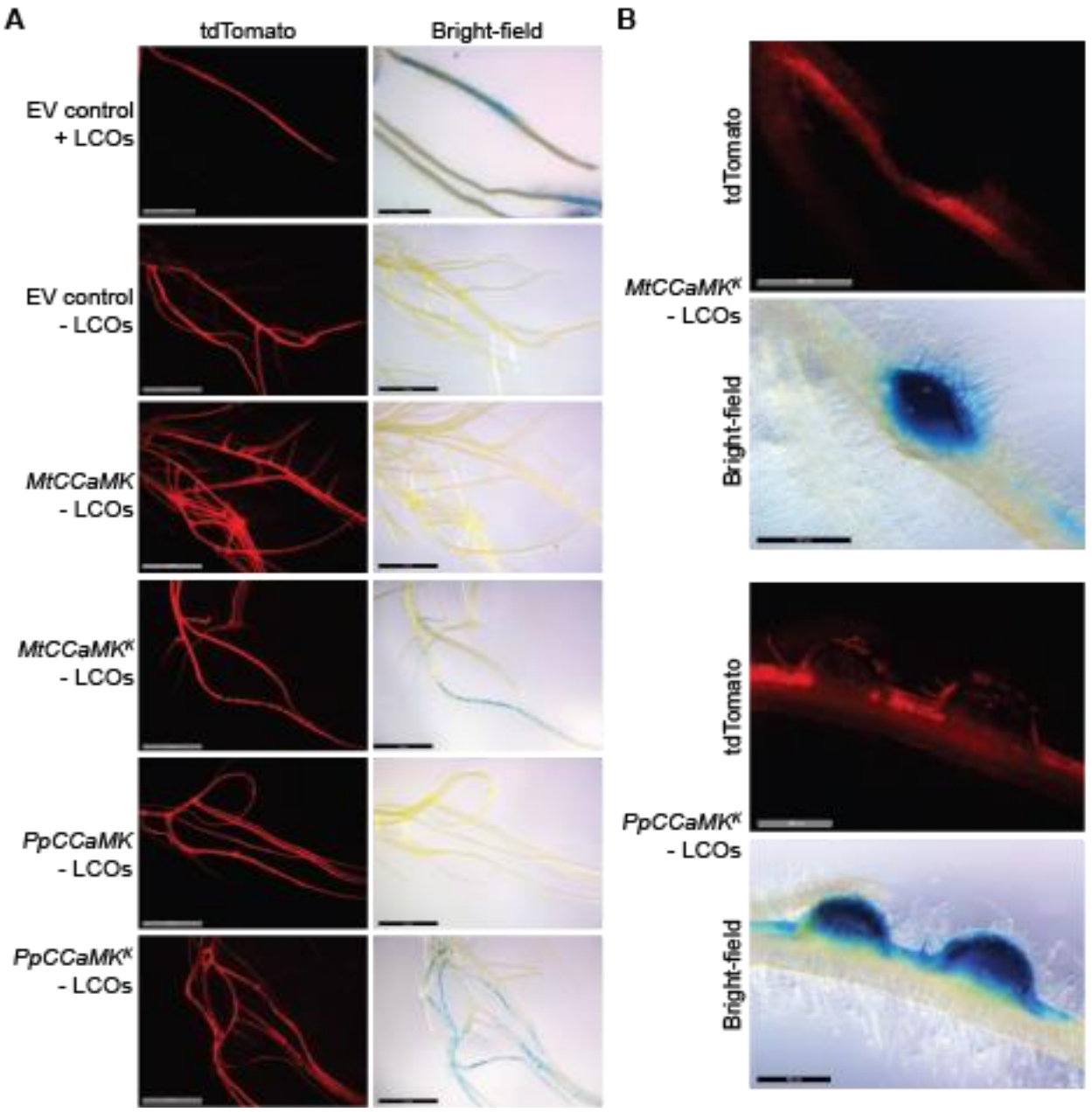

<u>Supplemental Figure 5.</u> Deletion of the C-terminal autoinhibition domain in PpCCaMK results in a gain-of-function isoform (PpCCaMK^K).

(A) Roots transformed with PpCCaMK^K, or a MtCCaMK^K positive control, strongly expressed *pENOD11::GUS* without addition of LCOs or rhizobia. Scale bars for EV control plants = 2 mm; for other plants = 5 mm.

(B) Roots expressing engineered forms of CCaMK from Physcomitrium (PpCCaMK^K) or Medicago (MtCCaMK^K) developed nodules in the absence of rhizobia. Scale bars = 500 µm.

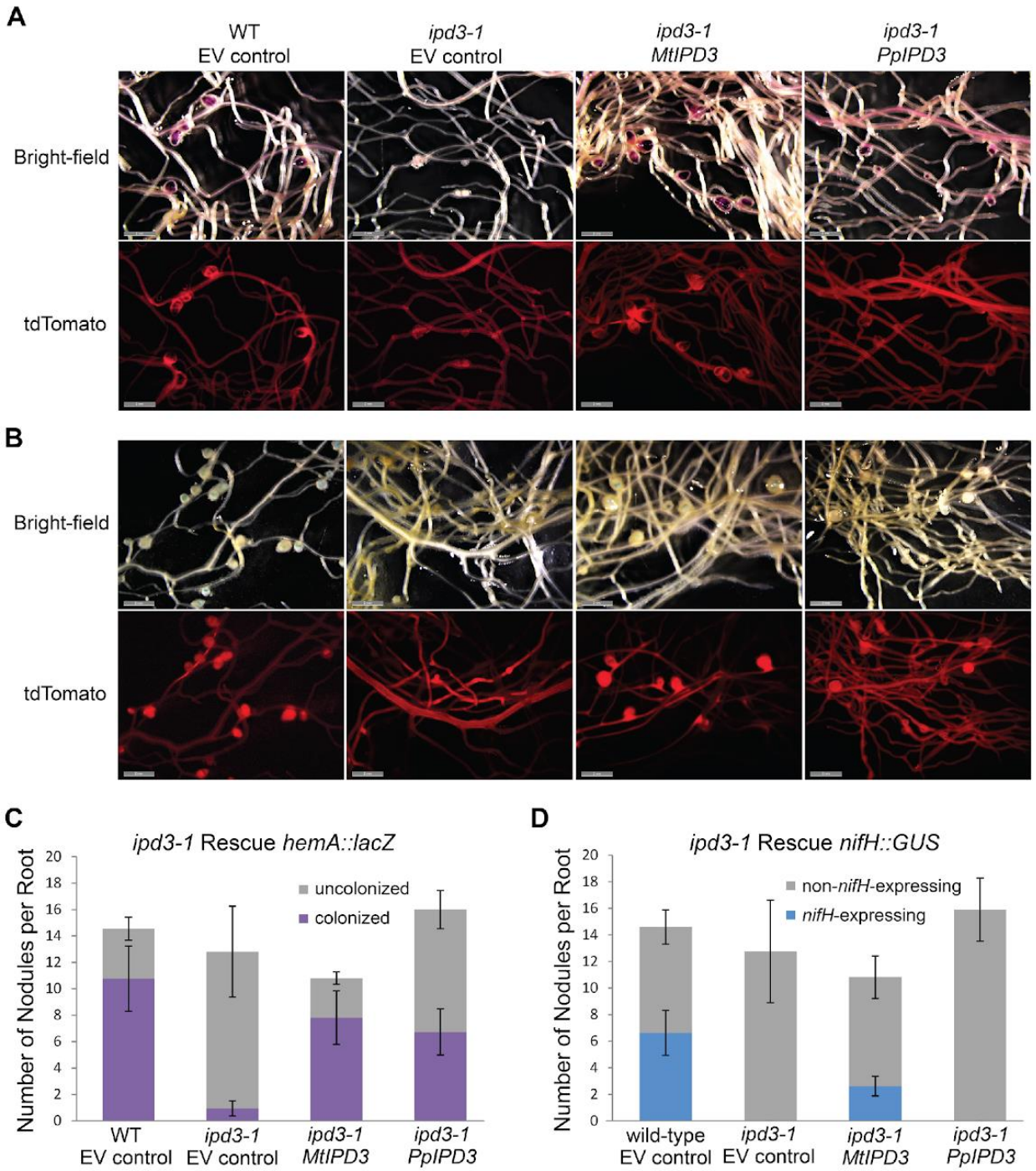

<u>Supplemental Figure 6.</u> ***PpIPD3*** **partially rescues nodule defects of** ***Medicago truncatula ipd3-1*** **mutants.**
(A) Roots transformed with *PpIPD3* developed colonized nodules after inoculation with *Sinorhizobium meliloti.* (B) Rhizobia inside the nodules did not express *nifH*. Scale bars = 2 mm. (C) A statistically significant difference in the number of colonized nodules per root was observed with a Dunn's test between *ipd3-1 MtIPD3* and *ipd3-1* EV control (p-value = 2.15 x 10^{-3}) and between *ipd3-1 PpIPD3* and *ipd3-1* EV control (p-value = 1.84

x 10^{-3}). (D) For number of nodules containing rhizobia expressing *nifH*, a statistically significant difference was observed using a Dunn's test between *ipd3-1 MtIPD3* and *ipd3-1* EV control (p-value = 2.73 x 10^{-3}).

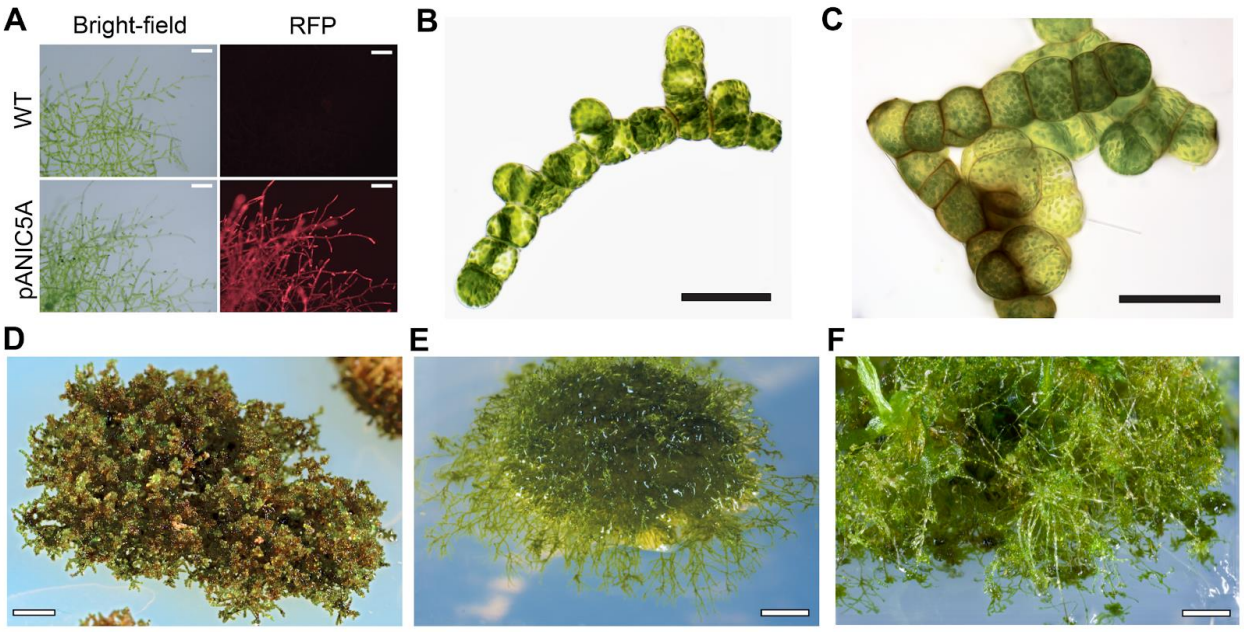

Supplemental Figure 7: Growth phenotypes of PpCCaMK or PpIPD3 gain-of-function lines.
(A) Physcomitrium genetically transformed with the empty pANIC5A vector, which was used to drive expression of each of native or modified forms of PpCCaMK or PpIPD3 in this study, did not show any growth defects or phenotypic aberrations compared to WT. Fluorescence from a red fluorescent protein (RFP) visual marker was used to validate transformation. Scale bars = 200 µm. (B) Example of juvenile cluster of cells expressing $PpIPD3^{DD}$. Sample was subcultured less than two weeks before imaging. Scale bar = 50 µm. (C) Example of cluster of cells expressing $PpIPD3^{DD}$ approximately three weeks after subculture. Note the prominent reddish cell wall thickenings. Scale bar = 50 µm. (D) Example of Physcomitrium line expressing $PpIPD3^{DD}$ more than 5 weeks after subculture. Note the dark pigmentation and that the entire visible population of cells are brood cells. Scale bar = 500 µm. (E) Example of Physcomitrium expressing $PpCCaMK^{D}$. Note the abundant presence of brood cells and the absence of gametophores. Scale bar = 500 µm. (F) Example of Physcomitrium expressing $PpCCaMK^{D}$. Note the presence of brood cells and that gametophores are stunted and malformed. Scale bar = 500 µm. All samples were grown in BCDAT medium with 16-hour days and approximately 50 mol m^{-2} s^{-1} light intensity and 22 degrees Celsius.

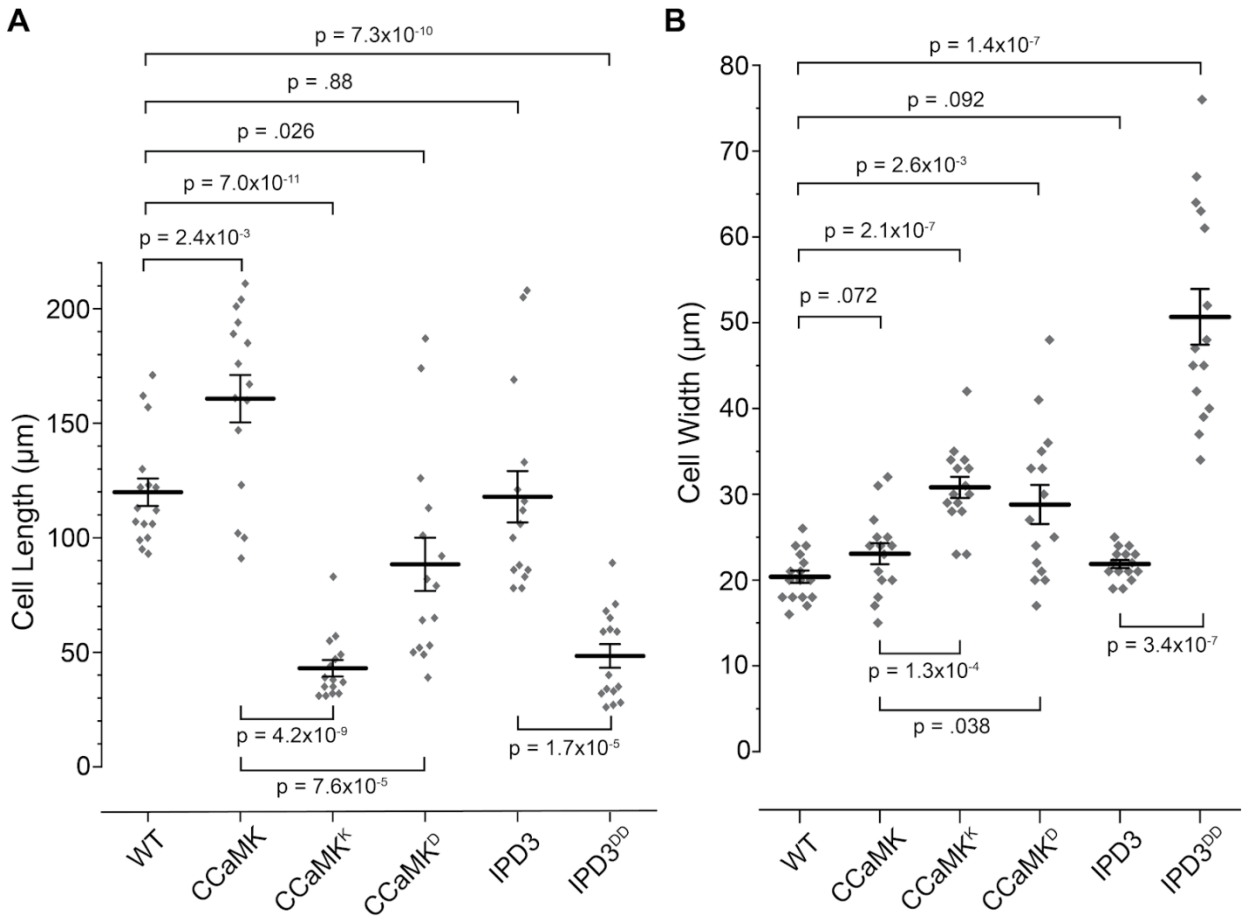

<u>Supplemental Figure 8:</u> Quantification and statistical analysis of protonemal cell dimensions of lines expressing native and modified forms of CCaMK or IPD3.
(A) Measured protonemal cell lengths of gain-of-function CCaMK or IPD3 lines in comparison to controls expressing unmodified forms or wild-type (WT). (B) Measured cell widths of gain-of-function CCaMK or IPD3 lines in comparison to controls expressing unmodified forms or WT. Thick lines indicate mean values. Whiskers indicate standard error of mean. Welch's t-test was used to calculate displayed p-values (n = 15-16).

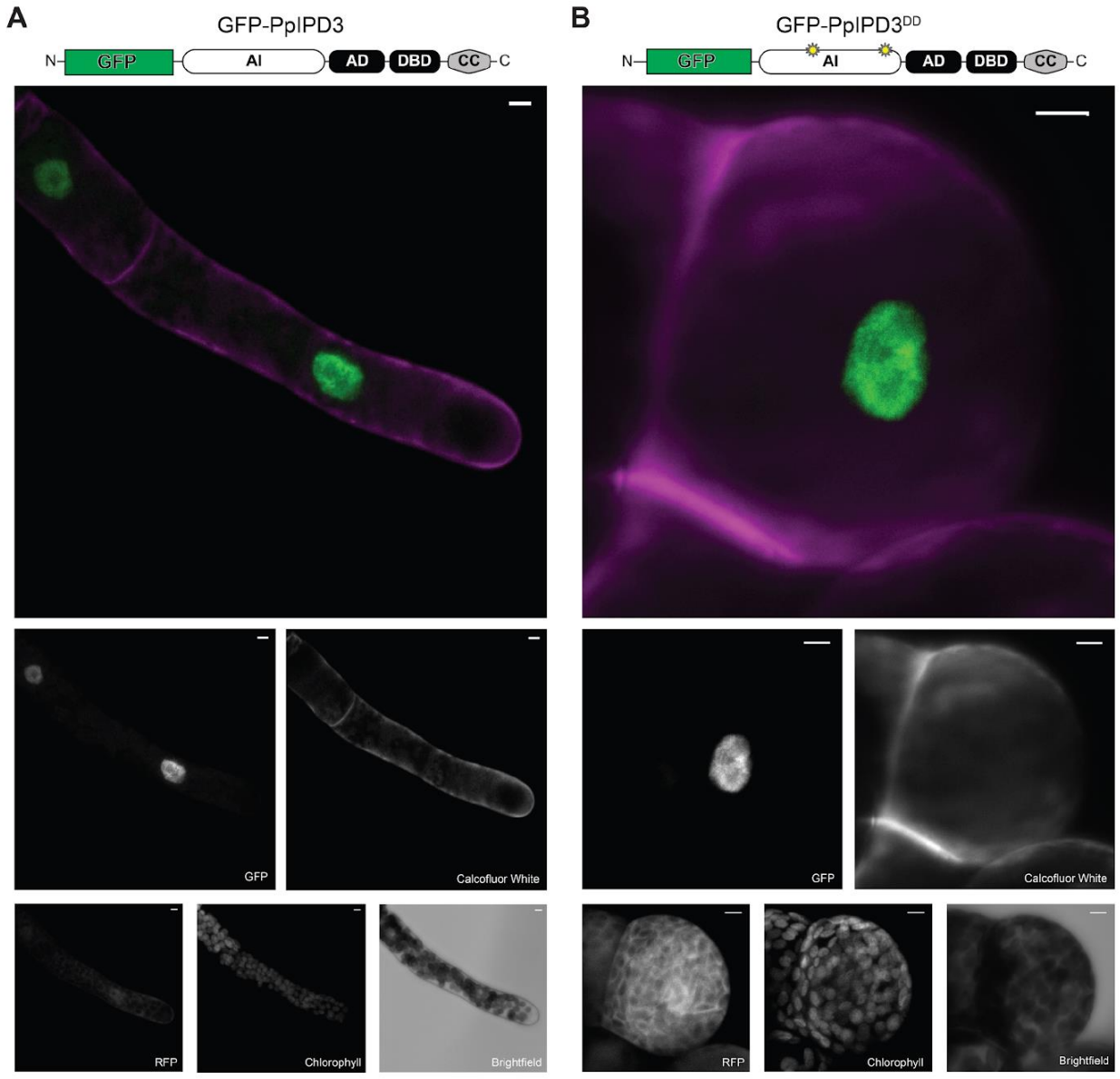

<u>Supplemental Figure 9:</u> Subcellular localization of GFP-tagged PpIPD3 and PpIPD3^{DD} driven by maize UBIQUITIN1 promoter.

Images are maximal projections of confocal z-stack acquisitions. Color image shows merged GFP (green) and calcofluor white (magenta) channels. Individual channels are labelled below. Free soluble red fluorescent protein (RFP) and chlorophyll autofluorescence were imaged for comparison. (A) N-terminally GFP-tagged native IPD3 localizes to nuclei, and protonemal growth and development is not noticeably affected. (B) N-terminally GFP-tagged native IPD3^{DD}, which differs by only two amino acid substitutions, also localizes to the nucleus and drives ectopic development of brood cells under non-stressed conditions. Scale bars = 5 μm.

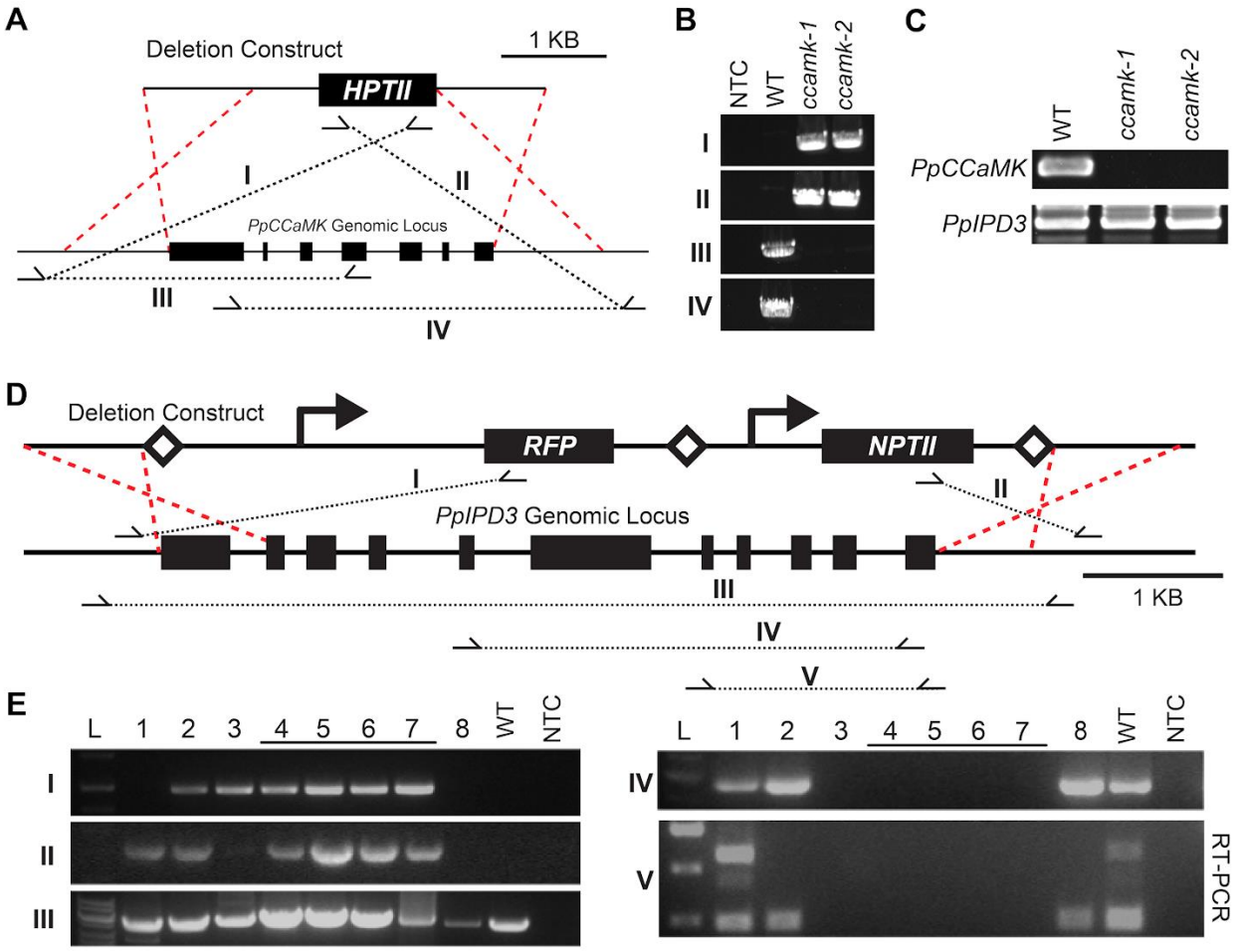

<u>Supplemental Figure 10:</u> Genotypic characterization of transformants and identification of Physcomitrium *ccamk* and *ipd3* deletion lines generated by homologous recombination-mediated gene targeting.

(A) Diagram summarizing strategy for genetic deletion of *IPD3*. Roughly 1 kilobase (KB) of genomic DNA was cloned upstream or downstream of the first and last exons of IPD3. The two fragments were used to sandwich a hygromycin B selectable marker gene (HPTII) construct. Primers specific to the flanking regions of the native and recombined locus were used to test for recombination events at the targeted locus. (B) Results of PCR reactions using genomic DNA extracted from two independent *ccamk* (*ccamk-1* and *ccamk-2*) deletion mutants, WT, and no template control (NTC). PCR amplicon indicated in A by roman numerals (I-IV). (C) RT-PCR analysis of *ccamk-1* and *ccamk-2* using oligonucleotide primers specific to the coding sequence (CDS) of *PpCCaMK*. Amplification of the *PpIPD3* from the same cDNA samples was used to validate cDNA quality. (D) Diagram illustrating strategy for deletion of *IPD3* and identification of knockout mutants. Deletion construct containing a red fluorescent protein (RFP) visible marker gene expression construct and neomycin resistance selectable marker gene (NPTII) expression construct is shown above the exon-intron structure of the *IPD3*. Expected homologous recombination events are depicted in red

dashed lines. PCR reactions with five different primer pairs (I-V) were used to identify *ipd3* deletion mutants. Expected PCR products are represented by arrows and dotted lines. (E) Results of PCR genotyping and RT-PCR. Panels I-IV show PCR results using genomic DNA samples. Panel V shows RT-PCR results. In each case, samples from eight lines stably transformed with ipd3 deletion constructs (1-8) were analyzed alongside DNA ladder (L), WT sample, and NTC.

2.9 – Supplementary Tables

	Medicago truncatula	*Lotus japonicus*	*Arabidopsis thaliana*	*Populus trichocarpa*	*Marchantia paleacea*	*Marchantia polymorpha*	*Physcomitrella patens*
DMI2	Medtr5g030920	Lj2g3v1467920	-	Potri.007G004700	1KP: LFVP_12404	-	Pp3c3_28930
DMI1	Medtr7g117580	Lj6g3v2275020 Lj1g3v5061360	AT5G49960	Potri.003G008800 Potri.004G223400	1KP: LFVP_10987	1KP: JPYU_1254	Pp3c6_21060
NUP85	Medtr1g006690	Lj1g3v0318210	AT4G32910	Potri.018G044300	1KP: IHWO_2064309	Mapoly0014s0066	Pp3c16_3750
NUP133	Medtr5g097260	Lj2g3v3337540	AT2G05120	Potri.002G221300	1KP: IHWO_2012039	Mapoly0061s0124	Pp3c21_14430
CCaMK	Medtr8g043970	Lj3g3v1739280	-	Potri.008G011400 Potri.010G247400	1KP: IHWO_2068101	-	Pp3c21_15330 Pp3c19_20580
IPD3	Medtr5g026850 NCBI: MG788323	Lj2g3v1549600	-	Potri.001G130800 Potri.003G103100	1KP: LFVP_585	-	Pp3c23_22500
NSP1	Medtr8g020840	Lj3g3v2579340.1	AT3G13840	Potri.001G168800 Potri.003G065400	-	1KP: JPYU_8216	Pp3c2_9730
NSP2	Medtr3g072710	Lj1g3v0785930	AT4G08250	Potri.002G086100 Potri.005G175300	-	-	-
RAM1	Medtr7g027190	NCBI: KU557503	-	Potri.001G326000	-	-	-
RAM2	Medtr1g040500	Lj1g3v2301880	-	Potri.006G198100 Potri.016G063900	1KP: LFVP_13817_3 1KP: LFVP_85930_3 1KP: LFVP_15570_2	1KP: JPYU_7323 1KP: JPYU_5852	Pp3c5_1510 Pp3c6_29200 Pp3c6_29290
STR	Medtr8g107450	Lj4g3v3115140	-	Potri.012G045100 Potri.015G036100	1KP: LFPV_2015253	-	-
STR2	Medtr5g030910	Lj0g3v0104499	-	Potri.007G004800	1KP: LFPV_2012505	-	-
VAPYRIN	Medtr6g027840	Lj0g3v0049599 Lj1g3v3975850	-	Potri.013G062000 Potri.010G185200	1KP: HMHL_4710	1KP: JPYU_2960	-

<u>Supplemental Table 1:</u> Database accession numbers for genes referenced in Figure 1A.

Accessions from the National Center for Biotechnology Information (NCBI, accessible at https://ncbi.nlm.nih.gov) or the 1000 Plants Initiative (1KP, accessible at https://www.onekp.com) are marked. Other accessions follow stanard genomic locus identified for each species. The *Lotus japonicus* genome is accessible at https://lotus.au.dk. All other data are accessible through Phytozome 12 (https://phytozome.jgi.doe.gov). Dashes indicate inferred ortholog losses.

Name	Mutation(s)	Predicted Effect	# Transformants	Reference(s)
PpCCaMK	None	-	12	-
PpCCaMK^{D}	S252D	Constitutive Activation	8	Banba *et al.*, 2008; Takeda *et al.*, 2012
PpCCaMK^{K}	Δ307-504	Constitutive Activation	14	Gleason *et al.*, 2006
PpIPD3	None	-	18	-
PpIPD3^{DD}	S107D, S241D	Constitutive Activation	>36	Singh *et al.*, 2014

Supplemental Table 2: Modified forms of PpCCaMK and PpIPD3 used in this study.

The name, introduced mutations (if applicable), and predicted effects of introduced mutations are listed. For each construct, the number (#) of independent transformants that were generated and analyzed is provided. The reference for each study that guided our directed mutagenesis are provided and cited in the main text.

Primer Name	Gene	Locus ID	Purpose	Orientation	Extension Type	Primer Extension Sequence (5' to 3')	Primer Sequence (5' to 3')	Source
CCaMK_CDS-F1g	CCaMK	Pp3c21_15330	Cloning Coding Sequence	Forward	Gateway AttB1	GGGGACAAGTTTGTACAAAAAAGCAGGCTTC	ATGAGTGATCCATATGGG	This study
CCaMK_CDS-R1g	CCaMK	Pp3c21_15330	Cloning Coding Sequence	Reverse	Gateway AttB2	GGGGACCACTTTGTACAAGAAAGCTGGGTC	ATTTCACTGGACCTGACC	This study
CCaMK_CDS-R2g	CCaMK	Pp3c21_15330	Cloning Truncated Coding Sequence	Reverse	Gateway AttB2 + Stop Codon	GGGGACCACTTTGTACAAGAAAGCTGGGTCTCA	TTGTAAGCGCATGAAAACG	This study
CCaMKb_CDS-F1g	CCaMKb	Pp3c19_20580	Cloning Coding Sequence	Forward	Gateway AttB1	GGGGACAAGTTTGTACAAAAAAGCAGGCTTC	AGGATGAGTGAGTATGGG	This study
CCaMKb_CDS-R1g	CCaMKb	Pp3c19_20580	Cloning Coding Sequence	Reverse	Gateway AttB2	GGGGACCACTTTGTACAAGAAAGCTGGGTC	TCAGTTCACCTCTCTGTTC	This study
IPD3_CDS-F1g	IPD3	Pp3c23_22500	Cloning Coding Sequence	Forward	Gateway AttB1	GGGGACAAGTTTGTACAAAAAAGCAGGCTTC	ATGGAGATGCAGGGAGAGC	This study
IPD3_CDS-R1g	IPD3	Pp3c23_22500	Cloning Coding Sequence	Reverse	Gateway AttB2	GGGGACCACTTTGTACAAGAAAGCTGGGTC	TTATGACTCGGGATTAATCAGTG	This study
CCaMK_S252D-F1	CCaMK	-	Site-directed Mutagenesis	Forward	-	-	CATGGAAGAAGAAGATTGGAGAGGTATTTC	This study
CCaMK_S252D-R1	CCaMK	-	Site-directed Mutagenesis	Reverse	-	-	GAAATACCTCTCCAATCTTCTTCTTCCATG	This study
IPD3_S107D-F1	IPD3	-	Site-directed Mutagenesis	Forward	-	-	GCTAGGGGAGACGACGAGGAGCTCTTC	This study
IPD3_S107D-R1	IPD3	-	Site-directed Mutagenesis	Reverse	-	-	GAAGAGCTCCTCGTCGTCTCCCCTAGC	This study
IPD3_S241D-F1	IPD3	-	Site-directed Mutagenesis	Forward	-	-	GTAACACGCAGTCGCGATTCAGAACTGAGG	This study
IPD3_S241D-R1	IPD3	-	Site-directed Mutagenesis	Reverse	-	-	CCTCAGTTCTGAATCGCGACTGCGTGTTAC	This study
IPD3_pro_cloning_F	IPD3	Medtr5g026850	Promoter Sequence Cloning	Forward	Golden-Gate L0 PU	TGTGGTCTCAGGAG	ATAGGAACCAAAAGTAGTGATTG	This study
IPD3_pro_cloning_R	IPD3	Medtr5g026850	Promoter Sequence Cloning	Reverse	Golden-Gate L0 PU	CGTGGTCTCACATT	TTCAACACTTTAAAGATGCTTGATTA	This study
IPD3_term_cloning_F	IPD3	Medtr5g026850	Terminator Sequence Cloning	Forward	Golden-Gate L0 T	TGTGGTCTCAGCTT	TGTTTTGTTTCGCTGTTATATCCTTA	This study
IPD3_term_cloning_R	IPD3	Medtr5g026850	Terminator Sequence Cloning	Reverse	Golden-Gate L0 T	CGTGGTCTCAAGCG	TTGAATGAATAGATAAGATACC	This study
eGFP-F1g	-	-	N-terminal tagging with eGFP	Forward	Gateway AttB1	GGGGACAAGTTTGTACAAAAAAGCAGGCTTC	ATGGTGAGCAAGGGCGAG	This study
eGFP_R1+linker	-	-	N-terminal tagging with eGFP	Reverse	Poly-glycine Linker	GCCTCCACCTCCGCC	CTTGTACAGCTCGTCCATGC	This study
IPD3_CDS-F1+linker	IPD3	Pp3c23_22500	N-terminal tagging with eGFP	Forward	Poly-glycine Linker	CAAGGGCGGAGGTGGAGGC	ATGGAGATGCAGGGAGAGC	This study
IPD3_CDS-R2g	IPD3	Pp3c23_22500	N-terminal tagging with eGFP	Reverse	Gateway AttB2	GGGGACCACTTTGTACAAGAAAGCTGGGTC	TTACATCTGCACATCACATCCC	This study
Phypa_166566-F1	LEA3.1	Pp3c12_22320.30	qPCR Query	Forward	-	-	GCAGACTGGCAACTATGTGTCCGA	Shinde *et al.*, 2012
Phypa_166566-R1	LEA3.1	Pp3c12_22320.30	qPCR Query	Reverse	-	-	ATCCCACTCAACCCTACTGTTTGG	Shinde *et al.*, 2012
Phypa_166566-F2	LEA3.1	Pp3c12_22320.30	qPCR Query	Forward	-	-	GACCTATGAACAGACCAAGGAG	This study
Phypa_166566-R2	LEA3.1	Pp3c12_22320.30	qPCR Query	Reverse	-	-	GTTTTGTCACCTACTTGCTGG	This study
Phypa_211998-F1	LEA3.2	Pp3c7_13140	qPCR Query	Forward	-	-	TGCTTCAACCATGCTAGTTAGGCG	Shinde *et al.*, 2012
Phypa_211998-R1	LEA3.2	Pp3c7_13140	qPCR Query	Reverse	-	-	TCCACCTGGATCTACGGAAGTTGA	Shinde *et al.*, 2012
Phypa_211998-F2	LEA3.2	Pp3c7_13140	qPCR Query	Forward	-	-	AAAAGAAGGATCAAGCATACGAC	This study
Phypa_211998-R2	LEA3.2	Pp3c7_13140	qPCR Query	Reverse	-	-	GTCTGTTTTGTTCCTTCCCATG	This study
Phypa_178090-F	-	Pp3c1_35630	qPCR Reference	Forward	-	-	GCAAGCCAATCAGTACACTC	LeBail *et al.*, 2013
Phypa_178090-R	-	Pp3c1_35630	qPCR Reference	Reverse	-	-	ATCTTAGCCAACAACCAATAACC	LeBail *et al.*, 2013
Phypa_430768-F	-	Pp3c14_21480	qPCR Reference	Forward	-	-	TACGGACCCTAATCCAGATGAC	LeBail *et al.*, 2013
Phypa_430768-R	-	Pp3c14_21480	qPCR Reference	Reverse	-	-	CAACCCATTGCATACTTCTGAG	LeBail *et al.*, 2013
Phypa_438496-F	-	Pp3c14_7550	qPCR Reference	Forward	-	-	ACGGACATTGCATTTAAGACCT	LeBail *et al.*, 2013
Phypa_438496-R	-	Pp3c14_7550	qPCR Reference	Reverse	-	-	GTCGATTACCTGTGGAGAAGAC	LeBail *et al.*, 2013
Phypa_443007-F	-	Pp3c8_16590	qPCR Reference	Forward	-	-	AGTATAGTCTAGAGTATGGTACCG	LeBail *et al.*, 2013
Phypa_443007-R	-	Pp3c8_16590	qPCR Reference	Reverse	-	-	TAGCAATTTGATGGCAGCTC	LeBail *et al.*, 2013
Phypa_451689-F	-	Pp3c27_6310	qPCR Reference	Forward	-	-	GTCTAGTTAGTCCTTTGGTCCT	LeBail *et al.*, 2013
Phypa_451689-R	-	Pp3c27_6310	qPCR Reference	Reverse	-	-	GCCTATTTCTATAATGACTCCGT	LeBail *et al.*, 2013
IPD3_GT-F1g	IPD3	Pp3c23_22500	5' Gene Targeting Flank	Forward	Gateway AttB1	GGGGACAAGTTTGTACAAAAAAGCAGGCTTA	TCGCATCTTCAGGTCCTTTCG	This study
IPD3_GT-R1g	IPD3	Pp3c23_22500	5' Gene Targeting Flank	Reverse	Gateway AttB4	GGGGACAACTTTGTATAGAAAAGTTGGGTG	TAAGGTTACGATCGGCCATCTC	This study
IPD3_GT-F2g	IPD3	Pp3c23_22500	3' Gene Targeting Flank	Forward	Gateway AttB3	GGGGACAACTTTGTATAATAAAGTTGTA	GTATCACTGATTAATCCCG	This study
IPD3_GT-R2g	IPD3	Pp3c23_22500	3' Gene Targeting Flank	Reverse	Gateway AttB2	GGGGACCACTTTGTACAAGAAAGCTGGGTA	ATGCAATATGCATAGCC	This study
RFP-F1g	-	-	Visual Marker Construct	Forward	Gateway AttB4r	GGGGACAACTTTTCTATACAAAGTTGTA	TTCAGCTGCAGGTTTGG	This study
RFP-R1g	-	-	Visual Marker Construct	Reverse	Gateway AttB5r	GGGGACAACTTTTGTATACAAAGTTGT	TCCCGATCTAGTAACATAGATG	This study
NPTII-F1g	-	-	Selectable Marker Construct	Forward	Gateway AttB5	GGGGACAACTTTGTATACAAAAGTTGTA	CTACTCCAAAAATGTCAAAG	This study
NPTII-R1g	-	-	Selectable Marker Construct	Reverse	Gateway AttB3r	GGGGACAACTTTATTATACAAAGTTGT	TGATCTGGATTTTAGTACTGG	This study
IPD3_KCA-F1	-	-	Knockout Construct Amplification	Forward	-	-	CGTTTCTTTTCTGCTCACTAGGTTTCTC	This study
IPD3_KCA-R1	-	-	Knockout Construct Amplification	Reverse	-	-	GTTTCCAAAACCGTCAGCGTTGAGC	This study
HPTII-F1	-	-	Genotyping -- 3' region (II)	Forward	-	-	GATGTGATTATCGTGAGATGTTTA	This study
HPTII-R2	-	-	Genotyping -- 5' region (I)	Reverse	-	-	TATCTGGGAACTACTCACACATTA	This study
CCaMK-CDS-R1	CCaMK	Pp3c21_15330	Genotyping -- 5' region (III)	Reverse	-	-	ACGCATGAAATTTACACGCA	This study
CCaMK-CDS-F2	CCaMK	Pp3c21_15330	Genotyping -- 3' region (IV)	Forward	-	-	GTTTGTACGTGAACCCCTTG	This study
CCaMK-gDNA-flank-F1	CCaMK	Pp3c21_15330	Genotyping--5' region (I/III)	Forward	-	-	AATAACGTGGCTTTTGGAAG	This study
CCaMK-gDNA-flank-R1	CCaMK	Pp3c21_15330	Genotyping--5' region (II/IV)	Reverse	-	-	AAAGGATCCAATCAACTCCA	This study
TB79-F	CCaMK	Pp3c21_15330	Knockout Construct Amplification	Forward	-	-	TGACCACATTCCCTTCTTCC	This study
TB79-R	CCaMK	Pp3c21_15330	Knockout Construct Amplification	Reverse	-	-	TTTCTTGTTCATATCCAAAAGACATTG	This study
IPD3_Ge-F1	IPD3	Pp3c23_22500	Genotyping -- 5' region (I)	Forward	-	-	TTCAGGTCCTTTCGTCATTTCCCTC	This study
RFP_Ge-R1	-	-	Genotyping -- 5' region (I)	Reverse	-	-	TACTCGTGCTAGTGGAAACCAAACAC	This study
NPTII_Ge-F2	-	-	Genotyping -- 3' region (II)	Forward	-	-	CATCGCCTTCTATCGCCTTC	This study
IPD3_Ge-R2	IPD3	Pp3c23_22500	Genotyping -- 3' region (II)	Reverse	-	-	ATGCATAGCCATTGTGACCATGACG	This study
IPD3_Ge-F3	IPD3	Pp3c23_22500	Genotyping -- entire locus (III)	Forward	-	-	TTGCATTCCCAATCCTCCAG	This study
IPD3_Ge-R3	IPD3	Pp3c23_22500	Genotyping -- entire locus (III)	Reverse	-	-	GTAAGGTCGGTTATTTGCTTGC	This study
IPD3_Ge-F4	IPD3	Pp3c23_22500	Genotyping -- deleted region (IV)	Forward	-	-	ATGTGGTTCGATTCACAGG	This study
IPD3_Ge-R4	IPD3	Pp3c23_22500	Genotyping -- deleted region (IV)	Reverse	-	-	CATCTGCACATCACATCCC	This study
IPD3_Ge-F5	IPD3	Pp3c23_22500	Genotyping -- RT-PCR (V)	Forward	-	-	TTAAGAACCAAGAACCCCTACC	This study
IPD3_Ge-R5	IPD3	Pp3c23_22500	Genotyping -- RT-PCR (V)	Reverse	-	-	TTCGGCATCAAAACTAAACAG	This study

<u>Supplemental Table 3:</u> Sequences and descriptions of oligonucleotide primers used in this study.

Names, descriptions, and DNA sequences (from 5’ to 3’) are provided. Locus IDs are for *Physcomitrium patens* genome version 3.3. Primer pairs used in previously published studies include the citation for the source.

2.10 – References

Ané, J.-M., Kiss, G.B., Riely, B.K., Penmetsa, R.V., Oldroyd, G.E.D., Ayax, C., Lévy, J., Debellé, F., Baek, J.-M., Kalo, P., *et al.* (2004). *Medicago truncatula DMI1* required for bacterial and fungal symbioses in legumes. Science *303*, 1364–1367.

Le Bail, A., Scholz, S., and Kost, B. (2013). Evaluation of reference genes for RT qPCR analyses of structure-specific and hormone regulated gene expression in *Physcomitrella patens* gametophytes. PLoS One *8*, e70998.

Bascom, C.S., Winship, L.J., and Bezanilla, M. (2018). Simultaneous imaging and functional studies reveal a tight correlation between calcium and actin networks. Proc. Natl. Acad. Sci. *115*, E2869-E2878.

Binder, A., Lambert, J., Morbitzer, R., Popp, C., Ott, T., Lahaye, T., and Parniske, M., (2014). A modular plasmid assembly kit for multigene expression, gene silencing and silencing rescue in plants. PLoS One *9*, 88218.

Bonfante, P., and Genre, A. (2008). Plants and arbuscular mycorrhizal fungi: an evolutionary-developmental perspective. Trends Plant Sci. *13*, 492–498.

Bopp, M. (2000). 50 Years of the Moss Story. In Progress in Botany, (Springer), pp. 3–34.

Broghammer, A., Krusell, L., Blaise, M., Sauer, J., Sullivan, J.T., Maolanon, N., Vinther, M., Lorentzen, A., Madsen, E.B., Jensen, K.J. and Roepstorff, P. (2012) Legume receptors perceive the rhizobial lipochitin oligosaccharide signal molecules by direct binding. Proc. Natl. Acad. Sci. *109*, 13859-13864.

Bressendorff, S., Azevedo, R., Kenchappa, C.S., Ponce de Leon, I., Olsen, J. V, Rasmussen, M.W., Erbs, G., Newman, M.-A., Petersen, M., and Mundy, J. (2016). An innate immunity pathway in the moss *Physcomitrella patens*. Plant Cell *28*, 1328–1342.

Buendia, L., Wang, T., Girardin, A., and Lefebvre, B. (2015). The LysM receptor-like kinase SlLYK10 regulates the arbuscular mycorrhizal symbiosis in tomato. New Phytol. *210*, 184–195.

Capoen, W., Sun, J., Wysham, D., Otegui, M.S., Venkateshwaran, M., Hirsch, S., Miwa, H., Downie, J.A., Morris, R.J., and Ané, J.-M. (2011). Nuclear membranes control symbiotic calcium signaling of legumes. Proc. Natl. Acad. Sci. *108*, 14348–14353.

Carleton, T.J. and Read, D.J. (1991). Ectomycorrhizas and nutrient transfer in conifer–feather moss ecosystems. Can. J. Bot. *69*, 778–785.

Chen, C., Ané, J., and Zhu, H. (2008). OsIPD3, an ortholog of the *Medicago truncatula* DMI3 interacting protein IPD3, is required for mycorrhizal symbiosis in rice. New Phytol. *180*, 311–315.

Correns, C. (1899). Untersuchungen über die Vermehrung der Laubmoose durch Brutorgane und Stecklinge (G. Fischer).

Davey, M.L., and Currah, R.S. (2006). Interactions between mosses (Bryophyta) and fungi. Botany *84*, 1509–1519.

Delaux, P.-M. (2017). Comparative phylogenomics of symbiotic associations. New Phytol. *213*, 89–94.

Delaux, P.-M., Séjalon-Delmas, N., Bécard, G., and Ané, J.-M. (2013). Evolution of the plant–microbe symbiotic 'toolkit.' Trends Plant Sci. *18*, 298–304.

Delaux, P.-M., Radhakrishnan, G. V., Jayaraman, D., Cheema, J., Malbreil, M., Volkening, J.D., Sekimoto, H., Nishiyama, T., Melkonian, M., Pokorny, L., *et al.* (2015). Algal ancestor of land plants was preadapted for symbiosis. Proc. Natl. Acad. Sci. *112*, 201515426.

Delaux, P.-M., Varala, K., Edger, P.P., Coruzzi, G.M., Pires, J.C., and Ané, J.M. (2014). Comparative phylogenomics uncovers the impact of symbiotic associations on host genome evolution. PLoS Genet. *10*, e1004487

Doyle, J.J. (2011). Phylogenetic perspectives on the origins of nodulation Mol. Plant Microbe Interact. *24*, 1289–1295.

Duckett, J.G., and Ligrone, R. (1992). A survey of diaspore liberation mechanisms and germination patterns in mosses. J. Bryol. *17*, 335–354.

Fliegmann, J., Canova, S., Lachaud, C., Uhlenbroich, S., Gasciolli, V., Pichereaux, C., Rossignol, M., Rosenberg, C., Cumener, M., Pitorre, D., Lefebvre, B., *et al.* (2013) Lipo-chitooligosaccharidic symbiotic signals are recognized by LysM receptor-like kinase LYR3 in the legume *Medicago truncatula*. ACS Chem. Biol. *8*, 1900-1906.

Frank, M.H., and Scanlon, M.J. (2015). Cell-specific transcriptomic analyses of three-dimensional shoot development in the moss *Physcomitrella patens*. Plant J. *83*, 743–751.

Galotto, G., Abreu, I., Sherman, C., Liu, B., Gonzalez-Guerrero, M., and Vidali, L. (2020). Chitin Triggers Calcium-Mediated Immune Response in the Plant Model Physcomitrella patens. Mol. Plant Microbe Interact. *33*, 911–920.

Garcia, K., Delaux, P., Cope, K.R., and Ané, J. (2015). Molecular signals required for the establishment and maintenance of ectomycorrhizal symbioses. New Phytol. *208*, 79–87.

Garcia, K., Chasman, D., Roy, S., and Ané, J.-M. (2017). Physiological responses and gene co-expression network of mycorrhizal roots under K^+ deprivation. Plant Physiol. *173*, 1811–1823.

Genre, A., Chabaud, M., Faccio, A., Barker, D.G., and Bonfante, P. (2008). Prepenetration apparatus assembly precedes and predicts the colonization patterns of arbuscular mycorrhizal fungi within the root cortex of both *Medicago truncatula* and *Daucus carota*. Plant Cell *20*, 1407–1420.

Gleason, C., Chaudhuri, S., Yang, T., Munoz, A., Poovaiah, B.W., and Oldroyd, G.E.D. (2006). Nodulation independent of rhizobia induced by a calcium-activated kinase lacking autoinhibition. Nature *441*, 1149–1152.

Gobbato, E., Marsh, J.F., Vernié, T., Wang, E., Maillet, F., Kim, J., Miller, J.B., Sun, J., Bano, S.A., and Ratet, P. (2012). A GRAS-type transcription factor with a specific function in mycorrhizal signaling. Curr. Biol. *22*, 2236–2241.

Hohe, A., Egener, T., Lucht, J.M., Holtorf, H., Reinhard, C., Schween, G., and Reski, R. (2004). An improved and highly standardised transformation procedure allows efficient production of single and multiple targeted gene-knockouts in a moss, *Physcomitrella patens*. Curr. Genet. *44*, 339–347.

Horváth, B., Yeun, L.H., Domonkos, Á., Halász, G., Gobbato, E., Ayaydin, F., Miró, K., Hirsch, S., Sun, J., Tadege, M., *et al.* (2011). *Medicago truncatula IPD3* is a member of the common symbiotic signaling pathway required for rhizobial and mycorrhizal symbioses. Mol. Plant Microbe Interact. *24*, 1345–1358.

Kamel, L., Keller-Pearson, M., Roux, C., and Ané, J.-M. (2016). Biology and evolution of arbuscular mycorrhizal symbiosis in the light of genomics. New Phytol. *213*, 531–536.

Kleist, T.J., Spencley, A.L., and Luan, S. (2014). Comparative phylogenomics of the CBL-CIPK calcium-decoding network in the moss *Physcomitrella*, *Arabidopsis*, and other green lineages. Front. Plant Sci. *5*, 187

Kleist, T.J., Cartwright, H.N., Perera, A.M., Christianson, M.L., Lemaux, P.G., and Luan, S. (2017). Genetically encoded calcium indicators for fluorescence imaging in the moss *Physcomitrella* : GCaMP3 provides a bright new look. Plant Biotechnol. J. *15*, 1235–1237.

Komatsu, K., Suzuki, N., Kuwamura, M., Nishikawa, Y., Nakatani, M., Ohtawa, H., Takezawa, D., Seki, M., Tanaka, M., and Taji, T. (2013). Group A PP2Cs evolved in land plants as key regulators of intrinsic desiccation tolerance. Nat. Commun. *4*.

Koske, R.E., and Gemma, J.N. (1989). A modified procedure for staining roots to detect VA mycorrhizas. Mycol. Res. *92*, 486–488.

Lang, C., Smith, L.S., and Long, S.R., 2018. Characterization of novel plant symbiosis mutants using a new multiple gene-expression reporter *Sinorhizobium meliloti* strain. Front. Plant Sci. *9*, 1–16.

Lang, D., Ullrich, K.K., Murat, F., Fuchs, J., Jenkins, J., Haas, F.B., Piednoel, M., Gundlach, H., Van Bel, M., Meyberg, R., *et al.* (2018). The *Physcomitrella patens*

chromosome-scale assembly reveals moss genome structure and evolution. Plant J. *93*, 515–533.

Levy, J., Bres, C., Geurts, R., Chalhoub, B., Kulikova, O., Duc, G., Journet, E.P., Ané, J.M., Lauber, E., Bisseling, T., and Denarie, J. (2004). A putative Ca^{2+} and calmodulin-dependent protein kinase required for bacterial and fungal symbioses. Science *303*, 1361–1364.

de León, I.P., Hamberg, M., and Castresana, C. (2015). Oxylipins in moss development and defense. Front. Plant Sci. *6*, 483.

Ma, F., Lu, R., Liu, H., Shi, B., Zhang, J., Tan, M., Zhang, A., and Jiang, M. (2012). Nitric oxide-activated calcium/calmodulin-dependent protein kinase regulates the abscisic acid-induced antioxidant defence in maize. J. Exp. Bot. *63*, 4835–4847.

Maillet, F., Poinsot, V., Andre, O., Puech-Pagès, V., Haouy, A., Gueunier, M., Cromer, L., Giraudet, D., Formey, D., and Niebel, A. (2011). Fungal lipochitooligosaccharide symbiotic signals in arbuscular mycorrhiza. Nature *469*, 58–63.

Mann, D.G.J., LaFayette, P.R., Abercrombie, L.L., King, Z.R., Mazarei, M., Halter, M.C., Poovaiah, C.R., Baxter, H., Shen, H., and Dixon, R.A. (2012). Gateway-compatible vectors for high-throughput gene functional analysis in switchgrass (*Panicum virgatum* L.) and other monocot species. Plant Biotechnol. J. *10*, 226–236.

Messinese, E., Mun, J.-H., Yeun, L.H., Jayaraman, D., Rougé, P., Barre, A., Lougnon, G., Schornack, S., Bono, J.-J., and Cook, D.R. (2007). A novel nuclear protein interacts with the symbiotic DMI3 calcium-and calmodulin-dependent protein kinase of *Medicago truncatula*. Mol. Plant Microbe Interact. *20*, 912–921.

Miller, J.B., Pratap, A., Miyahara, A., Zhou, L., Bornemann, S., Morris, R.J., and Oldroyd, G.E.D. (2013). Calcium/Calmodulin-dependent protein kinase is negatively and positively regulated by calcium, providing a mechanism for decoding calcium responses during symbiosis signaling. Plant Cell *25*, 5053–5066.

Miyata, K., Kozaki, T., Kouzai, Y., Ozawa, K., Ishii, K., Asamizu, E., Okabe, Y., Umehara, Y., Miyamoto, A., Kobae, Y., *et al.* (2014). Bifunctional plant receptor, OsCERK1, regulates both chitin-triggered immunity and arbuscular mycorrhizal symbiosis in rice. Plant Cell Physiol. *55*, 1864–1872.

Mun, T., Bachmann, A., Gupta, V., Stougaard, J., and Andersen, S.U. (2016). Lotus Base: An integrated information portal for the model legume *Lotus japonicus*. Sci. Rep. *6*, 1–18.

Okada, M., Takezawa, D., Tachibanaki, S., Kawamura, S., Tokumitsu, H., and Kobayashi, R. (2003). Neuronal calcium sensor proteins are direct targets of the insulinotropic agent repaglinide. Biochem. J. *375*, 87-97.

Oldroyd, G.E.D. (2013). Speak, friend, and enter: signalling systems that promote beneficial symbiotic associations in plants. Nat. Rev. Microbiol. *11*, 252–263.

Oliver, J.P., Castro, A., Gaggero, C., Cascón, T., Schmelz, E.A., Castresana, C., and de León, I.P. (2009). *Pythium* infection activates conserved plant defense responses in mosses. Planta *230*, 569–579.

Ondzighi-Assoume, C.A., Chakraborty, S., and Harris, J.M. (2016). Environmental nitrate stimulates abscisic acid accumulation in arabidopsis root tips by releasing it from inactive stores. Plant Cell *28*, 729–745.

Ortiz-Ramírez, C., Hernandez-Coronado, M., Thamm, A., Catarino, B., Wang, M., Dolan, L., Feijó, J.A.A., and Becker, J.D.D. (2016). A Transcriptome atlas of *Physcomitrella patens* provides insights into the evolution and development of land plants. Mol. Plant *9*, 205–220.

Parniske, M. (2008). Arbuscular mycorrhiza: the mother of plant root endosymbioses. Nat. Rev. Microbiol. *6*, 763–775.

Pirozynski, K.A., and Malloch, D.W. (1975). The origin of land plants: a matter of mycotrophism. Biosystems *6*, 153–164.

Ponce de León, I. (2011). The moss *Physcomitrella patens* as a model system to study interactions between plants and phytopathogenic fungi and oomycetes. J. Pathog. 719873.

Pressel, S., and Duckett, J.G. (2010). Cytological insights into the desiccation biology of a model system: moss protonemata. New Phytol. *185*, 944–963.

Pressel, S., Bidartondo, M.I., Ligrone, R., and Duckett, J.G. (2010). Fungal symbioses in bryophytes: new insights in the twenty first century. Phytotaxa *9*, 238.

R Core Team (2014). R: A language and environment for statistical computing. R Foundation for Statistical Computing, Vienna, Austria. Available online at https://www.R-project.org/.

Rabatin, S.C. (1980). The occurrence of the vesicular-arbuscular-mycorrhizal fungus *Glomus tenuis* with moss. Mycologia *72*, 191–195.

Radhakrishnan, G. V., Keller, J., Rich, M.K., Vernié, T., Mbadinga Mbadinga, D.L., Vigneron, N., Cottret, L., Clemente, H.S., Libourel, C., Cheema, J., Linde, A.M., Eklund, D.M., Cheng, S., Wong, G.K.S., Lagercrantz, U., Li, F.W., Oldroyd, G.E.D., and Delaux, P.M. (2020). An ancestral signalling pathway is conserved in intracellular symbioses-forming plant lineages. Nat. Plants *6*, 280–289.

Read, D.J., Duckett, J.G., Francis, R., Ligrone, R., and Russell, A. (2000). Symbiotic fungal associations in “lower” land plants. Philos. Trans. R. Soc. Lond. B. Biol. Sci. *355*, 815–830; discussion 830-831.

Redecker, D., Kodner, R., and Graham, L.E. (2000). Glomalean fungi from the Ordovician. Science *289*, 1920–1921.

Remy, W., Taylor, T.N., Hass, H., and Kerp, H. (1994). Four hundred-million-year-old vesicular arbuscular mycorrhizae. Proc. Natl. Acad. Sci. *91*, 11841–11843.

Rensing, S.A., Lang, D., Zimmer, A.D., Terry, A., Salamov, A., Shapiro, H., Nishiyama, T., Perroud, P.-F., Lindquist, E.A., and Kamisugi, Y. (2008). The *Physcomitrella* genome reveals evolutionary insights into the conquest of land by plants. Science *319*, 64–69.

Routray, P., Miller, J.B., Du, L., Oldroyd, G., and Poovaiah, B.W. (2013). Phosphorylation of S344 in the calmodulin-binding domain negatively affects CCaMK function during bacterial and fungal symbioses. Plant J. *76*, 287–296.

Schiessl, K., Lilley, J.L.S., Lee, T., Tamvakis, I., Kohlen, W., Bailey, P.C., Thomas, A., Luptak, J., Ramakrishnan, K., Carpenter, M.D., Mysore, K.S., Wen, J., Ahnert, S., Grieneisen, V.A., and Oldroyd, G.E.D. (2019). NODULE INCEPTION Recruits the Lateral Root Developmental Program for Symbiotic Nodule Organogenesis in *Medicago truncatula*. Curr. Biol. *29*, 3657-3668.

Schindelin, J., Arganda-Carreras, I., Frise, E., Kaynig, V., Longair, M., Pietzsch, T., Preibisch, S., Rueden, C., Saalfeld, S., Schmid, B. and Tinevez, J.Y. (2012). Fiji: an open-source platform for biological-image analysis. Nat. Methods *9*, 676-682.

Schnepf, E. and Reinhard, C. (1997). Brachycytes in *Funaria* protonemate: induction by abscisic acid and fine structure. J. Plant Physiol. *151*, 166–175.

Shi, B., Ni, L., Zhang, A., Cao, J., Zhang, H., Qin, T., Tan, M., Zhang, J., and Jiang, M. (2012). *OsDMI3* is a novel component of abscisic acid signaling in the induction of antioxidant defense in leaves of rice. Mol. Plant *5*, 1359–1374.

Shi, B., Ni, L., Liu, Y., Zhang, A., Tan, M., and Jiang, M. (2014). OsDMI3-mediated activation of OsMPK1 regulates the activities of antioxidant enzymes in abscisic acid signalling in rice. Plant Cell Environ. *37*, 341–352.

Shinde, S., Nurul Islam, M., and Ng, C.K. (2012). Dehydration stress-induced oscillations in LEA protein transcripts involves abscisic acid in the moss, *Physcomitrella patens*. New Phytol. *195*, 321–328.

Shinde, S., Shinde, R., Downey, F., and Ng, C.K. (2013). Abiotic stress-induced oscillations in steady-state transcript levels of Group 3 LEA protein genes in the moss, *Physcomitrella patens*. Plant Signal. Behav. *8*, e22535.

Singh, S., Katzer, K., Lambert, J., Cerri, M., and Parniske, M. (2014). CYCLOPS, A DNA-binding transcriptional activator, orchestrates symbiotic root nodule development. Cell Host Microbe *15*, 139–152.

Smith, S.E. and Read, D.J. (2010). Mycorrhizal symbiosis (Academic press).

Spatafora, J.W., Chang, Y., Benny, G.L., Lazarus, K., Smith, M.E., Berbee, M.L., Bonito, G., Corradi, N., Grigoriev, I., and Gryganskyi, A. (2016). A phylum-level phylogenetic classification of zygomycete fungi based on genome-scale data. Mycologia *108*, 1028–1046.

Strullu-Derrien, C., Kenrick, P., Pressel, S., Duckett, J.G., Rioult, J.P., and Strullu, D.G. (2014). Fungal associations in *Horneophyton ligneri* from the Rhynie Chert

(c. 407 million year old) closely resemble those in extant lower land plants: novel insights into ancestral plant-fungus symbioses. New Phytol. *203*, 964–979.

Strullu-Derrien, C., Wawrzyniak, Z., Goral, T., and Kenrick, P. (2015). Fungal colonization of the rooting system of the early land plant *Asteroxylon mackiei* from the 407-Myr-old Rhynie Chert (Scotland, UK). Bot. J. Linn. Soc. *179*, 201–213.

Sun, J., Miller, J.B., Granqvist, E., Wiley-Kalil, A., Gobbato, E., Maillet, F., Cottaz, S., Samain, E., Venkateshwaran, M., and Fort, S. (2015). Activation of symbiosis signaling by arbuscular mycorrhizal fungi in legumes and rice. Plant Cell *27*, 823–838.

Takeda, N., Maekawa, T., and Hayashi, M. (2012). Nuclear-localized and deregulated calcium- and calmodulin-dependent protein kinase activates rhizobial and mycorrhizal responses in *Lotus japonicus*. Plant Cell *24*, 810–822.

Takezawa, D., Watanabe, N., Ghosh, T.K., Saruhashi, M., Suzuki, A., Ishiyama, K., Somemiya, S., Kobayashi, M., and Sakata, Y. (2015). Epoxycarotenoid-mediated synthesis of abscisic acid in *Physcomitrella patens* implicating conserved mechanisms for acclimation to hyperosmosis in embryophytes. New Phytol. *206*, 209–219.

Tang, H., Krishnakumar, V., Bidwell, S., Rosen, B., Chan, A., Zhou, S., Gentzbittel, L., Childs, K.L., Yandell, M., Gundlach, H., *et al.* (2014). An improved genome release (version Mt4.0) for the model legume *Medicago truncatula*. BMC Genomics *15*, 1–14.

Tirichine, L., Imaizumi-Anraku, H., Yoshida, S., Murakami, Y., Madsen, L.H., Miwa, H., Nakagawa, T., Sandal, N., Albrektsen, A.S., Kawaguchi, M., *et al.* (2006). Deregulation of a Ca^{2+}/calmodulin-dependent kinase leads to spontaneous nodule development. Nature *441*, 1153–1156.

Tukey, J.W. (1949) Comparing individual means in the analysis of variance. Biometrics *5*, 99–114.

Venkateshwaran, M., Volkening, J.D., Sussman, M.R., and Ané, J.-M. (2013). Symbiosis and the social network of higher plants. Curr. Opin. Plant Biol. *16*, 118–127.

Vesty, E.F., Saidi, Y., Moody, L.A., Holloway, D., Whitbread, A., Needs, S., Choudhary, A., Burns, B., McLeod, D., and Bradshaw, S.J. (2016). The decision to germinate is regulated by divergent molecular networks in spores and seeds. New Phytol. *211*, 952–966.

Wang, B. and Qiu, Y.-L.Y.L. (2006). Phylogenetic distribution and evolution of mycorrhizas in land plants. Mycorrhiza *16*, 299–363.

Wang, B., Yeun, L.H., Xue, J.Y., Liu, Y., Ané, J.-M., and Qiu, Y.L. (2010). Presence of three mycorrhizal genes in the common ancestor of land plants suggests a key

role of mycorrhizas in the colonization of land by plants. New Phytol. *186*, 514–525.

Wang, C., Liu, Y., Li, S.-S., and Han, G.-Z. (2015). Insights into the origin and evolution of the plant hormone signaling machinery. Plant Physiol. *167*, 872–886.

Xue, L., Cui, H., Buer, B., Vijayakumar, V., Delaux, P.-M., Junkermann, S., and Bucher, M. (2015). Network of GRAS transcription factors involved in the control of arbuscule development in *Lotus japonicus*. Plant Physiol. *167*, 854–871.

Yan, J., Guan, L., Sun, Y., Zhu, Y., Liu, L., Lu, R., Jiang, M., Tan, M., and Zhang, A. (2015). Calcium and ZmCCaMK are involved in brassinosteroid-induced antioxidant defense in maize leaves. Plant Cell Physiol. *56*, 883–896.

Yang, C., Li, A., Zhao, Y., Zhang, Z., Zhu, Y., Tan, X., Geng, S., Guo, H., Zhang, X., and Kang, Z. (2011). Overexpression of a wheat *CCaMK* gene reduces ABA sensitivity of *Arabidopsis thaliana* during seed germination and seedling growth. Plant Mol. Biol. Report. *29*, 681–692.

Yano, K., Yoshida, S., Müller, J., Singh, S., Banba, M., Vickers, K., Markmann, K., White, C., Schuller, B., Sato, S., *et al.* (2008). CYCLOPS, a mediator of symbiotic intracellular accommodation. Proc. Natl. Acad. Sci. *105*, 20540–20545.

Yotsui, I., Saruhashi, M., Kawato, T., Taji, T., Hayashi, T., Quatrano, R.S., and Sakata, Y. (2013). ABSCISIC ACID INSENSITIVE3 regulates abscisic acid-responsive gene expression with the nuclear factor Y complex through the ACTT-core element in *Physcomitrella patens*. New Phytol. *199*, 101–109.

Young, N.D., Debellé, F., Oldroyd, G.E.D., Geurts, R., Cannon, S.B., Udvardi, M.K., Benedito, V.A., Mayer, K.F.X., Gouzy, J., Schoof, H., *et al.* (2011). The *Medicago* genome provides insight into the evolution of rhizobial symbioses. Nature *480*, 520–524.

Chapter 3 – Genetic dissection of the functional role of HMGRs in the common symbiosis pathway in legumes

3.1 – Abstract

The mevalonate pathway, controlled mainly at the point of 3-hydroxy-3-methylglutaryl coenzyme-A reductases (HMGR), is an essential metabolic pathway in eukaryotes for numerous cellular processes. The production of an extensive collection of isoprenoid compounds stemming from the mevalonate pathway serves a variety of roles in membrane structure, post-translational modifications, and electron transfer. Compared to other eukaryotes, large HMGR gene families in plants likely provide an increased ability to regulate HMGR activity and a diverse variety of isoprenoids with different functions. In addition to roles in photosynthesis and pathogen defense in plants, HMGR serves an essential role in symbiotic associations with rhizobia bacteria and arbuscular mycorrhizal fungi. It is currently unclear which HMGRs or how many of them function in these symbioses. In this chapter, we investigated the involvement of numerous HMGR family members in nodule development using the model legume *Medicago truncatula*. With an analysis of individual HMGR knockout mutants, we provided evidence for the role of multiple HMGRs, namely HMGR1 and HMGR2c, in root nodule symbiosis. The observed defects in nodules containing rhizobia expressing essential components for nitrogenase activity in these mutants also revealed a novel role for HMGRs in the late stages of nodule development. Also included are our attempts at targeting multiple HMGRs for knockout/knockdown of expression through CRISPR/Cas9 and amiRNA although these experiments were mostly inconclusive.

Together with previous knowledge, these findings suggest functional redundancy and additive roles of HMGRs in nodule development.

3.2 – Introduction

3-hydroxy-3-methylglutaryl coenzyme-A reductases (HMGRs) are enzymes that reduce HMG-CoA into mevalonate in a NADPH dependent process. This reaction serves as the rate-limiting step in the highly branched mevalonate pathway, which is conserved throughout eukaryotes and is present in some bacteria and archaea. Through the activity of HMGR and other downstream enzymes, the mevalonate pathway produces an extensive variety of isoprenoids (Friesen and Rodwell, 2004). These compounds are organic molecules consisting of multiple 5-carbon units and serve diverse physiological functions. Some such products produced throughout eukaryotes include dolichols, ubiquinone, isopentenylated tRNAs, and sterols, most notable being the essential cell membrane component cholesterol (Stermer et al., 1994).

HMGRs are typically composed of three separate domains: an N-terminal domain, a C-terminal domain, and a linker domain. The N-terminal region consists of multiple transmembrane helices anchoring the protein to lipid membranes (Li et al., 2014). Animal HMGRs contain eight membrane-spanning loops, while plant HMGRs differ in having only two (Stermer et al., 1994). This transmembrane region is responsible for localizing these proteins to the endoplasmic reticulum (Ferrero et al., 2015). The C-terminal domain serves as the catalytic region responsible for binding NADPH and HMG-CoA and catalyzing the reduction to mevalonate. The linker domain

connects the N- and C-terminal domains. While the linker and N-terminal transmembrane domain sequences vary considerably, the catalytic domain is highly conserved throughout HMGR proteins (Li et al., 2014).

The mevalonate pathway is even more extensive in plants due to multiple HMGR isoforms and additional branching points stemming from the main pathway. These features allow for differential regulation of the mevalonate pathway and a wider variety of produced isoprenoids. In combination with the plastid localized methylerythritol phosphate (MEP) pathway, the mevalonate pathway produces tens of thousands of different isoprenoid compounds, most unique to plants (Holstein and Hohl, 2004). Some plant isoprenoids, such as cytokinins, serve functions in growth regulation. Others are essential for photosynthesis, such as carotenoids and chlorophylls. In both plant and animal systems farnesyl pyrophosphate and geranylgeranyl pyrophosphate can serve as prenyl side chains to localize protein to membranes and regulate their activity. Other isoprenoids are plant defense molecules (monoterpenes), membrane components (sterols), and vitamins, to name a few (Holstein and Hohl, 2004). As observed in *hmgr1* knockout mutants in *Arabidopsis thaliana*, HMGRs are involved in endoplasmic reticulum organization as these mutants accumulate ER bodies near the nuclear envelope (Ferrero et al., 2015). *Arabidopsis thaliana hmgr1*, but not *hmgr2,* mutants also are dwarf, senesce early, and are male-sterile (Suzuki et al., 2004) Additionally, *hmgr1/2* double mutants in *A. thaliana* are also male-sterile are unable to synthesize mevalonate, demonstrating an essential role for HMGRs in male gametophyte development (Suzuki et al., 2009).

HMGR activity additionally has been identified as having a role in the subcellular signaling pathway responsible for forming beneficial plant-microbe interactions (Kevei et al., 2007). This signaling pathway shares numerous molecular components necessary for forming both the root nodule and arbuscular mycorrhizal symbioses, and is thus referred to as the “common symbiosis pathway.” In either case, the host plant typically detects the presence of the microbial partner through the binding of chitin-based signaling molecules by Lys-M receptor-like kinases (RLKs) located on the plasma membrane (Radutoiu et al., 2003). The signal activates another plasma membrane RLK, DMI2/NORK (Endre et al., 2002; Stracke et al., 2002). Various poorly understood secondary messengers transduce the signal from the plasma membrane to the nuclear envelope, ultimately leading to activation of nuclear ion channels, such as the calcium-sensitive calcium channel, DMI1, through unknown mechanisms (Ané et al., 2004; Kim et al., 2019). The activity of DMI1, combined with other ion channels and pumps, generates oscillations of high and low concentrations of calcium in the nucleus. These oscillations, or “nuclear calcium spikes,” are then interpreted by a calcium and calmodulin binding protein kinase, DMI3/CCaMK (Lévy et al., 2004). Activation of DMI3/CCaMK, in turn, phosphorylates the transcription factor IPD3/CYCLOPS, leading to a cascading induction of a network of other transcription factors which induce the expression of symbiotic genes responsible for the development of either nodules or arbuscules (Charpentier and Oldroyd, 2013).

Nodule development and bacterial colonization typically begin with the attachment of rhizobia to root hairs that curl around and entrap a bacterial microcolony. The bacteria then invade the root through invagination of the plant cell membrane,

termed an infection thread, at the point of attachment and travel through the root hair to the root epidermis. In the root cortex, below the infection zone, cortical cells re-enter the cell cycle to form a nodule meristem. As the nodule cells proliferate in a full nodule, the infection thread enters the nodule and branches throughout (Oldroyd, 2013). The bacteria are released into nodule cells through budding of the infection thread, encapsulated by the plant membrane into symbiosomes, and differentiate into bacteroids. The fully developed nodule expressing leghemoglobin provides an anaerobic environment for the bacteria to express *nifH*, *nifD,* and *nifK* for fixing nitrogen (Jones et al., 2007). The leguminous host plant then exchanges photosynthates for the microbially fixed ammonia, benefiting both organisms and ultimately preventing nitrogen deficiency, increasing crop yield.

An HMGR was initially identified as a possible component of the common symbiosis pathway through screening of interacting protein partners of DMI2/NORK, a major signaling component in the pathway. In *M. truncatula*, HMGR1 interacts with the symbiotic co-receptor DMI2/NORK, as confirmed by yeast two-hybrid and co-immunoprecipitation (Kevei et al., 2007). A role for HMGRs in symbiotic interactions is also supported by the ability of lovastatin, a pharmaceutical inhibitor of HMGR activity, to reduce nodulation in *M. truncatula*. Experiments knocking down the *MtHMGR* expression also resulted in a drastic reduction in nodule number (Kevei et al., 2007). Additionally, further evidence suggests that mevalonate, the product of HMGR activity, can stimulate multiple symbiotic signaling responses (Venkateshwaran et al., 2015).

While evidence points to a role for HMGR in symbiotic signaling for the development of root nodules in legumes, the involvement of specific HMGRs in this

process remains unclear. Herein, we investigate the possibility of functional redundancy between HMGRs and the extent to which various members of the HMGR protein family are essential for nodulation in *M. truncatula*. We used a combination of *Tnt1* retrotransposon insertion knockout, CRISPR/Cas9 deletion knockout, and amiRNA knockdown methods for altering the expression of individual and multiple HMGRs. With our findings, we showed that multiple HMGRs are involved in nodule development as individual *hmgr1-1* and *hmgr2c-1* display nodule defects.

3.3 – Materials and Methods

Sequence analysis of M. truncatula HMGRs. To identify all *HMGR* genes present in *M. truncatula* Jemalong A17 genome we performed BLASTn with the coding sequence of *HMGR1* described in Kevei et al., (2007) against *M. truncatula* Jemalong A17 genome assembly v5r1.7 CDS sequences (Pecrix et al., 2018). The Chr5g0409001 sequence was further analyzed with the Softberry online gene prediction tool, FGENESH, and revealed the presence of two genes in this region. To identify all *HMGRs* present in *M. truncatula* R108, BLASTn was performed with *HMGR* coding sequence from Jemalong A17 against the *M. truncatula* R108 v1.0 genome. The returned subject range of the top hits for each BLAST were then analyzed for the presence of HMGR-like genes with the FGENESH+ program (http://www.softberry.com/) using the protein sequence of the corresponding HMGR used for BLAST. Sequence similarity between *HMGRs* of *M. truncatula* R108 was determined using sequence alignment and genetic distance analysis with Geneious (https://www.geneious.com).

Identification of individual HMGR knockout mutant lines in Medicago truncatula. As *M. truncatula* is a model organism for the study of legumes, an extensive database of numerous genetic insertional knockout mutants is available, created through the use of the *Tnt1* retrotransposon (Tadege et al., 2008). This database was screened through BLASTn of each *M. truncatula* R108 *HMGR* sequence against the *Tnt1* flanking sequence tag (FST) - High Confidence sequences. The top 10 returned FST hits for each *HMGR* were then reciprocally aligned with each *HMGR* sequence to determine the most similar matches to particular *HMGRs*. For each *M. truncatula HMGR* sequence with strong alignments to FSTs (*HMGR1, HMGR2a, HMGR2b, HMGR2c, HMGR3, HMGR4, HMGR5*), the mutant seed lines corresponding to the top three FST matches were ordered. With PCR genotyping on leaves of a minimum of 10 plants per *Tnt1* insertion line, the presence of a *Tnt1* retrotransposon insert in the corresponding *HMGR* was confirmed and determined to be either a heterozygous or homozygous insertion. PCR screening was performed with three PCR reactions per plant; (1) using forward and reverse primers of the *HMGR* gene of interest, (2) using a forward *HMGR* gene of interest primer and a *Tnt1* forward outer primer, and (3) using a reverse *HMGR* gene of interest primer and a *Tnt1* forward outer primer. Lines with homozygous inserts were carried forward, and purified PCR products from amplification of the *Tnt1* to HMGR spanning region were sent to the UW-Madison Biotechnology Center for Sanger sequencing to determine the precise insert location.

Artificial miRNA design. Artificial miRNAs for the knockdown of the expression of various HMGRs were designed using the web microRNA designer tool, WMD3 (http://wmd3.weigelworld.org/cgi-bin/webapp.cgi). Combinations of *HMGR1* + *HMGR2a,*

HMGR2b+HMGR2c, HMGR2a+HMGR2b+HMGR2c, and *HMGR1* + *HMGR2a* + *HMGR2b* + *HMGR2c* coding sequences were submitted as targets using the *M. truncatula* Mt.3.5 genome from the J. Craig Venter Institute (JCVI) as a reference and accepting no off-targets. All returned miRNA sequences were manually verified to target each of the intended HMGR targets and have no unintended HMGR off-targets using sequence alignment of miRNAs to *M. truncatula* R108 *HMGR* coding sequences. Each *HMGR* amiRNA sequence was integrated into a pre-miR319a backbone with the corresponding amiRNA* and synthesized for compatibility with GoldenGate cloning.

CRISPR/Cas9 sgRNA design. For deleting the four tandem *HMGR* genomic region containing H*MGR2a, HMGR2c, HMGR2b,* and *HMGR1*, candidate sgRNA sequences targeting *HMGR1* and *HMGR2a* were generated with the CRISPOR web tool (Concordet and Haeussler, 2018). The genetic region spanning one kb upstream and downstream of the start codon of *HMGR2a* was searched for specific twenty bp gRNA sequences with “NGG” PAM sequences compatible with SpCas9. The same relative region of *HMGR1* was scanned for 20 bp gRNA sequences in the same way. We selected the top two specificity scoring sequences with two or more mismatches with the other *M. truncatula HMGR* sequences for both targeted regions and one gRNA sequence specific to both regions. The five selected gRNAs were connected together alternating with tRNA spacer sequences into a polycistronic fragment, followed by a poly T Pol III terminator, and synthesized for GoldenGate compatibility.

Molecular cloning and plasmid construction. All cloning was performed using GoldenGate methods (Binder et al., 2014; Engler et al., 2008). *HMGR* amiRNAs were

assembled into GoldenGate level 1 acceptors along with a *GmSUBI3* promoter and *AtuMas7* terminator. The *HMGR* CRISPR construct was assembled by first assembling the tDNA spaced five sgRNA sequence fragment with an *AtU6-26* promoter in a GoldenGate level 1 acceptor plasmid. For both HMGR amiRNA and HMGR CRISPR binary vector design, each GoldenGate level 1 part was subsequently inserted into a GoldenGate level 2 acceptor along with a red fluorescent reporter, tdTomato, and a nuclear-localized G-GECO1.2.

Agrobacterium-mediated plant transformation. All binary vectors for plant transformation were transformed into *Agrobacterium rhizogenes* MSU440 with electroporation. To generate transgenic roots, *M. truncatula* R108 plants were germinated and transformed with *A. rhizogenes* MSU440 containing the HMGR amiRNA or HMGR CRISPR binary vectors via the *Agrobacterium* mediated composite root transformation method (Delaux et al., 2015).

Medicago growth conditions and symbiotic phenotype screening. Wild-type, *Tnt1* mutant, and transgenic-root-containing *M. truncatula* R108 plants were grown at 22°C in a growth chamber with 100 µmol/m^2/s^1 continuous light. Nodulation assays were performed according to the procedures described in (Kim et al., 2019) using the multi-reporter *Sinorhizobium meliloti* strain CL304 (Lang et al., 2018). For experiments using *Tnt1* retrotransposon insertion lines, plants were harvested two weeks post-inoculation. For experiments using plants containing transgenic roots, plants were harvested three weeks post-inoculation. Following harvesting, whole root systems were stained according to (Schiessl et al., 2019) with GUS staining solution, without the

prefixation step, to observe *nifH::GUS* expression in nodules. HMGR amiRNA transformed roots used in qRT-PCR analysis were flash-frozen in liquid nitrogen after harvest and subject to RNA extraction using the Quick-RNA Miniprep Kit (Zymo Research), following the manufacturer's instructions. TURBO DNA-free Kit (Thermo Fisher Scientific) was used to remove the remaining DNA from the RNA samples. First-strand cDNA of 200ng RNA was synthesized using the RevertAid Reverse Transcriptase Kit (Thermo Fisher Scientific).

Quantitative Reverse Transcriptase PCR. Transgenic roots expressing *HMGR* amiRNA constructs were assayed for their relative *HMGR* transcript levels with qRT-PCR to verify a reduction in *HMGR* expression. SsoAdvanced Universal SYBR Green Supermix (Bio-Rad Laboratories) was used for the qRT-PCR in conjunction with a CFX Real-Time PCR System (Bio-Rad Laboratories). Due to high sequence similarity between many *HMGRs*, specific primers for each individual *HMGR* sequence were unable to be designed. We designed qRT-PCR primers spanning intron-exon junctions specifically for *HMGR1*; for any of *HMGR2a, HMGR2b, HMGR2c*; for any of *HMGR1, HMGR2a, HMGR2b, HMGR2c*; and specifically *HMGR6* and optimized them to determine their efficiency. Only primers with an efficiency between 90% and 110% were used. Expression levels of *HMGR1, HMGR2a, HMGR2b,* and *HMGR2c* combined and *HMGR6* were determined in each of the HMGR amiRNA mutants with primers targeting *HMGR1+HMGR2a+HMGR2b+HMGR2c* and primers for *HMGR6*. qRT-PCR was performed on three separate transgenic roots for each construct with three technical replicates for each biological replicate. Additionally, the expression of two housekeeping genes, *MtSecA* and *MtPDF2*, were measured and used for references in each sample.

The analysis of the qRT-PCR data was performed using CFX Manager Software (Bio-Rad Laboratories).

CRISPR/Cas9 deletion screening. Four rounds of *M. truncatula* R108 transformation were performed with the four HMGR-spanning CRISPR deletion constructs. A total of 183 transgenic tdTomato-expressing roots were identified with fluorescent microscopy and sampled. Each root sample was screened with PCR genotyping to identify roots containing the ≈17 Kb deletion spanning from *HMGR2a to HMGR1*. Two PCR reactions were performed on each sample, (1) using a primer upstream of the leftmost sgRNA target site (HMGR_5g_geno_F3) and primer downstream of the rightmost sgRNA target site in the opposite orientation (HMGR_5g_geno_R2) and (2) using a forward and reverse *MtHMGR1* primer.

Statistical analysis. For nodulation assays of *hmgr Tnt1* insertion mutants, each mutant line was compared to wild-type *M. truncatula* R108 plants for differences in total nodule number and number of nodules containing *PnifH::GUS* expressing rhizobia. The data were first tested for equality of variance with Levene's test for each wild-type vs. *hmgr Tnt1* mutant. For data sets with equal variance, we tested for differences in means with Student's T-Test. For data sets with unequal variance, differences in means were determined by Welch's T-Test. Samples sizes for *hmgr Tnt1* insert mutant nodulation assays ranged from 22 to 29 plants. Levene's test performed on HMGR amiRNA nodulation assay data determined equality of variance between samples for both observed phenotypes. As nodulation assays for HMGR1+2a amiRNA, HMGR2b+2c amiRNA, and HMGR2a+2b+2c amiRNA roots were performed side by side, samples

were compared for differences in means by one-way ANOVA. Statistical analysis for determining differences in total nodule number and number of nodules with *nifH::GUS* expressing rhizobia for HMGR12a+2b+2c amiRNA transgenic roots was performed as described for *hmgr Tnt1* mutant nodulation assays. The sample size was 44 plants for *HMGR1+2a+2b+2c amiRNA* nodulation analysis and was 61 roots for the analysis of HMGR1+2a amiRNA, HMGR2b+2c amiRNA, and HMGR1+2a+2b+2c amiRNA nodulation. Levene's test was performed on both the HMGR1+2a+2b+2c and HMGR6 qRT-PCR expression data to test for equal variance between the EV, HMGR1+2a, and HMGR1+2a+2b+2c amiRNA transformed samples. To compare differences in *HMGR1+2a+2b+2*c expression and in *HMGR6* expression between the EV, HMGR1+2a, and HMGR1+2a+2b+2c amiRNA transformed samples we performed a one-way ANOVA for each primer set. Each HMGR amiRNA group contained a sample size of three.

3.4 – Results

Medicago truncatula contains a large multigenic HMGR family

The expression of HMGR protein family members in plants is more complicated than in other eukaryotes due to the presence of multiple genes coding for HMGR. While not the largest, the HMGR family in *M. truncatula* genotypes is particularly extensive. We performed sequence analysis of both *M. truncatula* R108 and *M. truncatula* Jemalong A17 to identify all the genes coding for HMGR present in these genotypes and how they differ within and between ecotypes as both are often used as model organisms. Our genome analysis of *M. truncatula* A17 Mt5.0 (Pecrix et al., 2018) revealed the presence of eleven genes coding for HMGR, while previous publications

using an incomplete genome sequence only identified five full-length and two partial homologous sequences. MtrunA17_Chr5g0409031 (*HMGR1*), MtrunA17_Chr5g0407521 (*HMGR3*), MtrunA17_Chr5g0442831 (*HMGR4*), and MtrunA17_Chr8g0370001 (*HMGR5*) were named accordingly based on their sequence similarity to the previously identified *HMGRs*. Of the remaining seven *HMGR* sequences, six share extreme similarity to the previously named *HMGR2* sequence and are located in tandem near *HMGR1*. Therefore, we named these sequences *HMGR2a* (MtrunA17_Chr5g0408981), *HMGR2b* (MtrunA17_Chr5g0409021), *HMGR2c (MtrunA17_Chr5g0409011), HMGR2d* (MtrunA17_Chr5g0408991), *HMGR2e* (MtrunA17_Chr5g0409001), and *HMGR2f* (not annotated). The final newly identified *HMGR* sequence, MtrunA17_Chr5g0440371, was named HMGR6. Sequence analysis of *M. truncatula* R108 genome v1.0 revealed the presence of eight genes coding for HMGRs. *M. truncatula HMGR1, HMGR2a, HMGR2b, HMGR2c, and HMGR3, HMGR4,* and *HMGR6* are all located on chromosome five, while *HMGR5* is located on chromosome eight. The difference in *HMGR* number between these two genotypes is attributed to the lack of *HMGR2d, HMGR2e,* and *HMGR2f* in *M. truncatula* A17. The *M. truncatula HMGR2s* along with *HMGR1* span a roughly 18 kb chromosomal region (**Figure 1a)**. The ease of transformation and the presence of fewer *HMGR* genes in R108 ultimately led us to continue with this genotype for our research. HMGRs of *M. truncatula* share high sequence similarity with greater than 69% similarity at the protein level, and greater than 65% similarity at the CDS level in R108. The most similar sequences are those of the four tandem *HMGRs: HMGR1, HMGR2a, HMG2b*, and *HMGR2c*. These coding sequences share over 92% similarity with HMGR2b and

HMGR2c being nearly identical (99.8%) as there are only two base pair differences between them. The most genetically distant sequences are those of *HMGR1* and *HMGR6* which share only 65.5% coding sequence similarity (**Figure 1b**).

A

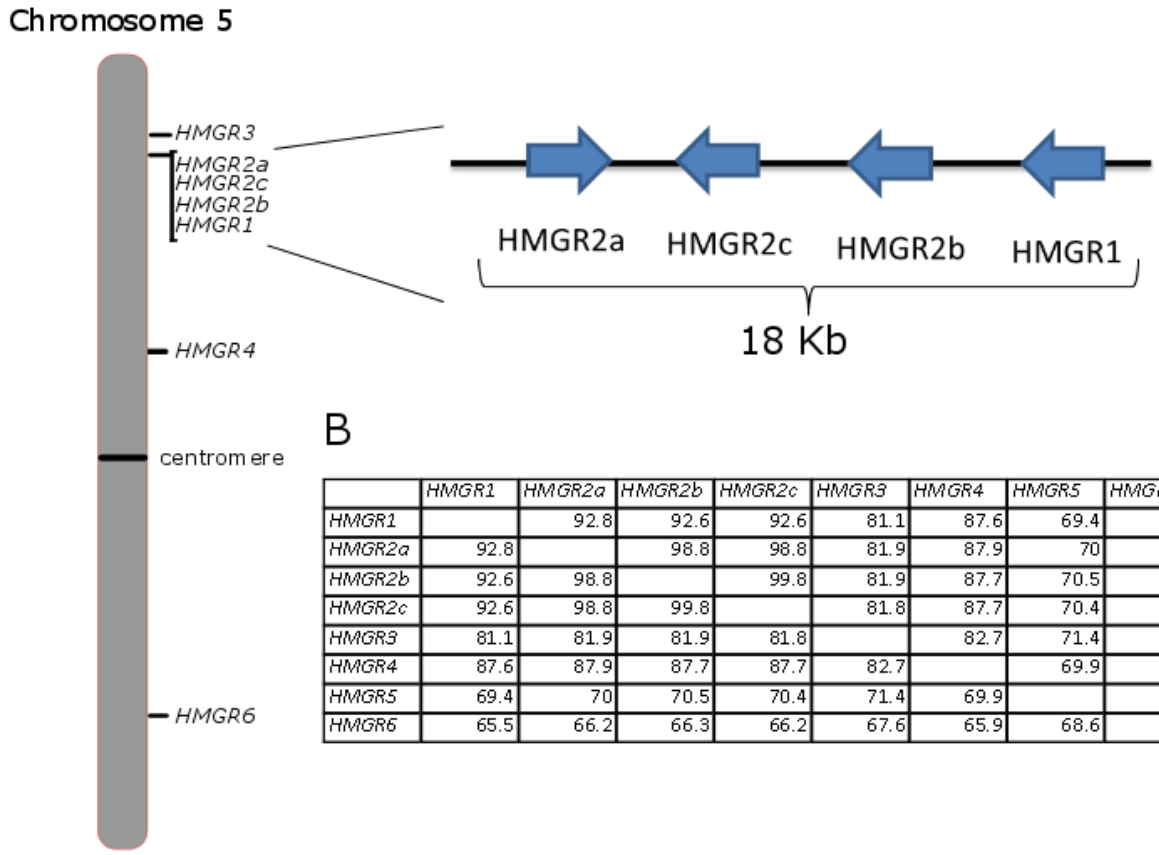

B

	HMGR1	HMGR2a	HMGR2b	HMGR2c	HMGR3	HMGR4	HMGR5	HMGR6
HMGR1		92.8	92.6	92.6	81.1	87.6	69.4	65.5
HMGR2a	92.8		98.8	98.8	81.9	87.9	70	66.2
HMGR2b	92.6	98.8		99.8	81.9	87.7	70.5	66.3
HMGR2c	92.6	98.8	99.8		81.8	87.7	70.4	66.2
HMGR3	81.1	81.9	81.9	81.8		82.7	71.4	67.6
HMGR4	87.6	87.9	87.7	87.7	82.7		69.9	65.9
HMGR5	69.4	70	70.5	70.4	71.4	69.9		68.6
HMGR6	65.5	66.2	66.3	66.2	67.6	65.9	68.6	

Figure 1: ***Medicago truncatula*** **R108 chromosomal map of HMGRs**
(**A**) Illustration of *M. truncatula* chromosome five showing the distribution of *HMGR* genes with a zoom-in of the region containing *HMGR2a, HMGR2c, HMGR2b*, and *HMGR1*. These four *HMGRs* are located in tandem spanning roughly 18 Kb with *HMGR2a* oriented on the forward strand *and HMGR2c, HMGR2b,* and *HMGR1* oriented on the reverse strand.
(B) Genetic distances between all *HMGR* coding sequences of *M. truncatula* R108. Values are shown as percent similarity between sequences.

Multiple individual HMGR knockout mutants exhibit defects in nodulation

Previous studies used RNAi to knockdown the expression of *HMGRs* and determined HMGRs are necessary for nodulation in *M. truncatula* (Kevei et al., 2007). Analysis of possible targets of the RNAi fragment (pRNAiMtHMGR1) used for knocking down *HMGR1* expression through sequence alignments with a more recent *M. truncatula* Jemalong A17 v5 genome sequence and assembly (Pecrix et al., 2018) revealed previously unidentified *HMGRs* were also targeted. In addition to pRNAiMtHMGR1 aligning with *HMGR1,* 41 bp aligned with *HMGR2a*, *HMGR2b*, *HMGR2c*, *HMGR2d, HMGR2e,* and *HMGR2f*. To assess the roles of specific individual *HMGRs* in nodule development, we used retrotransposon insertion mutant lines of *M. truncatula* R108 (Tadege et al., 2008). We identified candidate *Tnt1* mutant lines with insertions in individual *HMGRs* through BLAST and sequence alignment. We then confirmed the insertion sites with PCR genotyping and sequencing. Tnt1 mutant lines with homozygous insertions in *HMGR1* (NF1241, NF5803), *HMGR2b* (NF14664), *HMGR2c* (NF14668), *HMGR3* (NF16759), *HMGR4* (NF12019), and *HMGR5* (NF16526) were identified, while no lines containing an insert in either *HMGR2a* or *HMGR6* were found (**Figure 2**).

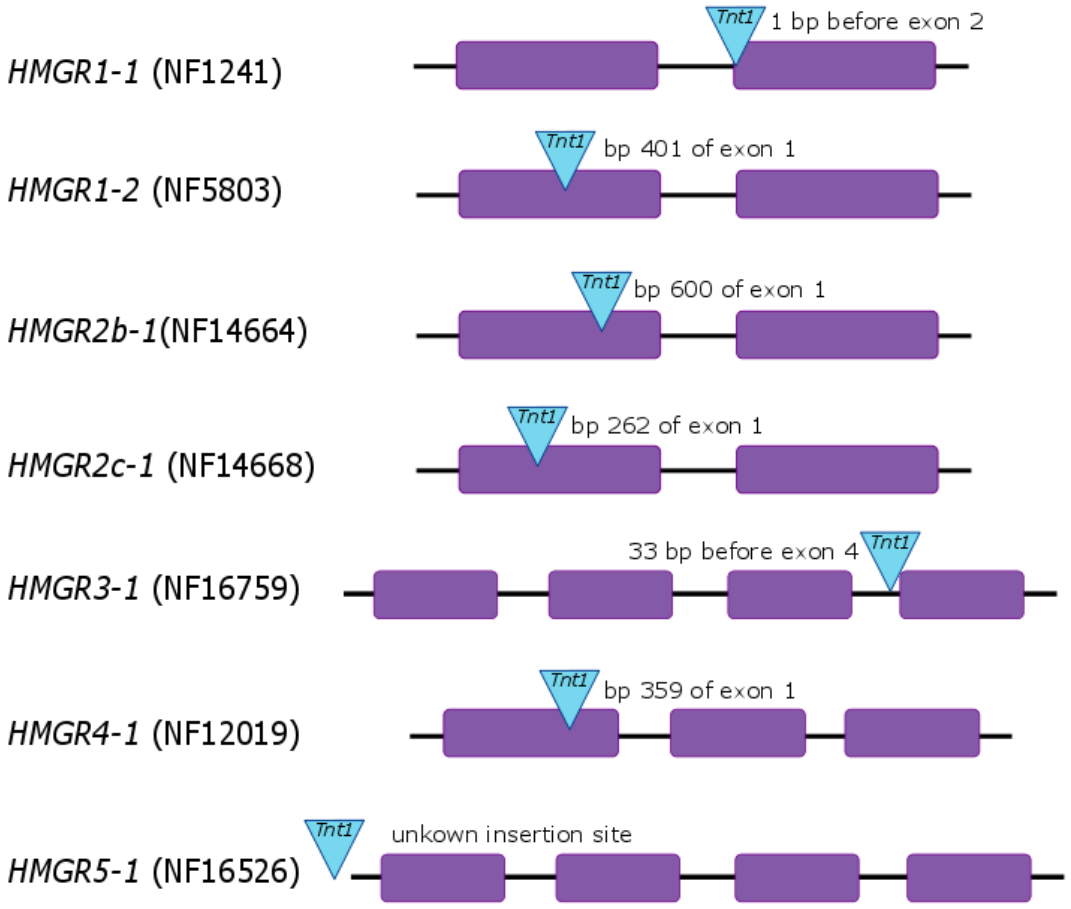

<u>Figure 2:</u> *Medicago truncatula Tnt1* insertion sites in *MtHMGRs*
Diagrammatic representation of the locations of *Tnt1* transposon insertions in *HMGR* genes in various mutant lines. Exons shown as rectangles, introns shown as solid lines between exons, and *Tnt1* insertions shown as blue triangles. Two *Tnt1* insert lines in this study contain inserts in *HMGR1,* with the insert located one base pair before exon one in NF1241 and after base pair 401 of exon one in NF5803. The insert in *HMGR2b* is located after base pair 600 of exon one in NF14664. In NF14668, the *Tnt1* insert is located after base pair 262 of exon one in *HMGR2c*. In NF16759, the insert is located 33 base pairs before exon four of *HMGR3*. In NF12019, the *Tnt1* insert is located after base pair 259 of exon one in *HMGR4*. The precise location of the *Tnt1* insert in the NF16526 mutant line is currently unknown. No lines containing inserts in either *HMGR2a* or *HMGR6* were identified.

Nodulation assays were performed on these *HMGR Tnt1* insertion lines. These assays assessed the total nodule number and the number of nodules that contained rhizobia expressing *nifH.* Mutant lines were grown alongside wild-type *M. truncatula* R108 as a positive control. Plants were inoculated with the *Sinorhizobium meliloti* strain CL304 containing a *PnifH::GUS* reporter. All assessed lines exhibited no difference in nodule number per plant compared to wild-type *M. truncatula* R108 plants. To examine the function of HMGRs in symbiosis downstream of nodule initiation, rhizobial expression of a nitrogenase component, *nifH,* in the nodules was assessed as a proxy for nodule functionality. *nifH* expression in nodules was significantly decreased in *hmgr1-1 plants* and abolished in *hmgr2c-1* plants, but no significant difference from wild-type was observed in *hmgr1-2*, *hmgr2b-1*, *hmgr3-1*, and *hmgr4-1* (**Figure 3**). Nodulation assays still need to be performed in the *hmgr5-1* lines. These findings specifically identify both *HMGR1* and *HMGR2c* as integral to the formation of functional nodules, specifically at later steps. However, we do not rule out a role for the other remaining *HMGRs* in nodulation. To confirm these results, it will be necessary to test for the ability of the native *HMGR1* and *HMGR2c* to rescue these phenotypes, respectively.

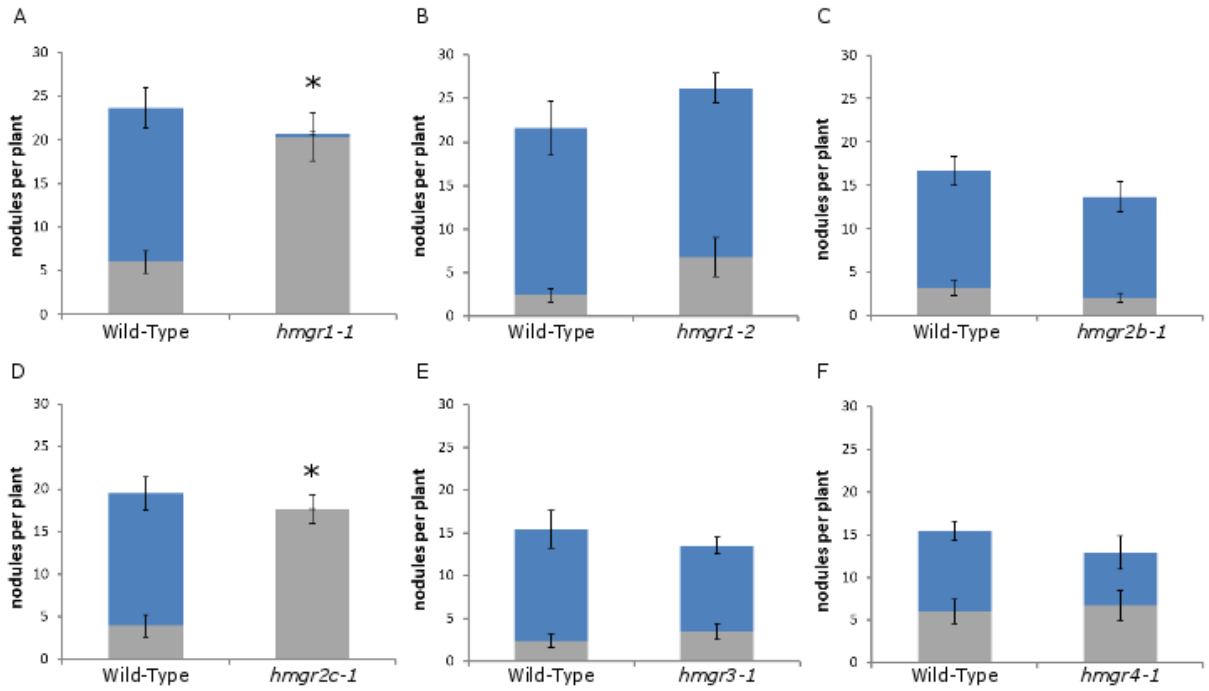

<u>Figure 3:</u> Nodulation phenotypes of *HMGR Tnt1* insertion mutants

Phenotypes from nodulation assays of *Tnt1* retrotransposon insertion lines with inserts located in *HMGR* genes assessing nodule number and presence of nodules containing rhizobia expressing *nifH::GUS.* Each mutant was compared to wild-type *M. truncatula* R108 grown alongside mutants as a negative control. Blue bars correspond to nodules containing *PnifH::GUS* expressing rhizobia. Grey bars correspond to unstained nodules. Error bars show standard error. Stars indicate a significant reduction in the number of nodules containing *PnifH::GUS* expressing rhizobia with a Student's t-test ($p < 0.05$).

A. NF1241 (*hmgr1-1*) mutants exhibited a decreased number of nodules containing *PnifH::GUS* expressing nodules (t-test, n= 15, $p = 3 \times 10^{-6}$), but not in overall nodule number per plant (t-test, n= 15, $p = 5 \times 10^{-1}$).

B. No difference was observed between NF5803 (*hmgr1-2*) mutants and wild-type in either nodule number (t-test, n= 12, $p = 3 \times 10^{-1}$) or nodules containing *PnifH::GUS* expressing rhizobia (t-test, n= 12, $p = 9 \times 10^{-1}$)

C. No difference was observed between NF14664 (*hmgr2b-1*) mutants and wild-type in either nodule number (t-test, n= 13, $p = 2 \times 10^{-1}$) or nodules containing *PnifH::GUS* expressing rhizobia (t-test, n= 13, $p = 5 \times 10^{-1}$).

D. NF14668 (*hmgr2c-1*) mutants exhibited a significant difference in *PnifH::GUS* expression compared to wild-type (t-test, n = 11, $p = 8.015 \times 10^{-5}$), as we observed no nodules containing *PnifH::GUS* expressing rhizobia. No difference in the total number of nodules was observed in these mutants (t-test, n = 11, $p = 6 \times 10^{-1}$).

E. No difference was observed between NF16759 (*hmgr3-1*) mutants and wild-type in either nodule number (t-test, n = 14, $p = 6 \times 10^{-1}$) or nodules containing *PnifH::GUS* expressing rhizobia(t-test, n = 14, $p = 6 \times 10^{-1}$).

F. No difference was observed between NF12019 (*hmgr4-1*) mutants and wild-type in either nodule number (t-test, n = 11, $p = 5 \times 10^{-1}$) or nodules containing *PnifH::GUS* expressing rhizobia (t-test, n = 11, $p = 1 \times 10^{-1}$).

No observed nodulation deficiencies with multi-HMGR knockdown with amiRNA

We observed different nodulation phenotypes between *HMGR* insertional knockout experiments and the RNAi experiment performed in Kevei et al., (2007). One explanation for this is functional redundancy between multiple HMGRs in nodule development. To determine if *HMGRs* serve a functionally redundant role in nodule development, we assessed knockdown mutants targeting an increasing number of *HMGRs* for additive nodulation defects. The most highly conserved *HMGR* sequences in *M. truncatula* are between *HMGR1*, *HMG2a*, *HMGR2b,* and *HMGR2c.* The high sequence similarity of these HMGRs and that they are the likely targets of the previous RNAi experiment led to our decision to knockdown combinations of these four *HMGRs*. We designed artificial microRNAs (amiRNAs) targeting *HMGR1* and *HMGR2a* (HMGR1+2a amiRNA); *HMGR2b* and *HMGR2c* (HMGR2b+2c amiRNA); *HMGR2a*, *HMGR2b*, and *HMGR2c* (HMGR2a+2b+2c amiRNA); as well as all four simultaneously (HMGR1+2a+2b+2c amiRNA). *M. truncatula* R108 roots were transformed via the standard *Agrobacterium rhizogenes*-based transformation method with constructs containing the various HMGR amiRNAs in combination with the visual marker, tdTomato, or an empty vector (EV) containing tdTomato marker alone. Total number of nodules and number of nodules containing *PnifH::GUS* expressing bacteria were assessed per root, instead of per plant, as each root is an independent transgenic event. Analysis of HMGR1+2a amiRNA, HMGR2b+2c amiRNA, and HMGR2a+2b+2c amiRNA, and HMGR1+2a+2b+2c transformed roots revealed no differences in nodule number between the mutants and EV control. Additionally, these same plants exhibited no differences in the number of nodules containing rhizobia expressing *PnifH::GUS*

(**Figure 4**). To determine if a lack of phenotype in these mutants is due to insufficient knockdown of expression we used qRT-PCR. For two of the amiRNA lines hypothesized to most likely show nodulation defects, HMGR1+2a amiRNA and HMGR 1+2a+2b+2c amiRNA, the gene expression level of *HMGR1, HMGR2a, HMGR2b,* and *HMGR2c* combined as well as of *HMGR6* for a control were measured and compared to those of EV control roots. In both sets of amiRNA mutant roots no statistically significant decrease in combined *HMGR1, HMGR2a, HMGR2b*, and *HMGR2c* expression was observed. With these findings, it remains unclear whether *HMGR2a* and *HMGR2b* additionally serve a role in nodulation and if separate *HMGRs* serve functionally redundant functions in nodulation. Additional transformation attempts with amiRNA constructs will be required to identify the knockdown efficiency of the various *HMGRs* and to determine their roles in nodulation.

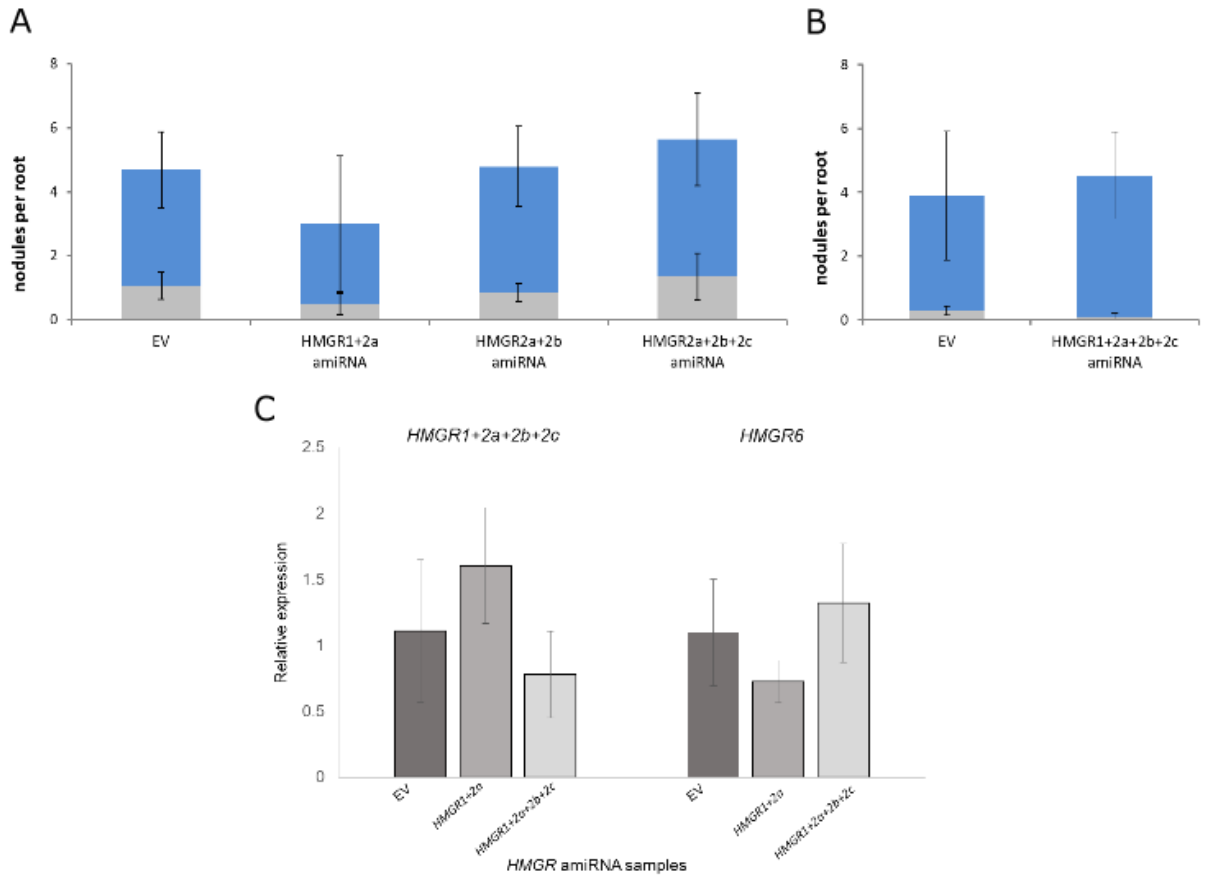

Figure 4: Nodulation and *HMGR* expression *HMGR* amiRNA mutants

Total nodule number and *nifH::GUS* expression phenotypes of *M. truncatula* R108 roots transformed with constructs for knocking down the expression of various *MtHMGRs* through artificial microRNAs. Blue bars correspond to nodules containing *PnifH::GUS* expressing rhizobia. Grey bars correspond to unstained nodules no containing PnifH::GUS expressing rhizobia. (A,B). Relative expression of *HMGR1, HMGR2a, HMGR2b,* and *HMGR2c* combined and of *HMGR6* in *M. truncatula* roots transformed with amiRNA constructs for knocking down *HMGR* expression. (C) Empty vector (EV) transformed *M. truncatula* R108 plants were used as negative controls. Error bars show standard error.

A. No statistically significant differences in total nodule number (n= 6, p = 9 x 10^{-1}) or presence of *nifH::GUS* expressing rhizobia (n= 6, p = 9 x 10^{-1}) between HMGR1+2a amiRNA, HMGR2b+2c amiRNA, HMGR2a+2b+2c, and EV transformed *M. truncatula* R108 plants were observed with an ANOVA.

B. No statistically significant difference was observed in total nodule number (n = 19, p = 8 x 10^{-1}) or presence of *nifH::GUS* expressing rhizobia (n = 19, p = 9 x 10^{-1}) between HMGR1+2a+2b+2c amiRNA and EV transformed *M. truncatula* R108 plants with a t-test.

C. No significant difference in combined *HMGR1*, *HMGR2a*, *HMGR2b*, and *HMGR2c* expression (n = 3, p = 5 x 10^{-1}) or *HMGR6* expression (n = 3, p = 5 x 10^{-1}) determined

by qRT-PCR was observed in *HMGR1+2a amiRNA* transformed roots or *HMGR1+2a+2b+2c* transformed roots as compared to EV roots.

Attempted deletion of *M. truncatula* genomic region containing four HMGRs

As our attempt to simultaneously knockdown expression of *HMGR1, HMGR2a, HMGR2b,* and *HMGR2c* provided unclear results due to possible lack of decreased expression we utilized the gene-editing tool CRISPR/Cas9 to eliminate the expression of these four *HMGRs* altogether to determine if these four HMGRs are necessary for nodule development. *M. truncatula* R108 contains these four HMGRs located in a tandem repeat spanning nearly 18 kb on chromosome five. We aimed to eliminate this chromosomal region with a single deletion to prevent the expression of each of these *HMGRs*. Multiple guide RNAs (gRNAs) were designed to target the most distant *HMGRs*; *HMGR1* and *HMGR2a,* and synthesized as a polycistronic fragment containing each of the gRNAs. Roots of a *M. truncatula* R108 line stably expressing *SpCas9* were transformed with a construct containing the HMGR gRNAs, as well as tdTomato and G-GECO fluorescent proteins via the *Agrobacterium rhizogenes*-mediated root transformation method. Using PCR genotyping, we assessed transgenic roots for full deletion of the *HMGR2a-HMGR1* chromosomal region. Screening of 183 *M. truncatula* R108 transgenic roots revealed none containing the desired 17kb deletion in the *HMGR2a-HMGR1* region, as a full *HMGR1* PCR product was amplified from all samples while a fragment spanning the would-be deleted region was not. Currently, we are unable to conclude the effect of a full HMGR1+HMGR2a+HMGR2b+HMGR2c knockout. Alternative methods for targeting the knockout of the four tandem *HMGRs* will be required to further assess the role of functional redundancy between *HMGRs* during nodulation.

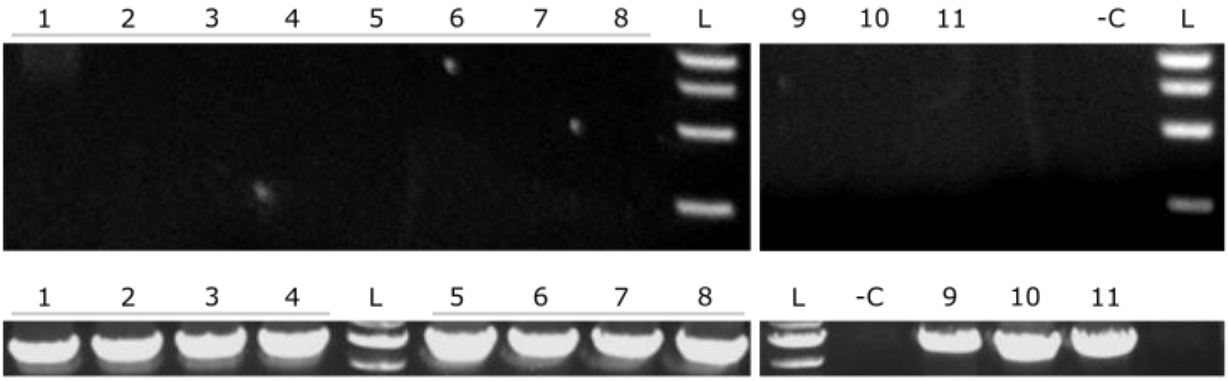

Figure 5: CRISPR/Cas9 deletion PCR screening
Results of PCR genotyping of a sampling of *M. truncatula* roots used in HMGR CRISPR deletion experiments.. DNA samples 1- 8 (underline) are from roots transformed with the HMGR CRISPR construct. DNA samples 9-11 are from samples transformed with an EV construct. 1 kb DNA ladder (L) and a no template negative control (-C) were run alongside DNA samples. Top two panels show PCR results with HMGR_5g_geno_F3 and HMGR_5g_geno_R2 primers flanking targeted deletion. No amplification of expected band size of 500-2000 bp if deletion occurred. Bottom two panels show PCR results using MtHMGR1 forward and reverse primers, in which a 2778 bp fragment corresponding to *MtHMGR1* is observed.

3.5 – Discussion

Phenotypic defects in Individual HMGR knockout mutants. Phenotypic defects of genetic mutants in various components of the symbiotic signaling pathway manifest in many different ways. Mutants may be defective in processes including root hair curling, infection thread formation, initiation of nodule primordia, release of bacteria into the nodule, or bacteroid differentiation. *M. truncatula* hmgr1-1 and hmgr2c-1 mutant lines exhibited no difference in nodule number compared to wild-type plants. However, we observed that fewer nodules contained nifH-expressing rhizobia. While hmgr1-1 mutants produce very few nodules containing nifH-expressing rhizobia, no nodules produced on hmgr2c-1 mutants contain nifH-expressing rhizobia. Bacterial expression of nifH in nodules strongly corresponds to nitrogen fixation as nifH codes for a

nitrogenase enzyme subunit. As these mutant plants are defective in nitrogen fixation but still produce a comparable number of nodules compared to wild-type plants, it suggests a new role for these HMGRs in the late stages of nodule development. The decreased nitrogen fixation ability could be due to various reasons. Further experiments of transcriptome analysis by RNAseq, observing the differentiation of bacteroids, or observing the presence of leghemoglobin in nodules could provide insights into which precise processes require these HMGRs.

Unfortunately, *Tnt1* insertion lines contain an estimated 50 copies of the *Tnt1* retrotransponson (Tadege et al., 2008). Recent screening of flanking sequences near other *Tnt1* inserts in the *hmgr1-1* and *hmgr2c-1* lines allude to possible insertions in known symbiotic signaling genes as well. Through PCR screening, a heterozygous *Tnt1* insert in *CCaMK* and a homozygous *Tnt1* insert in *PLC* were identified in the *hmgr1-1* and *hmgr2c-1* lines, respectively. We cannot rule out the possibility that the observed phenotypes in these mutant lines are due to mutations in other genes, including but not limited to *CCaMK* and *PLC*. Backcrossing the individual mutant lines to wild-type *M. truncatula* R108 could eliminate the background mutations and pinpoint the observed phenotypes to the genes-of-interest. Also, complementing these mutants with the native *HMGR* will be necessary to prove whether the insertions in the *HMGRs* are the cause of the observed nodulation defects.

In the other available *HMGR* insertion lines, we were unable to observe any defects in nodule development. No symbiotic phenotypes were observed in the *hmgr2b-1*, *hmgr3-1*, *hmgr4-1*, *hmgr5-1* insertion mutants, which may signify that these HMGRs are not involved in nodule development. However, a lack of phenotype may be due to

incomplete knockout of gene expression or redundancy amongst the *HMGRs*. Future experiments measuring gene expression of each of the individual *HMGRs* in these mutants would help clarify our findings by determining if the targeted genes show decreased expression and if it, in turn, leads to increased expression of the remaining *HMGRs.*

No *Tnt1* lines were identified to have insertions located in either *HMGR2a* or *HMGR6*. Two possible explanations include incomplete coverage of the *M. truncatula* genome by the methods used to develop the mutant database or lethality caused by defects in the expression of these genes. However, it is unlikely that an *HMGR2a* mutation is lethal since it shares extreme sequence similarity to *HMGR1*, *HMGR2b*, and *HMGR2c,* which all do not exhibit mutant lethality. *HMGR6* mutants, on the other hand, are more likely to be lethal since *HMGR6* shares higher sequence similarity to the ancestral form. Knocking out the expression of these two genes with other methods, such as CRISPR/Cas9, could answer whether the deletion of these genes is lethal or if they serve a symbiotic function.

Differences in the observed phenotypes between the mutants in the various *HMGRs* imply possible specialized roles for different *HMGRs*. The duplication of these genes and subsequent differentiation may allow for the evolution of new functions. Differential expression patterns, expression levels, or regulation of *HMGRs* may be responsible for these different mutant phenotypes.

***Multi-HMGR knockdown with artificial microRNAs*.** Unlike traditional RNAi methods, artificial microRNAs allow for specific knockdowns of individual or multiple genes with limited to no off-targets. We designed artificial microRNAs targeting

combinations of multiple *HMGR1* and *HMGR2* sequences. Assessment of roots transformed with the amiRNA constructs targeting several *HMGR* genes served to determine whether partial functional redundancy exists between specific *HMGRs.* No nodulation defects were observed in roots transformed with any HMGR amiRNA construct tested. With these findings, we cannot conclude whether *HMGR1, HMGR2a, HMGR2b,* and *HMGRc* are functionally redundant in their role in symbiotic signaling for nodule development. No significant decrease of *HMGR* expression in the amiRNA roots as determined by qRT-PCR likely explains a lack of observed nodulation defects. Low knockdown efficiency could prevent our detection of decreased expression and corresponding phenotype. Additional replicates with a larger samples size may allow for the identification of transgenic roots with sufficient knockdown of *HMGR* expression for further analysis. Otherwise, to determine the effects of knocking down the expression of multiple HMGRs for assessing functional redundancy, these experiments will need to be repeated with newly designed amiRNAs.

CRISPR/Cas9 for deletion of four HMGR containing genomic region. The *M. truncatula* R108 genome contains eight sequences coding for HMGR with high sequence similarity in its genome. While the tandem duplication and maintenance of several nearly identical HMGR sequences may be an artifact of in progress expansion, this could also serve as a mechanism to increase expression levels or assure the prevention of the loss of an important function. We investigated whether this is the case for certain *HMGRs* in *M. truncatula* through CRISPR/Cas9 deletion of four tandem *HMGRs*. Screening of 183 transgenic roots revealed none that carried deletions of the region of interest. As no mutants were found, we were unable to determine the genetic

role of the *HMGR1*, *HMGR2a*, *HMGR2b*, and *HMGR2c* chromosomal region and the impact that knocking out the expression of these genes has on nodule development. The inability to delete these four HMGRs may be due to the combination of our expression methods and the designed deletion size. We will continue the investigation of these *HMGRs* through more efficient deletion methods. The chosen promoters, Cas9 sequence, and the presence of an exonuclease can all impact CRISPR deletion ability and efficiency. Using a construct with a constitutive Pol II promoter driving polycistronic expression of our five tRNA spaced HMGR sgRNAs, a TREX2 exonuclease, and an optimized Cas9 for transforming wild-type *M.truncatula* R108 plants should increase the likelihood of obtaining the desired deletion. Besides the possibility of low expression, the chosen individual sgRNAs may exhibit weak activity. Before performing transformations, each sgRNA should be test for their in-vitro cleavage ability. Additionally, creating a stable transgenic line with this deletion instead of multiple independently transformed transgenic roots would also allow for a more detailed and clearer assessment of the role of these *HMGRs*.

3.6 – Acknowledgements

I would like to thank Christina Arther for her contributions to this work. Christina performed the qRT-PCR analysis of gene expression for the HMGR amiRNA experiments.

3.7 – Supplementary Tables

Primer Name	Gene	Purpose	Sequence (5' to 3')
HMGR_5g_geno_F3	HMGR2a	genotyping	TGCAGTTCCCTCACTCTCTG
HMGR_5g_geno_R2	HMGR1	genotyping	CCTCGTTGTTCACGAGTTCC
HMGR1_R108_F2	HMGR1	genotyping	CCCTTAAATTGTTCATTTTGTTCA
HMGR1_R108_R2	HMGR1	genotyping	CCACCAATTTACAAAGCATGACAG
HMGR2a_R108_F	HMGR2a	genotyping	CAGTTCCCTCACTCTCTGACTCT
HMGR2a_R108_R	HMGR2a	genotyping	CGTGAGAATCACTTTGGCTATG
HMGR2b_R108_F	HMGR2b	genotyping	GCCTTGGAACCAATCTTAGTAAAC
HMGR2b_R108_R	HMGR2b	genotyping	GAGATTCTTCTAGTGCGCTTCTTG
HMGR2c_R108_F	HMGR2c	genotyping	TTCCAAACAACTTCAGGACAAG
HMGR2c_R108_R	HMGR2c	genotyping	CGTGCTCCTATGTTTTTCTTCTA
HMGR3_R108_F	HMGR3	genotyping	CAACCCTTTTTCCACTCTGTCC
HMGR3_R108_R	HMGR3	genotyping	CATGCATTGGGAGGAAAGTATTC
HMGR4_R108_F	HMGR4	genotyping	TTACCAATCAATCTCCCTGAA
HMGR4_R108_R	HMGR4	genotyping	GGGAATTGAGACATACTACAGCAC
HMGR5_R108_F	HMGR5	genotyping	TCGTAGATTCAAAACTCGTCGG
HMGR5_R108_R	HMGR5	genotyping	CTACAAGTTTATTGTTGTGTTGTGTG
HMGR6-R108-F	HMGR6	genotyping	CCATTCATTCATTCTCCAATTC
HMGR6-R108-R	HMGR6	genotyping	CAATGTCTTGGTTAAGGAAATGG
Tnt1_Fwd_out	Tnt1	genotyping	GTATTTACCTCCGACCTACAAAGTG
LTR3-F	Tnt1	sequencing	AGTTGCTCCTCTCGGGGTCGTGGT
PDF2_ qrtPCR_F	MtPDF2	qRT-PCR	GTGTTTTGCTTCCGCCGTT
PDF2_ qrtPCR_R	MtPDF2	qRT-PCR	CCAAATCTTGCTCCCTCATCTG
SecAgent_qrtPCR_F	MtSecA	qRT-PCR	GGCAGGTCTGCCTATGGTTA
SecAgent_qrtPCR_R	MtSecA	qRT-PCR	GGTCAGACGCACAGATTTGA
HMGR12a2b2c_qrtPCR_F1	HMGR1, HMGR2a, HMGR2b, HMGR2c	qRT-PCR	CTCACACTTTCAACAAGTCAAGTAG
HMGR12a2b2c_qrtPCR_R1	HMGR1, HMGR2a, HMGR2b, HMGR2c	qRT-PCR	CCAGATATACCAATAACATCCATATC
HMGR6_qrtPCR_F2	HMGR6	qRT-PCR	CACAGGTCAAGATCCAGCTCA
HMGR6_qrtPCR_R2	HMGR6	qRT-PCR	TACCGTACCCACCTCAATGGAT

Supplementary Table 1: Primer sequences
Table provides primer names, gene targets, and DNA sequences for all primers used. Each primer is specified for its experimental purpose.

3.8 – References

Ané, J.-M., Kiss, G.B., Riely, B.K., Penmetsa, R.V., Oldroyd, G.E.D., Ayax, C., Lévy, J., Debellé, F., Baek, J.-M., Kaló, P., Rosenberg, C., Roe, B.A., Long, S.R., Dénarié, J., Cook, D.R., 2004. Medicago truncatula DMI1 required for bacterial and fungal symbioses in legumes. Science. 303, 1364–1367. https://doi.org/10.1126/science.1092986

Binder, A., Lambert, J., Morbitzer, R., Popp, C., Ott, T., Lahaye, T., Parniske, M., 2014. A modular plasmid assembly kit for multigene expression, gene silencing and silencing rescue in plants. PLoS One 9. https://doi.org/10.1371/journal.pone.0088218

Charpentier, M., Oldroyd, G.E.D., 2013. Nuclear Calcium Signaling in Plants. Plant Phys. 1 163, 496–503. https://doi.org/10.1104/pp.113.220863

Concordet, J.P., Haeussler, M., 2018. CRISPOR: Intuitive guide selection for CRISPR/Cas9 genome editing experiments and screens. Nucleic Acids Res. 46, 242–245. https://doi.org/10.1093/nar/gky354

Delaux, P.M., Radhakrishnan, G. V., Jayaraman, D., Cheema, J., Malbreil, M., Volkening, J.D., Sekimoto, H., Nishiyama, T., Melkonian, M., Pokorny, L., Rothfels, C.J., Sederoff, H.W., Stevenson, D.W., Surek, B., Zhang, Y., Sussman, M.R., Dunand, C., Morris, R.J., Roux, C., Wong, G.K.S., Oldroyd, G.E.D., Ane, J.M., 2015. Algal ancestor of land plants was preadapted for symbiosis. Proc. Natl. Acad. Sci. U. S. A. 112, 13390–13395. https://doi.org/10.1073/pnas.1515426112

Endre, G., Kereszt, A., Kevei, Z., Mihacea, S., Kaló, P., Kiss, G.B., 2002. A receptor kinase gene regulating symbiotic nodule development. Nature 417, 962–966. https://doi.org/10.1038/nature00842

Engler, C., Kandzia, R., Marillonnet, S., 2008. A one pot, one step, precision cloning method with high throughput capability. PLoS One 3. https://doi.org/10.1371/journal.pone.0003647

Ferrero, S., Grados-Torrez, R.E., Leivar, P., Antolín-Llovera, M., López-Iglesias, C., Cortadellas, N., Ferrer, J.C., Campos, N., 2015. Proliferation and Morphogenesis of the Endoplasmic Reticulum Driven by the Membrane Domain of 3-Hydroxy-3-Methylglutaryl Coenzyme A Reductase in Plant Cells. Plant Physiol. 168, 899–914. https://doi.org/10.1104/pp.15.00597

Friesen, J.A., Rodwell, V.W., 2004. The 3-hydroxy-3-methylglutaryl coenzyme-A (HMG-CoA) reductases. Genome Biol. 5. https://doi.org/10.1186/gb-2004-5-11-248

Holstein, S.A., Hohl, R.J., 2004. Isoprenoids : Remarkable Diversity of Form and Function. Lipds 39, 293–309.

Jones, K.M., Kobayashi, H., Davies, B.W., Taga, M.E., Walker, G.C., 2007. How rhizobial symbionts invade plants: the Sinorhizobium-Medicago model. Nat. Rev. Microbiol. 5, 619–33. https://doi.org/10.1038/nrmicro1705

Kevei, Z., Lougnon, G., Mergaert, P., Horváth, B., Kereszt, A., Jayaraman, D., Zaman,

N., Marcel, F., Regulski, K., Kiss, G.B., Kondorosi, A., Endre, G., Kondorosi, E., Ané, J.-M., Horváth, G. V, Horvath, G. V, 2007. 3-hydroxy-3-methylglutaryl coenzyme A reductase1 interacts with NORK and is crucial for nodulation in Medicago truncatula. Plant Cell 19, 3974–3989. https://doi.org/10.1105/tpc.107.053975

Kim, S., Zeng, W., Bernard, S., Liao, J., Ane, J., Jiang, Y., Venkateshwaran, M., 2019. Ca2+-regulated Ca2+ channels with an RCK gating ring control plant symbiotic associations. Nat. Commun. 10, 1–12. https://doi.org/10.1038/s41467-019-11698-5

Lang, C., Smith, L.S., Long, S.R., 2018. Characterization of Novel Plant Symbiosis Mutants Using a New Multiple Gene-Expression Reporter Sinorhizobium meliloti Strain. Front. Plant Sci. 9, 1–16. https://doi.org/10.3389/fpls.2018.00076

Lévy, J., Bres, C., Geurts, R., Chalhoub, B., Kulikova, O., Duc, G., Journet, E.-P., Ané, J.-M., Lauber, E., Bisseling, T., Dénarié, J., Rosenberg, C., Debellé, F., 2004. A Putative Ca 2 and Calmodulin- Dependent Protein Kinase Required. Science 303, 1361–1364.

Li, W., Liu, W., Wei, H., He, Q., Chen, J., Zhang, B., Zhu, S., 2014. Species-specific expansion and molecular evolution of the 3-hydroxy-3-methylglutaryl coenzyme A reductase (HMGR) gene family in plants. PLoS One 9, 1–10. https://doi.org/10.1371/journal.pone.0094172

Oldroyd, G.E.D., 2013. Speak, friend, and enter: Signalling systems that promote beneficial symbiotic associations in plants. Nat. Rev. Microbiol. 11, 252–263. https://doi.org/10.1038/nrmicro2990

Pecrix, Y., Staton, S.E., Sallet, E., Lelandais-Brière, C., Moreau, S., Carrère, S., Blein, T., Jardinaud, M.F., Latrasse, D., Zouine, M., Zahm, M., Kreplak, J., Mayjonade, B., Satgé, C., Perez, M., Cauet, S., Marande, W., Chantry-Darmon, C., Lopez-Roques, C., Bouchez, O., Bérard, A., Debellé, F., Muños, S., Bendahmane, A., Bergès, H., Niebel, A., Buitink, J., Frugier, F., Benhamed, M., Crespi, M., Gouzy, J., Gamas, P., 2018. Whole-genome landscape of Medicago truncatula symbiotic genes. Nat. Plants 4, 1017–1025. https://doi.org/10.1038/s41477-018-0286-7

Radutoiu, S., Madsen, L.H., Madsen, E.B., Felle, H.H., Umehara, Y., Grønlund, M., Sato, S., Nakamura, Y., Tabata, S., Sandal, N., Stougaard, J., Gronlund, M., Sato, S., Nakamura, Y., Tabata, S., Sandal, N., Stougaard, J., 2003. Plant recognition of symbiotic bacteria requires two LysM receptor-like kinases. Nature 425, 585–592. https://doi.org/10.1038/nature02039

Schiessl, K., Lilley, J.L.S., Lee, T., Tamvakis, I., Kohlen, W., Bailey, P.C., Thomas, A., Luptak, J., Ramakrishnan, K., Carpenter, M.D., Mysore, K.S., Wen, J., Ahnert, S., Grieneisen, V.A., Oldroyd, G.E.D., 2019. NODULE INCEPTION Recruits the Lateral Root Developmental Program for Symbiotic Nodule Organogenesis in Medicago truncatula. Curr. Biol. 29, 3657-3668. https://doi.org/10.1016/j.cub.2019.09.005

Stermer, B. a, Bianchini, G.M., Korth, K.L., 1994. Regulation of HMG-CoA reductase activity in plants. J. Lipid Res. 35, 1133–40.

Stracke, S., Kistner, C., Yoshida, S., Mulder, L., Sato, S., Kaneko, T., Tabata, S., Sandal, N., 2002. A plant receptor-like kinase required for both bacterial and fungal symbiosis. Nature 417, 959–962.

Suzuki, M., Kamide, Y., Nagata, N., Seki, H., Ohyama, K., Kato, H., 2004. Loss of

function of 3-hydroxy-3-methylglutaryl coenzyme A reductase 1 (HMG1) in Arabidopsis leads to dwaring , early senescence and male sterility , and reduced sterol levels Plant J. 1, 750–761. https://doi.org/10.1111/j.1365-313X.2003.02003.x

Suzuki, M., Nakagawa, S., Kamide, Y., Kobayashi, K., Ohyama, K., 2009. Complete blockage of the mevalonate pathway results in male gametophyte lethality 60, 2055–2064. https://doi.org/10.1093/jxb/erp073

Tadege, M., Wen, J., He, J., Tu, H., Kwak, Y., Eschstruth, A., Cayrel, A., Endre, G., Zhao, P.X., Chabaud, M., Ratet, P., Mysore, K.S., 2008. Large-scale insertional mutagenesis using the Tnt1 retrotransposon in the model legume Medicago truncatula. Plant J. 54, 335–347. https://doi.org/10.1111/j.1365-313X.2008.03418.x

Venkateshwaran, M., Jayaraman, D., Chabaud, M., Genre, A., Balloon, A.J., Maeda, J., Forshey, K.L., den Os, D., Kwiecien, N.W., Coon, J.J., Barker, D.G., Ané, J.-M., 2015. A role for the mevalonate pathway in early plant symbiotic signaling. Proc. Natl. Acad. Sci. 112, 201413762. https://doi.org/10.1073/pnas.1413762112

Chapter 4 - Repurposing of multiple signaling mechanisms for cytoplasmic signal transduction in the common symbiosis pathway

4.1 – Abstract

The formation of the beneficial root nodule and arbuscular mycorrhizal plant-microbe symbioses require numerous shared molecular components in the subcellular signal transduction pathway for inducing the necessary genetic and physiological changes following the detection of their symbiotic partner, which together comprise the “common symbiosis pathway.” Receptor-like kinases detect rhizobia and arbuscular mycorrhizal fungi produced signals and require an additional co-receptor, Does not Make Infections 2 (DMI2), for signaling downstream of the plasma membrane. The following induction of oscillations of calcium levels in the nucleus controlled by calcium channels and pumps then regulates symbiotic gene expression. The signal transduction process spanning from the plasma membrane to the nuclear envelope remains elusive. However, 3-Hydroxy-3-Methylglutaryl CoA Reductase 1 (HMGR1) interacts with DMI2 and is required for nuclear calcium oscillations and subsequent development of symbiotic associations. In this chapter, we investigated the mechanism by which HMGR activity transduces signals in the common symbiosis pathway. We showed that HMGR activity is sufficient for the induction of symbiotic gene expression. Additionally, limiting the activity of farnesyl pyrophosphate synthase or prenyltransferase inhibits symbiotic gene expression. Furthermore, the regulation of symbiotic gene expression by HMGR activity relies on the activity of phospholipases. Therefore, this work demonstrated that the common symbiosis pathway employs

downstream metabolites of the mevalonate pathway and protein prenylation, followed by phospholipase activity for signal transduction.

4.2 – Introduction

The root nodule symbiosis and arbuscular mycorrhizal symbiosis are two of the most agronomically important plant microbe interactions because they are capable of assisting in attaining essential nutrients. In the root nodule symbiosis, bacteria reduce atmospheric nitrogen into usable ammonium and supply it to the host plant in exchange for fixed carbon (Lindström and Mousavi, 2020). In the arbuscular mycorrhizal symbiosis, which forms between the majority of land plants and Glomeromycotina, fungi obtain phosphorus, potassium, nitrogen, water, and many micronutrients from the soil with their large hyphal networks and exchange these nutrients for carbon (Fellbaum et al., 2011; Kiers et al., 2012; Wang et al., 2017). The overwhelming benefits of these two symbioses has led to extensive research investigating the molecular mechanisms that allow these interactions to occur. Interestingly, the signaling pathway is highly conserved between root nodule symbiosis and arbuscular mycorrhizal symbiosis, and is thus referred to as the “common symbiosis pathway” (CSP) (Catoira et al., 2000; Riely et al., 2004).

Both microbial partners in these two symbiotic relationships produce chitin-based signaling molecules, in the form of chitooligosaccharides or lipid-containing lipochitooligosaccharides (LCOs) (Dénarié et al., 1996; Genre et al., 2013; Maillet et al., 2011). These compounds are recognized by pairs of LysM receptor-like kinases (RLKs) on the surface of the host plant’s plasma membrane. In the case of *M. truncatula*, the

LCO receptors are referred to as NFP and LYK3 (Amor et al., 2003; Limpens et al., 2003; Moling et al., 2014). Activation of the receptor complex initiates the subcellular symbiotic signaling cascade through the interaction with another RLK, DMI2/NORK (Antolín-Llovera et al., 2014; Bersoult et al., 2005). From the plasma membrane, secondary messengers transduce the signal through the cytoplasm through not-yet-well-understood mechanisms. Through these unknown secondary messengers, ion channels and pumps at the nuclear envelope are activated. This leads to a symbiosis-specific response of an influx of calcium into the nucleus and repeated oscillations of high and low calcium concentrations. DMI1, in particular, is a calcium mediated calcium channel that is essential for symbiotic associations and nuclear calcium oscillations, as displayed by *dmi1* mutants (Ané et al., 2004; Catoira et al., 2000; Charpentier et al., 2016; Charpentier and Oldroyd, 2013; Kanamori et al., 2006; Kim et al., 2019). These nuclear calcium oscillations activate a nuclear-localized calcium and calmodulin binding protein kinase (DMI3/CCaMK) (Miller et al., 2013; Mitra et al., 2004). DMI3/CCaMK then binds to and phosphorylates IPD3, a key transcription factor in symbiotic signaling responsible for initiating the activation of a complex network of various other transcription factors (Horváth et al., 2011; Limpens et al., 2011; Messinese et al., 2007). Ultimately, this process allows for the regulation of symbiotic genes for the colonization and physiological modifications necessary for forming either association with rhizobia or arbuscular mycorrhizal fungi.

How the signal is transduced from the plasma membrane to the nucleus remains one of the most elusive aspects of the CSP. Components implicated in this process include HMGRs, phospholipases, and G-proteins (Choudhury and Pandey, 2013; Den

Hartog et al., 2001; Kevei et al., 2007). HMGR1 interacts with the symbiotic co-receptor DMI2/NORK, and knockdown of HMGR expression inhibits nodule formation (Kevei et al., 2007).

HMGRs perform the rate-limiting step in the mevalonate pathway, reducing HMG-CoA to mevalonate in an NADPH-dependent manner. This pathway is highly conserved across eukaryotes and is responsible for generating tens of thousands of different isoprenoid products (Friesen and Rodwell, 2004). While animals contain only a single *HMGR*, the family is greatly expanded in plants. Larger numbers of HMGR encoding genes and resulting differential regulation likely leads to the increased abundance of isoprenoids synthesized by plants (Stermer et al., 1994). Isoprenoids serving numerous different functions are generated through the activity of enzymes downstream of HMGR, branching off at various points along the mevalonate pathway (**Figure 1**). Cytokinins and isoprene donors of tRNAs are synthesized from dimethylallyl pyrophosphate (DMAPP) and serve roles in plant growth regulation and translation; monoterpenes are synthesized from geranyl pyrophosphate and are involved in microbial defense, as well as repelling and attracting insects sesquiterpenes, sterols, dolichols, and isoprene side chains quinones are all produced from farnesyl pyrophosphate and serve in microbial defense, membrane structure, *N*-glycosylation, and electron transport; and gibberellins, carotenoids, and chlorophylls are derived from geranylgeranyl pyrophosphate and are important for plant growth regulation and photosynthesis. Additionally, both farnesyl pyrophosphate and geranylgeranyl pyrophosphate are used as prenyl side chains in the prenylation of proteins which affect protein localization (Holstein and Hohl, 2004). With such wide-spanning functions of

isoprenoids, there are many mechanisms by which HMGR activity may serve in forming symbiotic associations.

In this study, we aimed to determine the ability of HMGR activity to stimulate symbiotic responses and clarify the mechanism by which HMGRs transduce the symbiotic signal. The identification of numerous symbiotic-specific genes induced by the completion of the CSP allows for the use of them as a readout for the activation of the signaling pathway. Using this method has allowed for the identification of various key components in symbiotic signaling. We used this method to assess the ability of activating or inhibiting mevalonate pathway enzymes to alter symbiotic responses. We identified that in addition to HMGR activity, activity of other downstream mevalonate pathway enzymes are necessary for symbiotic signaling. Additionally, we developed a genetic system to induce constitutive activity of HMGR and identified *in vivo* HMGR activity is sufficient to stimulate symbiotic responses. We further determined that phospholipases are essential for the activation of the symbiotic signaling pathway with this inducible HMGR system, while two core symbiotic signaling components, DMI1 and DMI2, are not.

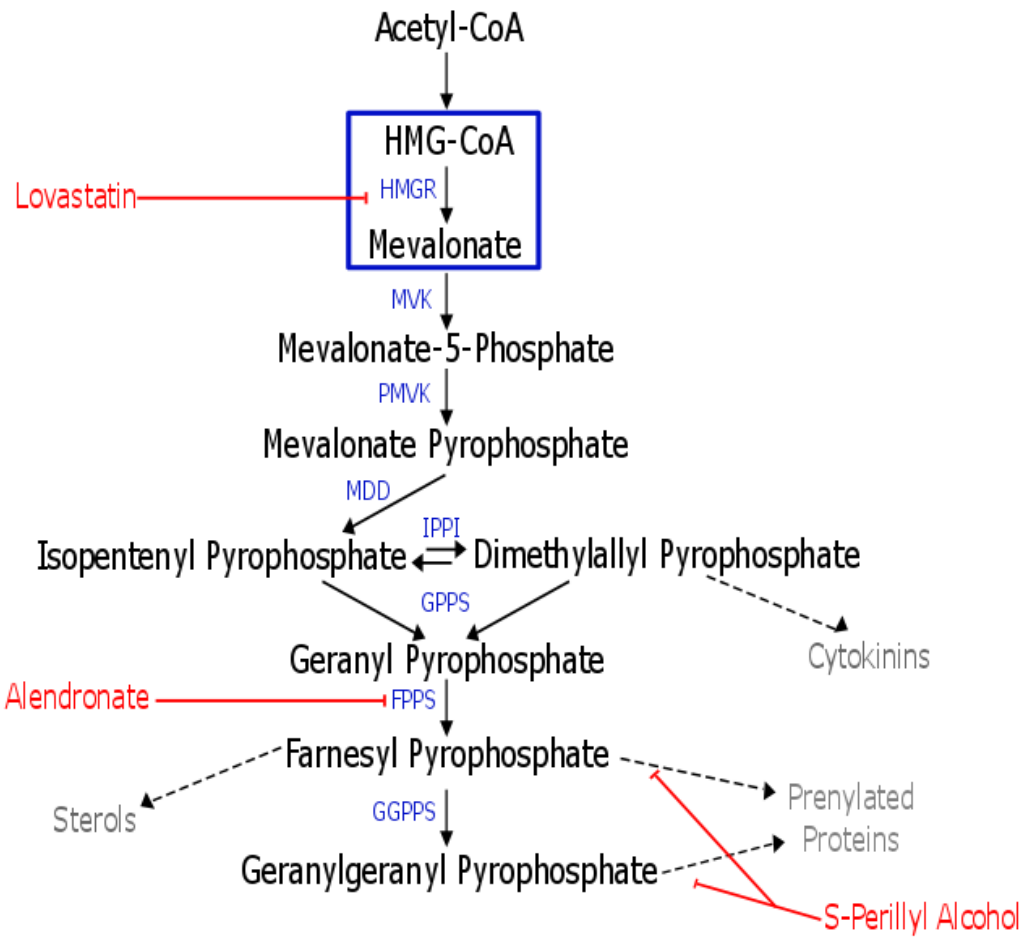

Figure 1: Mevalonate pathway

Simplified mevalonate pathway diagram illustrating the core enzymatic steps and products. 3-hydroxy-3-methylglutaryl coenzyme A reductase (HMGR) converts two acetyl-CoA molecules to mevalonate. Mevalonate kinase (MVK) phosphorylates mevalonate creating mevalonate-5-phosphate. Phosphomevalonate kinase (PMVK) phosphorylates mevalonate-5-phosphate creating mevalonate pyrophosphate. Mevalonate pyrophosphate decarboxylase (MDD) produces isopentenyl pyrophosphate through decarboxylation of mevalonate pyrophosphate. Isopentenyl pyrophosphate isomerase (IPPI) catalyzes the reversible reaction converting isopentenyl pyrophosphate to dimethylallyl pyrophosphate. The condensation of dimethylallyl pyrophosphate with isopentenyl pyrophosphate isomerase by geranyl pyrophosphate synthase (GPPS) creates geranyl pyrophosphate. Farnesyl pyrophosphate synthase (FPPS) forms farnesyl pyrophosphate from geranyl pyrophosphate. Geranylgeranyl pyrophosphate synthase (GGPPS) converts farnesyl pyrophosphate to geranylgeranyl pyrophosphate. Examples of mevalonate pathway end products stemming from various branches are denoted in grey. Core mevalonate pathway enzymes are denoted in blue, core mevalonate pathway products are denoted in black, biochemical inhibitors of the enzymatic activity are denoted in red. Solid arrows represent direct enzymatic activity of core mevalonate pathway enzymes, while dashed arrows indicate multi-enzyme activity.

4.3 – Results

In vivo HMGR activity is sufficient to activate symbiotic signaling

Previous research has used exogenous application of the product of HMGR activity, mevalonate, to determine its ability to stimulate symbiotic responses, and identified mevalonate to trigger both nuclear calcium spiking and *ENOD11* expression (Venkateshwaran et al., 2015). However, the biologically relevant concentration of mevalonate is unknown, and the use of high concentrations and the inability to confirm how much enters inside the cells are problematic with this method. Still, the mechanism by which mevalonate activates the signaling pathway and if HMGR activity is directly involved in the activation is still unclear. As has been shown with an *Arabidopsis thaliana* HMGR expressed in bacteria, the modification of HMGR1 by deleting the transmembrane domain led to the generation of an autoactive form of the enzyme (Dale et al., 1995). Using an equivalent modification of MtHMGR1 (**Figure 2a**), we investigated whether an autoactive HMGR1 (MtHMGR1cat) can activate the symbiotic signaling pathway and lead to symbiotic responses, such as *ENOD11* expression. To control the timing of expression, and therefore HMGR activity, we used an ethanol inducible promoter system to regulate the expression of the modified MtHMGR1cat. *M. truncatula* plants containing *pENOD11*::GUS were transformed with constructs containing the ethanol inducible *MtHMGR1cat* or an ethanol inducible luciferase (as a negative control). To verify the functionality of our ethanol inducible promoter, we drove the expression of GUS with this promoter in wild-type *M. truncatula.* These plants treated with 2% ethanol strongly expressed GUS, while no expression was observed in plants only treated with water, showing strong expression in the presence of ethanol

and the absence of background expression. Ethanol inducible *MtHMGR1cat* plants were then treated with 2% ethanol or water (negative control) and observed for *ENOD11* expression. As an additional negative control, inducible luciferase transformed M. truncatula roots were treated with 2% ethanol (not shown). For a positive control, roots containing the ethanol inducible luciferase were treated with LCOs to compare to classical symbiotic expression levels of *ENOD11*. Inducible *MtHMGR1cat* transformed *M. truncatula* roots treated with ethanol showed far stronger *pENOD11:GUS* expression than LCO-treated positive controls (**Figure 2b**). In contrast, water-treated roots ethanol inducible *MtHMGR1cat* transformed roots, and ethanol-treated inducible luciferase transformed roots exhibited no detectable *pENOD11:GUS* expression. These results indicate that *in vivo* HMGR activity induces the expression of symbiotic marker genes.

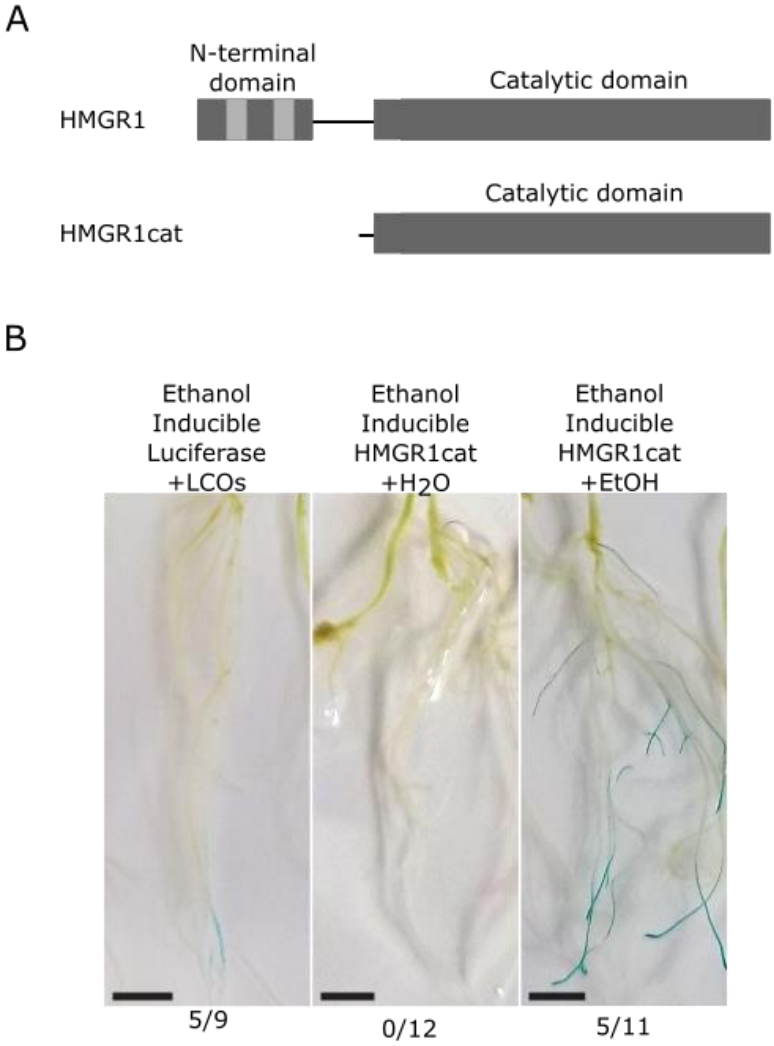

Figure 2: HMGR activity triggers symbiotic gene expression in *M. truncatula*

Protein structure of wild-type MtHMGR1 and MtHMGR1cat (A) and *pENOD11:GUS* reporter expression in *M. truncatula* roots (B). *M. truncatula* HMGR1 consists of an N-terminal domain with 2 transmembrane spanning regions (light gray), a linker region (thin line), and a large catalytic domain at the C-terminus. HMGR1cat is a modified autoactive HMGR generated by the truncation of *M. truncatula* HMGR1 leaving the catalytic domain and four amino acids of the upstream linker (A). Ethanol inducible luciferase transformed roots treated with LCOs show standard staining. Ethanol inducible HMGR1cat transformed plants treated with water exhibit no background ENOD11 expression. Ethanol inducible HMGR1cat transformed roots treated with 2% ethanol exhibited strong GUS staining, signifying higher expression of ENOD11 than the response to LCOs. Roots of a representative plant for each treatment were imaged (B). Ratio represents number of plants with staining over total plants observed. Scale bars = 0.5 cm

Position of HMGR activity in the symbiotic signaling pathway

As HMGR activity drove symbiotic responses, it led us to investigate where HMGRs act in the signaling pathway. The newly designed ethanol inducible HMGR system provided us with a simple way to determine whether symbiotic responses triggered by HMGR activity are dependent on other known signaling components. *M. truncatula dmi1-1 and dmi2-1* mutants and wild-type plants, all containing *pENOD11::GUS* were transformed with the inducible HMGR1cat construct. When treated with ethanol, both wild-type and mutant roots strongly expressed *pENOD11:GUS*. The ability of HMGR activity to drive *pENOD11::GUS* expression in *dmi2-1* mutants indicates HMGR stimulated symbiotic responses are independent of DMI2, with HMGR activity likely occurring downstream of DMI2. The induction of symbiotic gene expression in *dmi1-1* mutants also signifies that HMGR activity can stimulate symbiotic responses independently of DMI1. HMGR activity may occur downstream of DMI1, as well, but more likely plays is capable of circumventing DMI1 through other ion channels **(Figure 3).**

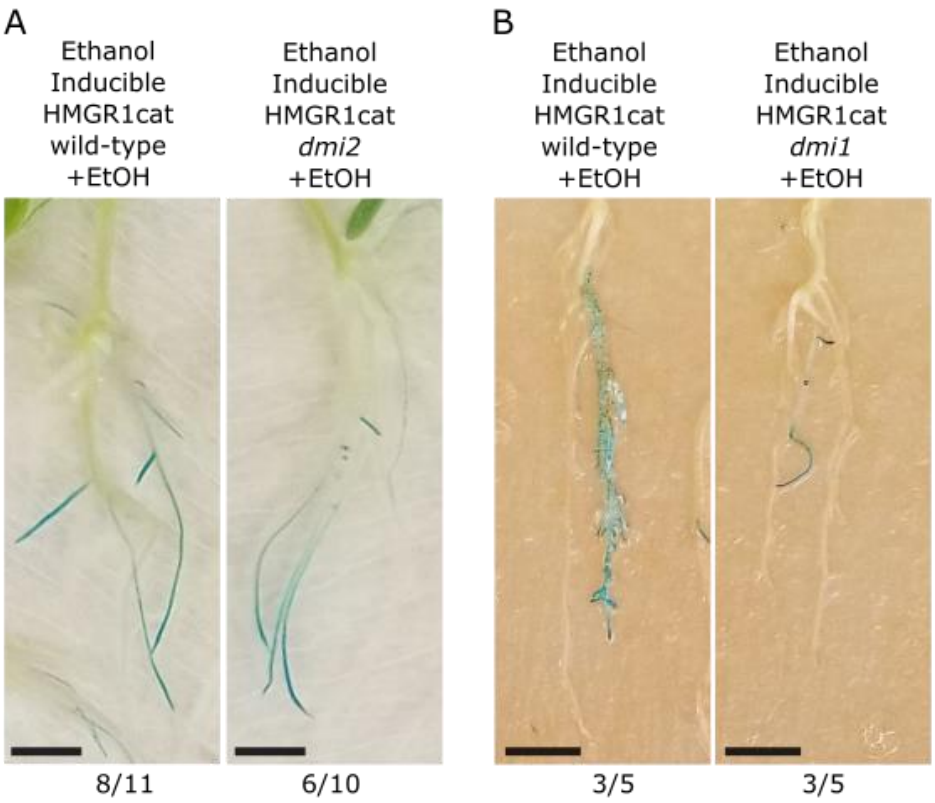

<u>Figure 3:</u> HMGR activity triggered symbiotic gene expression in symbiotic mutants
Images show expression of *pENOD11:GUS* in *M. truncatula* roots. Representative roots from plants for each treatment were imaged. Ethanol-treated ethanol inducible HMGR1cat transformed roots of wild-type and *dmi2-1* mutant plants show strong staining (A). Ethanol-treated ethanol inducible HMGR1cat transformed roots of wild-type and *dmi1-1* mutants show strong staining (B). Ratio represents number of plants with staining over total plants observed. Scale bars = 0.5 cm

Downstream mevalonate pathway products are involved in symbiotic signaling

HMGR activity is essential for the legume-rhizobia symbiosis, as RNAi knock-down and pharmacological inhibition of HMGRs causes a reduction of nodule number and prevents early symbiotic signaling (Kevei et al., 2007; Venkateshwaran et al., 2015). Due to the conservation of the mevalonate pathway in humans, we have numerous pharmacological inhibitors of different enzymes in the pathway at our

disposal for determining whether additional mevalonate pathway components are also essential for symbiotic signaling.

We first confirmed the requirement of HMGR activity in symbiotic signaling by growing *M. truncatula* containing *pENOD11*::GUS in the presence of 0.5 µM lovastatin, a general inhibitor of HMGR activity, then treating these plants with LCOs. A concentration of 0.5 µM was used as it was previously shown to inhibit nodulation without effects on root growth (Kevei et al., 2007). We observed extremely weak expression of *pENOD11:GUS* in these plants **(Figure 4a)**. This confirms previous results suggesting HMGR activity is necessary for the common symbiosis pathway.

To determine the identity of the isoprenoid products that transduce the symbiotic signal, we utilized alendronate, which inhibits the farnesyl pyrophosphate synthase, blocking the central pathway downstream of HMGR (**Figure 1**). We grew *M. truncatula* containing *pENOD11*::GUS on media containing 100 µM alendronate and treated the roots with LCOs. Similar to lovastatin treated roots, alendronate treated roots displayed dramatically weaker *pENOD11:GUS* expression in response to LCOs than untreated roots **(Figure 4b)**. This demonstrates that producing the essential isoprenoid involved in symbiotic signaling requires the activity of farnesyl pyrophosphate synthase and suggests it is not derived form a branch earlier in the pathway, such as cytokinins (**Figure 1**). Alternatively, cell death or inhibition of off-target processes could be responsible for the observed defects and will need to be ruled out.

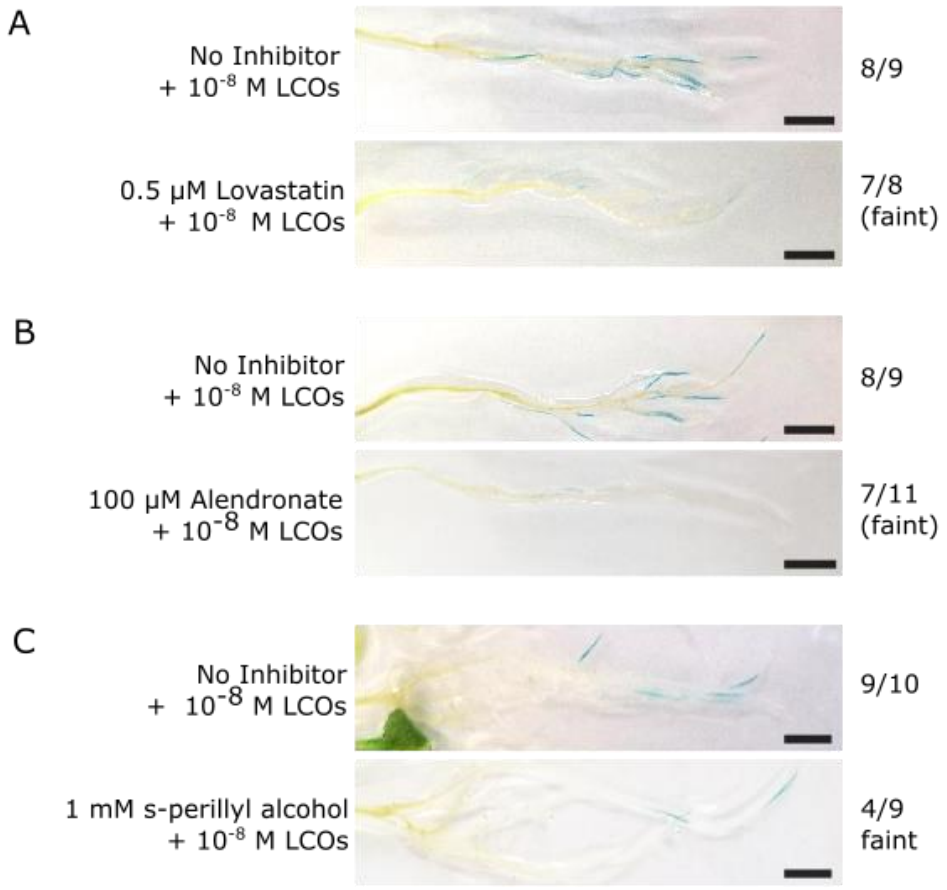

Figure 4: Mevalonate pathway components required for symbiotic signaling
Images show the expression of a *pENOD11::GUS* reporter in *M. truncatula* in response to LCOs from *S. meliloti.* Roots of *M. truncatula* in the presence of no inhibitor exhibit strong GUS staining 24 hours after LCO treatment, contrasting with plants grown in the presence of 0.5 µM lovastatin (A), plants grown in the presence of 100 µM alendronate (B), and plants grown in the presence of 1 mM s-perillyl alcohol (C) which all show weak GUS staining.Ratio represents number of plants with staining over total plants observed. Scale bars = 0.5 cm

One significant process downstream of farnesyl pyrophosphate synthase involved in signaling is protein prenylation. We investigated a requirement for prenylation in symbiotic signaling using s-perillyl alcohol, an inhibitor of both farnesyl and geranylgeranyl prenylation. *M. truncatula* plants containing *pENOD11*::GUS were treated with 1 mM s-perillyl alcohol and LCOs. Once again, s-perillyl alcohol-treated

roots exhibited lower levels of *pENOD11::GUS* expression in response to LCOs than untreated roots **(Figure 4c)**. This suggests that symbiotic signal transduction involves protein prenylation for the expression of *ENOD11*. S-perrilyl alcohol may otherwise inhibit other cell processes or lead to cell death and be responsible for the observed symbiotic defect.

Connection between HMGR activity and phospholipase signaling in symbiosis

Phospholipase signaling components have been implicated in the cytoplasmic segment of the common symbiosis pathway. Chemical inhibition of either phospholipase C (PLC) or phospholipase D (PLD) inhibits LCO-induced symbiotic responses (Den Hartog et al., 2001). We investigated the order in which phospholipases and HMGRs play a role in the signaling pathway by using chemical inhibitors of phospholipases in combination with inducible HMGR activity. Neomycin and 1-butanol inhibit PLC activity and the formation of PLD-derived phosphatidic acid, respectively (Den Hartog et al., 2001). Roots of *M. truncatula* plants containing a *pENOD11::GUS* reporter were transformed with ethanol inducible HMGR1cat, treated with 100 μM neomycin, 0.5% 1-butanol, or water, and then treated with 2% ethanol. Roots treated only with water were used as negative controls. Roots treated with ethanol without either inhibitor expressed high levels of *pENOD11::GUS*, as expected. In contrast, we observed minimal to no *pENOD11::GUS* expression in ethanol-treated plants in the presence of neomycin or 1-butanol. Both neomycin and 1-butanol inhibit HMGR-induced expression of *pENOD11::GUS,* indicating that the phospholipase activity of both PLC and PLD is required for HMGR activation of the symbiotic signaling pathway. As with the other

biochemical inhibitor experiments, cell death or inhibition of additional targets are also possible explanations and will need to be ruled out.

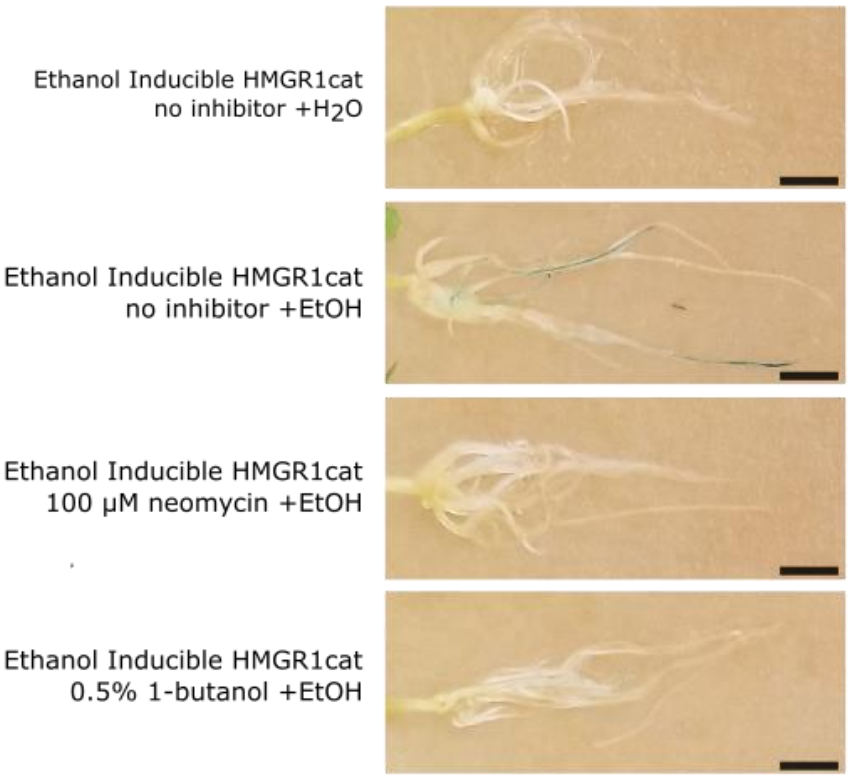

<u>Figure 5:</u> Inhibition of HMGR-activated symbiotic signaling by phospholipase inhibitors

Ethanol inducible HMGR1cat transgenic roots of *M. truncatula* plants containing *pENOD11::GUS* treated with water (A), with 2% ethanol alone (B), or 2% ethanol with 100 µM neomycin (C) or 0.5% 1-butanol (D). Autoactive HMGR did not drive *pENOD11::GUS* expression in *M. truncatula* treated with inhibitors of phospholipases. A representative root system for each treatment is shown. Ratio represents number of plants with staining over total plants observed. Scale bars = 0.5 cm

4.4 – Materials and Methods

Inducible HMGR1cat, GUS, and luciferase construct design

An autoactive version of HMGR has previously been generated from an *Arabidopsis thaliana* HMGR1 by truncation, leaving only the catalytic domain (Dale et al., 1995). To generate an autoactive version of HMGR for *M. truncatula* (HMGR1cat), we employed the same method using *MtHMGR1*. To create an equivalent modification, the last 933 bp of the c-terminus of *MtHMGR1* containing the catalytic domain and four amino acids of the upstream linker region was synthesized with GoldenGate CDS overhangs, with BsaI, BpiI, and BbmI type IIs restriction sites removed via silent mutations (Engler et al., 2014). As a way to control the expression of the autoactive HMGR, we designed and synthesized an ethanol-inducible promoter. This promoter consists of a fusion between an *AlcA* promoter and a minimal CaMV35S promoter. Previous research identified a system using a similar fusion promoter and the presence of the regulatory component, AlcR, to be highly controllable by ethanol concentrations in tobacco (Caddick et al., 1998). To create a GoldenGate compatible ethanol inducible promoter, we synthesized a fragment containing the *AlcA* promoter from *Aspergillus nidulans,* followed by the -31 to +5 region of the CaMV35S promoter sequence. This fragment was also synthesized with modifications to eliminate any type IIs restriction sites and to contain the correct overhang sequences for a Pro + 5U GoldenGate part.

All cloning and construct assembly was performed using GoldenGate cloning methodology (Engler et al., 2014). To create the level 1 inducible HMGR1cat expression cassette, the level 0 ethanol inducible promoter, HMGR1cat, and 35S terminator parts were assembled into a level 1 acceptor. Additionally, we created the negative control

inducible GUS and inducible luciferase level 1 parts by assembling either the level 0 GUS CDS or luciferase CDS by assembly with the ethanol-inducible promoter and 35s terminator level 0 parts. The corresponding level 2 plasmids were constructed by the assembly of the inducible HMGR1cat, inducible GUS, or inducible luciferase level 1 part along with the *AlcR* regulator of *AlcA*, tdTomato-ER fluorescent reporter, and nuclear-localized G-GECO1.2 level 1 parts into the binary GoldenGate level 2 acceptor plasmid.

***Medicago truncatula Agrobacterium*-mediated transformation**

Each of the desired binary expression vectors was transformed into *Agrobacterium rhizogenes* MSU440 using electroporation. Germinated *M. truncatula* seedlings were transformed using *Agrobacterium rhizogenes* MSU440 containing the inducible HMGR1cat, GUS, or luciferase binary vectors to generate transgenic roots using the *Agrobacterium*-mediated root transformation method (Delaux et al., 2015)

***Medicago truncatula* growth conditions and treatments**

Wild-type or *pENOD11::GUS M. truncatula* Jemalong A17 seeds were surface-sterilized with sulfuric acid and germinated on agar plates containing 1 µM gibberellic acid in the dark for 48 hours at 4°C followed by 24 hours at 20°C. *M. truncatula* seedings (12 per plate) were then grown on modified Fahräeus medium agar (Vincent, 1970) in large 24.5 x 24.5 cm square petri dishes under light racks with 65 µmol m^{-2} s^{-1} continuous light at 20°C. For the induction of inducible promoter-driven gene expression, 2-3 weeks post-transformation, plants containing transgenic roots were removed from their plates, submerged in 50 ml of 2% ethanol for one hour, and placed back on their plates for 24 hours. For biochemical induction of the symbiotic signaling

pathway, plants were removed from their plates, submerged in 10^{-8} M LCOs from *S. meliloti* (GM16390), and placed back on their plates for 24 hours. Chemical inhibition of HMGR and farnesyl pyrophosphate synthase activity were performed by transferring three-day-old *M. truncatula* seedlings to Fahräeus medium agar plates containing either 0.5 µM lovastatin or 100 µM alendronate, respectively, for ten days before treatment with LCOs and subsequent placement back on the inhibitor-containing Fahräeus medium agar plates for 24 hours. S-perillyl treatment for the inhibition of prenyltransferase activity was performed by submerging the roots of two-week-old *M. truncatula* in 50 ml of 1 mM s-perillyl alcohol for one hour before the addition of LCOs. The plants were then placed back on Fahräeus medium agar plates, and the root systems of each plant were covered with 0.5 ml of 1 mM s-perillyl alcohol. For inhibition of PLC and PLD signaling with neomycin and 1-butanol, respectively, we removed the transgenic plants from modified Fahräeus medium agar plates 2-3 weeks post-transformation, submerged the roots in 50ml of 100 µM neomycin or 0.5% 1-butanol for a one-hour pretreatment before the addition of ethanol, placed back on Fahräeus medium agar plates, and each root system was covered with 0.5 ml of either neomycin or 1-butanol.

Symbiotic gene expression analysis

In *M. truncatula plants* containing the *pENOD11::GUS* reporter, expression of ENOD11 was observed by GUS staining. Whole plants were submerged in GUS staining solution containing X-Gluc 24 hours after ethanol or LCO treatment, vacuum infiltrated for 10 minutes, and incubated at 37°C for 3-6 hours (Journet et al., 2001)

4.5 – Discussion

Research justification. HMGR knockdown mutants in *M. truncatula* are defective in nodule development, showing the importance of HMGR in forming root nodule symbiosis (Kevei et al., 2007). Complete association between a leguminous host plant and the rhizobia partners for the development of a functional nitrogen-fixing nodule requires many complex cellular processes in which HMGR could serve an essential function. HMGR1 interacts with the symbiotic co-receptor, DMI2/NORK, and HMGR1 knockout mutants are defective in symbiotic nuclear calcium-spiking, suggesting that HMGR activity is necessary for signal transduction (Kevei et al., 2007; Venkateshwaran et al., 2015). The use of exogenous application of the immediate product of HMGR activity, mevalonate, demonstrated that it induces both nuclear calcium spiking and expression of the symbiotic marker gene *ENOD11* (Venkateshwaran et al., 2015). These results point to a role of HMGR in the signal transduction process necessary for root nodule and arbuscular mycorrhizal symbioses. Many isoprenoids are derived from the mevalonate pathway, but unlike mevalonate, the inability of the exogenous application of downstream products, such as isopentenyl pyrophosphate, to stimulate symbiotic responses has left the identity of the isoprenoid secondary messenger unknown (Venkateshwaran et al., 2015).

In the present study, we further support a role for HMGR activity in the symbiotic signaling pathway and elucidate additional signaling mechanisms downstream of HMGR and mevalonate.

HMGR activity in the common symbiosis pathway. Through the development and use of an inducible constitutively active HMGR system, we show that HMGR

activity alone is sufficient to stimulate the expression of the symbiosis marker gene *ENOD11*. While mevalonate, the product of HMGR activity, was already shown to induce symbiotic signaling, exogenous chemical application introduces alterations to external conditions, which may cause unintended cellular responses. *In vivo* generation of mevalonate by activation of HMGR eliminates the possibility of cell surface receptor-ligand responses. The addition of more controls for our inducible system will be necessary for these experiments. The expression of luciferase and HMGRcat will need to be assessed through either qRT-PCR or western blot to confirm the expression of the HMGR1 catalytic domain is responsible for inducing *ENOD11* expression. ENOD11 expression is only one of many known symbiotic responses. To complement our *pENOD11::GUS* staining assays, additional experiments using qRT-PCR to quantify the induction of other symbiotic specific genes and experiments observing for calcium-spiking in response to the induction of HMGR1cat expression will be performed. These experiments will provide further evidence of HMGR activity being sufficient for symbiotic responses.

Using this same inducible constitutively active HMGR system in *dmi1* and *dmi2 M. truncatula* mutants, we show that HMGR-activated symbiotic responses are not dependent on either DMI1 or DMI2, as symbiotic gene expression in response to HMGR activity was still observed in these plants. This is consistent with prior reports in *dmi2* mutants but contradicts the previous finding that mevalonate was unable to trigger symbiotic responses in *dmi1* mutants (Venkateshwaran et al., 2015). Our results suggest a model where HMGR activity is positioned downstream of DMI2 and is capable of circumventing *dmi1*. Differences in *dmi1* phenotypes may be explained by

possible higher subcellular concentrations or continued presence of mevalonate caused by autoactivate HMGR. A similar ability to trigger calcium spiking in *dmi1* mutants is observed with the application of the G-protein agonist Mas7 (Sun et al., 2007). High concentrations of mevalonate may be able to circumvent *DMI1* in symbiotic signaling through excessive stimulation of other nuclear calcium channels. The presence of *MtCASTOR*, whose homolog in *Lotus japonicus* is an ion channel similar to DMI1 which serves a role in calcium spiking, may compensate for the loss of *DMI1* and be sufficient for calcium spiking with a large stimulus (Venkateshwaran et al., 2012). Alternatively, HMGR activity may otherwise occur downstream of DMI1. As HMGR stimulated symbiotic responses still occur in both mutants we tested, further experiments testing the ability of HMGR activity to stimulate symbiotic signaling in mutants of other components involved in later stages of the pathway, such as *dmi3,* will further clarify the relative position of HMGR. Observing for calcium spiking in *dmi1* mutants in response to autoactive HMGR will also provide support for the function of HMGR activity in the pathway.

Mevalonate pathway branching. To identify which isoprenoid products generated from HMGR activity are responsible for signal transduction, we used biochemical inhibitors of different processes along the mevalonate pathway. Starting with inhibitors of enzymes near the beginning of the pathway and moving down, we aimed to identify where the mevalonate pathway branches during symbiotic signaling. First, we determined that inhibition of HMGR activity with lovastatin decreased expression of the symbiotic reporter gene *ENOD11* in response to LCOs. This

confirmed our expectation, as it agrees with the ability of lovastatin to limit nodulation and our finding that HMGR triggers symbiotic responses (Kevei et al., 2007).

We then targeted a process far down the mevalonate pathway to assess whether isoprenoids generated from late steps or early steps are necessary for the symbiotic signaling transduction. Using alendronate, we determined farnesyl pyrophosphate synthase activity is necessary for LCO induction of *ENOD11* gene expression. This rules out the involvement of isoprenoids generated from earlier branches as being sufficient for symbiotic signal transduction. The last two steps of the core mevalonate pathway include the production of farnesyl pyrophosphate and geranylgeranyl pyrophosphate. Our finding suggests a process utilizing either farnesyl pyrophosphate or geranylgeranyl pyrophosphate as precursors in symbiotic signal transduction. As described above, many isoprenoids are generated from these precursors.

Prenylation is one specific process with a connection to signaling, as the addition of prenyl groups (farnesyl and geranylgeranyl) to proteins is known to alter protein localization and functionality (Hála and Žárský, 2019). There are hundreds of plant proteins known to be targeted for prenylation (Running, 2014). To determine whether prenylation is involved in symbiotic signaling, we used the general prenyltransferase inhibitor s-perillyl alcohol, which inhibits both farnesyltransferase and geranylgeranyltransferase (Courdavault et al., 2005). The application of s-perillyl alcohol led to decreased induction of *ENOD11* expression by LCOs, signifying an important role for prenylation in the continuation of symbiotic signaling.

Inhibitor assays, unfortunately, exhibit some pitfalls for interpreting the mechanism responsible for their observed biological effect. However, each of the

biochemical inhibitors used here have been well studied in plants and verified for their inhibition of their targeted activity. Still, the possibility of other unknown enzyme targets of these inhibitors are difficult to rule out. Experiments using other known inhibitors of HMGR, FPPS, and prenyl transferase activity for the verification of similar decreases in symbiotic responses will help eliminate concerns with the possibility of off-target effects. To rule out the possibility that cell death is responsible for the observed decreases in pENOD11:GUS expression when treated with mevalonate pathway inhibitors, we will also need to observe for continued cytoplasmic streaming or changes in housekeeping gene expression by qRT-PCR.

Our study did not identify the type of prenylation involved or the prenylation target involved in this process. Further experiments carried out in a similar manner but with specific inhibitors of either farnesyltransferase or geranylgeranyltransferase will clarify whether the lack of farnesylation or geranylgeranylation is responsible for the defect in symbiotic gene expression. This would further narrow down the possible prenylation targets involved in this pathway as specific proteins are either farnesylated or geranylgeranylated based on their CaaX sequence motif (Hála and Žárský, 2019). Prenylation targets involved in symbiotic signaling could further be identified through prenylomics experiments comparing the prenylation status of proteins in LCO treated plants compared to untreated plants.

Connecting multiple signaling mechanisms. Additional signal transduction mechanisms are employed in the CSP, but how these signaling mechanisms relate to other components remains uncertain. This is the case for the role of phospholipase signaling; PLC and PLD activity are both induced by the application of LCOs, and

inhibition of PLC and PLD decreases symbiotic responses (Den Hartog et al., 2001). We tested for a possible link between mevalonate pathway signaling and phospholipase signaling using inhibitors of PLC and PLD activity in combination with induction of HMGR activity. We determined that both PLD and PLC activity is necessary for HMGR-induced *ENOD11* expression. Our results place PLC and PLD activity downstream of HMGR activity in the CSP. As with the mevalonate pathway inhibitor experiments, these experiments will need to be followed up with the observation for cytoplasmic streaming, qRT-PCR for detection of maintained housekeeping gene expression, and experiments with additional PLC and PLD inhibitors to assure the observed responses are not due to off-target inhibitor effects or cell death.

We suggest a model for symbiotic signal transduction in the cytoplasm in which phospholipase signaling plays a role downstream of HMGR activity and the mevalonate pathway. In this model, HMGRs are activated by the detection of microbial signals (LCOs/COs) and produce mevalonate. The continuation of the mevalonate pathway through the activity of farnesyl pyrophosphate synthase converts mevalonate into farnesyl pyrophosphate. An unknown protein/proteins is prenylated with farnesyl pyrophosphate by a prenyltransferase, localizing it to the plasma membrane. PLC and PLD are then activated, leading to the production of diacylglycerol (DAG) and inositol triphosphate (IP3), and phosphatidic acid, respectively. One or more of these products then, directly or indirectly, stimulate ion channels/pumps at the nuclear envelope (**Figure 6)**.

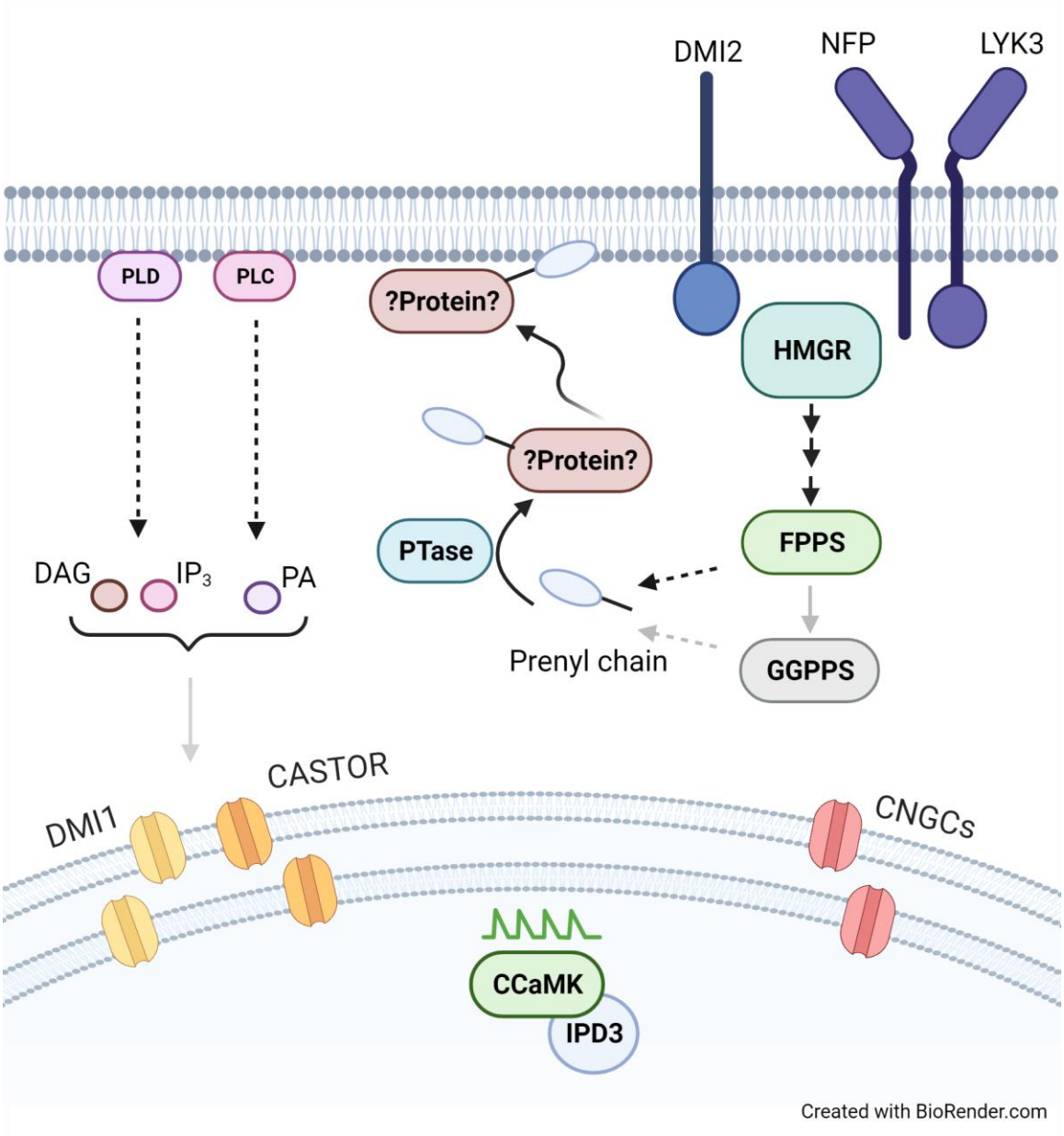

Figure 6: Model for connection between mevalonate pathway and phospholipase signaling in the common symbiosis pathway

HMGR activity is stimulated by the detection of LCOs, producing mevalonate. The continuation of the mevalonate pathway through FPPS, and possibly GGPPS, subsequently convert mevalonate into the prenyl group, FPP or GGPP. Prenylation of an unknown protein by a prenyltransferase (PTase) alters its localization to the plasma membrane and leads to the activation of PLC and PLD. Products of PLC and PLD, either directly or indirectly, activate ion channels/pumps at the nuclear envelope.

4.6 – References

Amor, B. Ben, Shaw, S.L., Oldroyd, G.E.D., Maillet, F., Penmetsa, R.V., Cook, D., Long, S.R., Dénarié, J., Gough, C., 2003. The NFP locus of Medicago truncatula controls an early step of Nod factor signal transduction upstream of a rapid calcium flux and root hair deformation. Plant J. 34, 495–506. https://doi.org/10.1046/j.1365-313X.2003.01743.

Ané, J.-M., Kiss, G.B., Riely, B.K., Penmetsa, R.V., Oldroyd, G.E.D., Ayax, C., Lévy, J., Debellé, F., Baek, J.-M., Kaló, P., Rosenberg, C., Roe, B.A., Long, S.R., Dénarié, J., Cook, D.R., 2004. Medicago truncatula DMI1 required for bacterial and fungal symbioses in legumes. Science. 303, 1364–1367. https://doi.org/10.1126/science.1092986

Antolín-Llovera, M., Ried, M.K., Parniske, M., 2014. Cleavage of the symbiosis receptor-like kinase ectodomain promotes complex formation with nod factor receptor 5. Curr. Biol. 24, 422–427. https://doi.org/10.1016/j.cub.2013.12.053

Bersoult, A., Camut, S., Perhald, A., Kereszt, A., Kiss, G.B., Cullimore, J. V., 2005. Expression of the Medicago truncatula DMI2 gene suggests roles of the symbiotic nodulation receptor kinase in nodules and during early nodule development. Mol. Plant-Microbe Interact. 18, 869–875. https://doi.org/10.1094/MPMI-18-0869

Caddick, M.X., Greenland, A.J., Jepson, I., Krause, K.-P., Qu, N., Riddel, K. V., Salter, M.G., Wolfgang, S., Sonnewald, U., Tomsett, B.A., 1998. An ethanol inducible gene switch for plants used to manipulate carbon metabolism. Nat. Biotechnol. 16, 291–294.

Catoira, R., Galera, C., de Billy, F., Penmetsa, R. V, Journet, E.P., Maillet, F., Rosenberg, C., Cook, D., Gough, C., Dénarié, J., 2000. Four genes of Medicago truncatula controlling components of a Nod factor transduction pathway. Plant Cell 12, 1647–1666. https://doi.org/10.1105/tpc.12.9.1647

Charpentier, M., Oldroyd, G.E.D., 2013. Nuclear Calcium Signaling in Plants. Plant Phys. 1 163, 496–503. https://doi.org/10.1104/pp.113.220863

Charpentier, M., Sun, J., Martins, T. V., Radhakrishnan, G. V., Findlay, K., Soumpourou, E., Thouin, J., Very, A.-A., Sanders, D., Morris, R.J., Oldroyd, G.E.D., 2016. Nuclear-localized cyclic nucleotide-gated channels mediate symbiotic calcium oscillations. Science. 352, 1102–1105. https://doi.org/10.1126/science.aae0109

Choudhury, S.R., Pandey, S., 2013. Specific Subunits of Heterotrimeric G Proteins Play Important Roles during Nodulation in Soybean. Plant Physiol. 162, 522–533. https://doi.org/10.1104/pp.113.215400

Courdavault, V., Thiersault, M., Courtois, M., Gantet, P., Oudin, A., Doireau, P., St-Pierre, B., Giglioli-Guivarc'h, N., 2005. CaaX-prenyltransferases are essential for expression of genes involved in the early stages of monoterpenoid biosynthetic pathway in Catharanthus roseus cells. Plant Mol. Biol. 57, 855–870. https://doi.org/10.1007/s11103-005-3095-0

Dale, S., Arro, M., Becerra, B., Morrice, N.G., Boronat, A., Hardie, D.G., Ferrer, A., 1995. Bacterial Expression of the Catalytic Domain of 3-Hydroxy-3-Methylglutaryl-CoA Reductase (Isoform HMGR1) from Arabidopsis thaliana, and Its Inactivation by Phosphorylation at Ser577 by Brassica oleracea 3-Hydroxy-3-Methylglutaryl-CoA Reductase Kinase. Eur. J. Biochem. 233, 506–513. https://doi.org/10.1111/j.1432-

1033.1995.506_2.x
Delaux, P.M., Radhakrishnan, G. V., Jayaraman, D., Cheema, J., Malbreil, M., Volkening, J.D., Sekimoto, H., Nishiyama, T., Melkonian, M., Pokorny, L., Rothfels, C.J., Sederoff, H.W., Stevenson, D.W., Surek, B., Zhang, Y., Sussman, M.R., Dunand, C., Morris, R.J., Roux, C., Wong, G.K.S., Oldroyd, G.E.D., Ane, J.M., 2015. Algal ancestor of land plants was preadapted for symbiosis. Proc. Natl. Acad. Sci. U. S. A. 112, 13390–13395. https://doi.org/10.1073/pnas.1515426112
Den Hartog, M., Musgrave, A., Munnik, T., 2001. Nod factor-induced phosphatidic acid and diacylglycerol pyrophosphate formation: A role for phospholipase C and D in root hair deformation. Plant J. 25, 55–65. https://doi.org/10.1046/j.1365-313X.2001.00931.x
Dénarié, J., Debellé, F., Promé, J.C., 1996. Rhizobium lipo-chitooligosaccharide nodulation factors: signaling molecules mediating recognition and morphogenesis. Annu Rev Biochem 65, 503–535.
Engler, C., Youles, M., Gruetzner, R., Ehnert, T.M., Werner, S., Jones, J.D.G., Patron, N.J., Marillonnet, S., 2014. A Golden Gate modular cloning toolbox for plants. ACS Synth. Biol. 3, 839–843. https://doi.org/10.1021/sb4001504
Fellbaum, C.R., Gachomo, E.W., Beesetty, Y., Choudhari, S., Strahan, G.D., Pfeffer, P.E., 2011. Carbon availability triggers fungal nitrogen uptake and transport in arbuscular mycorrhizal symbiosis. PNAS 109, 2666-2671. https://doi.org/10.1073/pnas.1118650109/-/DCSupplemental.www.pnas.org/cgi/doi/10.1073/pnas.1118650109
Friesen, J.A., Rodwell, V.W., 2004. The 3-hydroxy-3-methylglutaryl coenzyme-A (HMG-CoA) reductases. Genome Biol. 5. https://doi.org/10.1186/gb-2004-5-11-248
Genre, A., Chabaud, M., Balzergue, C., Puech-Pagès, V., Novero, M., Rey, T., Fournier, J., Rochange, S., Bécard, G., Bonfante, P., Barker, D.G., 2013. Short-chain chitin oligomers from arbuscular mycorrhizal fungi trigger nuclear Ca2+ spiking in Medicago truncatula roots and their production is enhanced by strigolactone. New Phytol. 198, 190–202. https://doi.org/10.1111/nph.12146
Hála, M., Žárský, V., 2019. Protein prenylation in plant stress responses. Molecules 24, 1–14. https://doi.org/10.3390/molecules24213906
Holstein, S.A., Hohl, R.J., 2004. Isoprenoids : Remarkable Diversity of Form and Function. Lipids 39, 293–309.
Horváth, B., Yeun, L.H., Domonkos, Á., Halász, G., Gobbato, E., Ayaydin, F., Miró, K., Hirsch, S., Sun, J., Tadege, M., Ratet, P., Mysore, K.S., Ané, J.-M., Oldroyd, G.E.D., Kaló, P., 2011. Medicago truncatula IPD3 is a member of the common symbiotic signaling pathway required for rhizobial and mycorrhizal symbioses. Mol. Plant-Microbe Interact. 24, 1345–1358. https://doi.org/10.1094/mpmi-01-11-0015
Journet, E.P., El-Gachtouli, N., Vernoud, V., De Billy, F., Pichon, M., Dedieu, A., Arnould, C., Morandi, D., Barker, D.G., Gianinazzi-Pearson, V., 2001. Medicago truncatula ENOD11: A novel RPRP-encoding early nodulin gene expressed during mycorrhization in arbuscule-containing cells. Mol. Plant-Microbe Interact. 14, 737–748. https://doi.org/10.1094/MPMI.2001.14.6.737
Kanamori, N., Madsen, L.H., Radutoiu, S., Frantescu, M., Quistgaard, E.M.H., Miwa, H., Downie, J.A., James, E.K., Felle, H.H., Haaning, L.L., Jensen, T.H., Sato, S., Nakamura, Y., Tabata, S., Sandal, N., Stougaard, J., 2006. A nucleoporin is

required for induction of Ca2+ spiking in legume nodule development and essential for rhizobial and fungal symbiosis. Proc. Natl. Acad. Sci. U. S. A. 103, 359–364. https://doi.org/10.1073/pnas.0508883103

Kevei, Z., Lougnon, G., Mergaert, P., Horváth, B., Kereszt, A., Jayaraman, D., Zaman, N., Marcel, F., Regulski, K., Kiss, G.B., Kondorosi, A., Endre, G., Kondorosi, E., Ané, J.-M., Horváth, G. V, Horvath, G. V, 2007. 3-hydroxy-3-methylglutaryl coenzyme A reductase1 interacts with NORK and is crucial for nodulation in Medicago truncatula. Plant Cell 19, 3974–3989. https://doi.org/10.1105/tpc.107.053975

Kiers, E.T., Kiers, E.T., Duhamel, M., Beesetty, Y., Mensah, J.A., Franken, O., Verbruggen, E., Fellbaum, C.R., Kowalchuk, G.A., Hart, M.M., Bago, A., Palmer, T.M., West, S.A., Vandenkoornhuyse, P., Jansa, J., Bücking, H., 2012. Reciprocal Rewards Stabilize Cooperation in the Mycorrhizal Symbiosis. Science 880, 10–13. https://doi.org/10.1126/science.1208473

Kim, S., Zeng, W., Bernard, S., Liao, J., Ane, J., Jiang, Y., Venkateshwaran, M., 2019. Ca2+-regulated Ca2+ channels with an RCK gating ring control plant symbiotic associations. Nat. Commun. 10, 1–12. https://doi.org/10.1038/s41467-019-11698-5

Limpens, E., Franken, C., Smit, P., Willemse, J., Bisseling, T., Geurts, R., 2003. LysM Domain Receptor Kinases Regulating Rhizobial Nod Factor-Induced Infection. Science 302, 630–633. https://doi.org/10.1126/science.1090074

Limpens, E., Ovchinnikova, E., Journet, E.P., Chabaud, M., cosson, viviane, Ratet, P., Duc, G., Fedorova, E.E., Liu, W., Op den Camp, R., Zhukov, V., Tikhonovich, I.A., Borisov, A., Bisseling, T., 2011. IPD3 controls the formation of nitrogen-fixing symbiosomes in pea and Medicago. Mol. Plant-Microbe Interact. 24, 1333-1344. https://doi.org/10.1094/mpmi-01-11-0013

Lindström, K., Mousavi, S.A., 2020. Effectiveness of nitrogen fixation in rhizobia. Microb. Biotechnol. 13, 1314–1335. https://doi.org/10.1111/1751-7915.13517

Maillet, F., Poinsot, V., André, O., Puech-Pagés, V., Haouy, A., Gueunier, M., Cromer, L., Giraudet, D., Formey, D., Niebel, A., Martinez, E.A., Driguez, H., Bécard, G., Dénarié, J., 2011. Fungal lipochitooligosaccharide symbiotic signals in arbuscular mycorrhiza. Nature 469, 58–64. https://doi.org/10.1038/nature09622

Messinese, E., Mun, J.-H.H., Yeun, L.H., Jayaraman, D., Rougé, P., Barre, A., Lougnon, G., Schornack, S., Bono, J.-J., Cook, D.R., Ané, J.-M., Rouge, P., 2007. A novel nuclear protein interacts with the symbiotic DMI3 calcium- and calmodulin-dependent protein kinase of Medicago truncatula. Mol. Plant-Microbe Interact. 20, 912–921. https://doi.org/10.1094/MPMI-20-8-0912

Miller, J.B., Pratap, A., Miyahara, A., Zhou, L., Bornemann, S., Morris, R.J., Oldroyd, G.E.D., 2013. Calcium/calmodulin-dependent protein kinase is negatively and positively regulated by calcium, providing a mechanism for decoding calcium responses during symbiosis signaling. Plant Cell 25, 5053–5066. https://doi.org/10.1105/tpc.113.116921

Mitra, R.M., Gleason, C.A., Edwards, A., Hadfield, J., Downie, J.A., Oldroyd, G.E.D., Long, S.R., 2004. A Ca2+/calmodulin-dependent protein kinase required for symbiotic nodule development: Gene identification by transcript-based cloning. Proc. Natl. Acad. Sci. U. S. A. 101, 4701–4705. https://doi.org/10.1073/pnas.0400595101

Moling, S., Pietraszewska-Bogiel, A., Postma, M., Fedorova, E.E., Hink, M.A., Limpens, E., Gadella, T.W.J., Bisseling, T., 2014. Nod Factor Receptors Form Heteromeric Complexes and Are Essential for Intracellular Infection in Medicago Nodules. Plant Cell 26, 4188-4199. https://doi.org/10.1105/tpc.114.129502

Riely, B.K., Ané, J.M., Penmetsa, R.V., Cook, D.R., 2004. Genetic and genomic analysis in model legumes bring Nod-factor signaling to center stage. Curr. Opin. Plant Biol. 7, 408–413. https://doi.org/10.1016/j.pbi.2004.04.005

Running, M.P., 2014. The role of lipid post-translational modification in plant developmental processes. Front. Plant Sci. 5, 1–9. https://doi.org/10.3389/fpls.2014.00050

Stermer, B. a, Bianchini, G.M., Korth, K.L., 1994. Regulation of HMG-CoA reductase activity in plants. J. Lipid Res. 35, 1133–40.

Sun, J., Miwa, H., Downie, J.A., Oldroyd, G.E.D., 2007. Mastoparan activates calcium spiking analogous to Nod factor-induced responses in Medicago truncatula root hair cells. Plant Physiol 144, 695–702.

Venkateshwaran, M., Cosme, A., Han, L., Banba, M., Satyshur, K.A., Ané, J.-M., Schleiff, E., Parniske, M., Imaizumi-Anraku, H., 2012. The Recent Evolution of a Symbiotic Ion Channel in the Legume Family Altered Ion Conductance and Improved Functionality in Calcium Signaling. Plant Cell 24, 2528–2545. https://doi.org/10.1105/tpc.112.098475

Venkateshwaran, M., Jayaraman, D., Chabaud, M., Genre, A., Balloon, A.J., Maeda, J., Forshey, K.L., den Os, D., Kwiecien, N.W., Coon, J.J., Barker, D.G., Ané, J.-M., 2015. A role for the mevalonate pathway in early plant symbiotic signaling. Proc. Natl. Acad. Sci. 112, 9781-9786. https://doi.org/10.1073/pnas.1413762112

Wang, W., Shi, J., Xie, Q., Jiang, Y., Yu, N., Wang, E., 2017. Nutrient Exchange and Regulation in Arbuscular Mycorrhizal Symbiosis. Mol. Plant 10, 1147–1158. https://doi.org/10.1016/j.molp.2017.07.012

Chapter 5 – Discussion

5.1 – Justification and aims of research

This dissertation sought to clarify the subcellular signal transduction process for the formation of beneficial plant-microbe interactions, relating specifically to AM symbiosis and RN symbiosis. As these two beneficial plant-microbe interactions are some of the most agriculturally important, they have been the subject of extensive research elucidating numerous molecular components shared between both processes (Oldroyd, 2013).The evolutionary conservation of these components and the cytoplasmic signaling mechanisms involved in symbiotic signal transduction are areas that have been enigmatic and are, therefore, the focus of the included work.

5.2 – Conclusions regarding the conservation of CCaMK and IPD3 in *Physcomitrium*

Non-host plants for AM and RN symbiosis lack numerous genes associated with these two symbioses, indicating loss of the ability to form these associations leads to the loss of multiple symbiosis-specific genes (Delaux et al., 2014; Griesmann et al., 2018). The retention of *CCaMK* and *IPD3* homologs in *Physcomitrium patens*, which do not show either RN or AM-like symbioses, raises questions regarding its conservation and function. Therefore, in **chapter 2,** we investigated the biochemical, molecular, and biological features of these two genes in *P. patens.*

We identified CCaMK and IPD3 homologs in the *P. patens* genome with similar sequence and biochemical features to angiosperm CCaMK and IPD3. Research in legumes generated molecular tools to study the functionality of CCaMK and IPD3 through the generation of gain-of-function variants using phosphomimetic mutations

and/or truncations eliminating the autoinhibitory domain (Gleason et al., 2006; Tirichine et al., 2006). We adapted these strategies for genetic studies of these genes in *P. patens*. Transformations of *M. truncatula* with constitutively active *PpCCaMK* phenocopies the early symbiotic gene expression and spontaneous nodulation responses seen using the equivalent *M. truncatula* variant. Expression of unaltered *PpCCaMK* in *dmi3*/*ccamk* mutants in *M. truncatula* also rescues the lack-of-nodulation and -mycorrhization phenotypes in these mutants. Similar rescue experiments in *M. truncatula ipd3-1* mutants with *PpIPD3* restored the ability to generate nodules, but these nodules did not fix nitrogen, suggesting a lack of all necessary transcription-factor binding sites. Our results indicate partial conservation of the molecular function of the CCaMK and IPD3 components in *P. patens* for symbiotic signaling. AM-like associations have never been demonstrated in *P. patens,* suggesting the retention of these genes is for an unknown biological role. We investigated the response of *P. patens* to the activity of CCaMK and IPD3 using the constitutively active variants. The activity of both CCaMK and IPD3 stimulated stress-related responses, inducing brood cell formation and ABA signaling. These genes, however, were not required for osmotic stress-stimulated ABA responses, which occurred as expected in the *P. patens ccamk* and *ipd3* mutants. We hypothesize that CCaMK and IPD3 are involved in signaling for an unknown non-drought induced stress response. Further research regarding the physiology of *P. patens* during stress responses will be instrumental to uncovering the native biological function of PpCCaMK and PpIPD3 in mosses.

5.3 – Conclusions regarding the role of the HMGR family in root nodule symbiosis

Continued research identifying essential signaling mechanisms will provide further insight into the evolutionary aspects of AM and RN symbioses and additionally aid in the long-time goal of improving the associations. The molecular mechanisms for symbiotic signal transduction between the plasma membrane and the nuclear envelope are poorly understood, but prior work has demonstrated a requirement for HMGR activity. However, their methodology leaves open the possibility of the involvement of an individual or multiple HMGR family members (Kevei et al., 2007).

The research discussed in **Chapter 3** aimed to identify the specific HMGR gene required to form symbiotic associations. Through reverse genetics screening of individual HMGR knockout mutants in *M. truncatula*, *HMGR1* and *HMGR2c* were revealed to both be essential for RN symbiosis. The drastic reduction or absence of bacterial *NifH* expression in these *HMGR* mutant nodules identifies another role for HMGR activity in late stages of nodule development, in addition to the previously identified role in early nodule organogenesis. The observed differences between RNAi knockdown and insertion knockout may be explained by an overall reduction in *HMGR* expression and functional redundancy between multiple *HMGRs*. A similar dual role in nodulation is observed with NORK/DMI2, as knockout mutants do not nodulate while RNAi knockdown lines form nodules but are defective in nitrogen fixation (Catoira et al., 2000; Limpens et al., 2005). The overlap in mutant phenotype patterns between DMI2/NORK and HMGRs fits well with a model in which they work together for symbiotic signal transduction.

5.4 – Conclusions regarding downstream symbiotic signaling in the cytoplasm

The enzymatic activity of HMGRs produces an intermediate that feeds into the complex and highly branched mevalonate pathway and thus drives many biological functions. We aimed to identify the role of HMGRs in symbiotic signaling. Previously, attempts had been made to identify the mevalonate pathway enzymes functioning downstream of HMGR in symbiosis via the use of biochemical activators, but these were unsuccessful (Venkateshwaran et al., 2015). We aimed to address the questions regarding signaling downstream of HMGR through the use of biochemical inhibitors (**Chapter 4)**.

Cytokinins, products of DMAPP activity in the mevalonate pathway, are known to participate in the induction of nodule organogenesis (Gamas et al., 2017). However, experiments using an inhibitor of farnesyl pyrophosphate synthase demonstrated that symbiotic signaling requires a product derived from farnesyl pyrophosphate, not products branching from DMAPP. We also demonstrated that the expression of early symbiotic genes requires prenyltransferase activity, and by inference, involves the prenylation of unknown target proteins. This suggests the role of HMGR activity in symbiotic signaling is for the production of prenyl side chains to alter protein localization and activate the next steps in signal transduction.

Besides mevalonate pathway signaling, phospholipase signaling is implicated in the induction of symbiotic responses (Den Hartog et al., 2001; Pingret et al., 1998). Phospholipases are likely involved in the cytoplasm due to their localization, but their placement in relation to other known signaling components was unknown. Using biochemical inhibitors, we showed that activation of symbiotic responses by HMGR

activity requires both phospholipase C and phospholipase D activity. Placing phospholipase activity downstream of HMGR activity in the signaling pathway suggests that a PLC or PLD product acts as the secondary messenger responsible for nuclear ion channel activation.

5.5 – Future directions in the study of the commons symbiosis pathway

Continued research uncovering symbiotic signaling molecular mechanisms will be essential for our understanding of the diverging processes responsible for AM-specific or RN-specific responses. Ultimately this knowledge will provide an opportunity for targeted modifications of AM host plants to allow them to associate with rhizobia.

HMGR functional redundancy*.* The identification of numerous *HMGRs* with important roles in nodule development brings up questions regarding functional redundancy between HMGRs. High sequence similarity between *HMGR1* and the three *HMGR2* genes supports this idea (**Chapter 3**). In addition to rescue experiments overexpressing the *HMGR* knocked out in the mutant, rescues with overexpression of an alternate *M. truncatula HMGR* sequence could identify the HMGRs with similar functionality. The reason why some HMGR knockout mutants cause observable nodulation phenotypes while others do not could be due to differential expression between functionally similar HMGRs. Transcript abundance approaches have left our knowledge of *M. truncatula HMGR* expression lacking due to problems differentiating extremely similar *HMGR* coding sequences. Promoter-GUS fusions for each *M. truncatula HMGR* would circumvent this issue, allowing for an accurate determination of which are expressed in roots and/or nodules and clarity as to which HMGR could serve a biological role in nodulation. The continued development of multi-*HMGR* knockout

mutants and their assessment of any additive nodulation phenotypes would further clarify any functional redundancy between HMGRs in nodulation, and hopefully, explain the different phenotypes observed between *HMGR* single knockout mutants and the RNAi knockdown line (Kevei et al., 2007).

***Regulation of HMGRs in symbiosis*.** A stable line with a more severe nodulation phenotype will also greatly serve our efforts to uncover the placement of HMGRs in the signaling pathway and their mechanism of action. With numerous gain-of-function mutants in known symbiotic signaling components with the ability to stimulate symbiotic responses at our disposal, we can test for the requirement of *HMGRs* at multiple steps along the common symbiosis pathway (Gleason et al., 2006; Saha et al., 2014). As NORK/DMI2 interacts with LCO receptors as well as HMGR1, the possibility of HMGR interactions with LYK3 and NFP are of interest (Antolín-Llovera et al., 2014; Jayaraman et al., 2017). Protein interactions between HMGRs and the symbiotic RLKs may serve in regulating HMGR activity. What remains cryptic is how HMGRs are activated during symbiosis. Following protein interaction assays between HMGRs and the symbiotic RLKs, kinase assays between these proteins and analysis of the effects of phosphomimetic-HMGR mutants would answer how incoming symbiotic signals activate HMGRs.

Link between HMGRs and phospholipases. The findings in **chapter 4** identify a role for prenylation and phospholipase activity downstream of HMGRs in symbiotic signaling. No known direct connection between prenylation, or HMGR activity in general, and the activity of PLC or PLD has been established. Therefore, we predict an intermediate protein, which is prenylated, is responsible for continuing signal

transduction between HMGRs and phospholipases. A prenylomics approach comparing the differential prenylation status of proteins between untreated, LCO-treated, and autoactive HMGR plants could illuminate possible prenylation targets during symbiotic signaling. Heterotrimer G-proteins, which are prenylated during other signaling mechanisms, are candidate targets downstream of HMGR activity in the common symbiosis pathway (Muntz et al., 1992). G-proteins have already been identified as important signaling components in nodulation with a role upstream of phospholipases (Den Hartog et al., 2001). In other systems, the prenylation of G-proteins has been determined to be directly responsible for their ability to activate PLCs (Fogg et al., 2001). To confirm this hypothetical role for G-proteins linking the NORK/HMGR complex to PLC activation, biochemical G-protein inhibitors could be applied to the inducible auto-active HMGR line created in this work. Further analysis of G-protein knockout mutants in *M. truncatula* and attempted rescues with modified unprenylatable G-protein subunits would also help confirm a connection between HMGR activity and phospholipase activity.

Signal for activating ion channels. The final question in cytoplasmic symbiotic signal transduction remains: what activates ion channels at the nuclear envelope responsible for calcium-spiking? Inositol triphosphate remains a likely candidate due to its known role in calcium release in mammals (Taylor and Tovey, 2010). Inhibitors of IP3 calcium release in mammals are capable of blocking LCO induced symbiotic nuclear calcium spiking (Engstrom et al., 2002). However, no IP3 regulated ion channels have been identified in plants to date (Krinke et al., 2007). A continued search for IP3 regulated ion channels in plants may be necessary to determine whether IP3 is

the secondary messenger required for symbiotic signaling. However, phosphatidic acid cannot be ruled out as the signaling molecule responsible for initiating calcium spiking, as recent research has identified ion channels regulated by phosphatidic acid in plants (Shen et al., 2020).

Functional differences between PpIPD3 and MtIPD3. In regards to symbiotic signaling components in mosses, the biological function of PpCCaMK and PpIPD3 remains unclear. It is difficult to conclude whether the ABA and brood cell formation response to autoactive forms of IPD3 and CCaMK in *P. patens* is a direct response controlled by these signaling components or an off-target effect due to unnatural activity levels. Abscisic acid is known to regulate nodulation and mycorrhization but does so in a negative manner at high concentrations (Charpentier et al., 2014; Tominaga et al., 2010). In legumes, there is no observed ABA or stress response to autoactive CCaMK similar to that in moss (Takeda et al., 2012). Analysis comparing ABA responses between autoactive PpIPD3 and MtIPD3 in both *P. patens* and *M. truncatula* could help clarify if PpIPD3 is neofunctionalized for a role in stress response. A transcriptomics approach in *P. patens* would greatly aid in our broader understanding of the biological role of CCaMK-IPD3 signaling in moss. Specifically, comparing differentially regulated genes between wild-type and *ipd3 P. patens* mutants in response to AM fungi or fungal pathogens may provide answers to whether its biological function is for microbe interactions. Additionally, further investigation into the lack of complete rescue of *M. truncatula ipd3* mutants will help us understand the mechanism of action of IPD3 in legumes. Specifically, the use of DAPseq with MtIPD3 and PpIPD3 will illuminate differences in their ability to activate necessary transcription factors.

5.6 – Future of the field of plant-microbe interactions

A significant gap in knowledge remains in the plant-microbe interactions field as to how plants differentiate beneficial microbes from pathogens. The rhizosphere consists of a diverse microbiome with both pathogens and beneficial microbes simultaneously interacting with plants (Mendes, 2013). Therefore, plants need to constantly regulate their innate immunity and defense responses to allow for symbiotic associations while keeping pathogens at bay. Microbial symbionts need to remain undetected or suppress host immunity to evade plant defenses. On the plant side, this process requires the precise recognition of the nearby microbes and the determination of whether they are harmful or helpful (Bozsoki et al., 2020). The microbial signals, or "molecular associated molecular patterns" (PAMPs), responsible for triggering the first layer of defense are highly conserved features of microbes, including those which are beneficial (Newman et al., 2013). Interestingly, MAMPs are detected similarly to symbiotic LCOs and COs through binding to a complex of kinase-active and kinase-inactive RLKs (Couto and Zipfel, 2016). Numerous models have suggested a mechanism in which long-chain COs signify pathogens and induce defense, whereas LCOs or short-chain COs signify beneficial microbes and induce symbiosis (Chiu and Paszkowski, 2021; Zhang et al., 2021). In nature, however, plants are subject to a mixture of these compounds and must respond accordingly. Additionally adding obscurity to the determination to promote association or ramp up defenses, both symbiotic and pathogenic fungi likely produce short and long-chain chitin molecules, and more recently, LCOs have been shown to be nearly ubiquitous throughout the

fungal kingdom (Feng et al., 2019; Rush et al., 2020). While much has been uncovered about the individual mechanisms for symbiotic responses and defense responses, there is much more to the story involving the interplay between them that we are missing and will be an exciting area to watch in the upcoming years. With the similarities between symbiotic signaling and immunity signaling, a valid concern regarding engineering improved symbiotic associations or transfer of nodulation into non-host is the possibility of off-target unfavorable effects on pathogen susceptibility. Understanding the integration of many incoming microbial signals, their signaling pathways, and factors responsible for the different outcomes will be tremendously important for the plant-microbe interaction field and will aid in preventing unintended consequences of engineered symbiosis.

5.7 – References

Antolín-Llovera, M., Ried, M.K., Parniske, M., 2014. Cleavage of the symbiosis receptor-like kinase ectodomain promotes complex formation with nod factor receptor 5. Curr. Biol. 24, 422–427. https://doi.org/10.1016/j.cub.2013.12.053

Bozsoki, Z., Gysel, K., Hansen, S.B., Lironi, D., Krönauer, C., Feng, F., de Jong, N., Vinther, M., Kamble, M., Thygesen, M.B., Engholm, E., Kofoed, C., Fort, S., Sullivan, J.T., Ronson, C.W., Jensen, K.J., Blaise, M., Oldroyd, G., Stougaard, J., Andersen, K.R., Radutoiu, S., 2020. Ligand-recognizing motifs in plant LysM receptors are major determinants of specificity. Science 369, 663–670. https://doi.org/10.1126/science.abb3377

Catoira, R., Galera, C., de Billy, F., Penmetsa, R. V, Journet, E.P., Maillet, F., Rosenberg, C., Cook, D., Gough, C., Dénarié, J., 2000. Four genes of Medicago truncatula controlling components of a Nod factor transduction pathway. Plant Cell 12, 1647–1666. https://doi.org/10.1105/tpc.12.9.1647

Charpentier, M., Sun, J., Wen, J., Mysore, K.S., Oldroyd, G.E.D., 2014. Abscisic acid promotion of arbuscular mycorrhizal colonization requires a component of the PROTEIN PHOSPHATASE 2A complex. Plant Physiol. 166, 2077–2090. https://doi.org/10.1104/pp.114.246371

Chiu, C.H., Paszkowski, U., 2021. How membrane receptors tread the fine balance between symbiosis and immunity signaling. Proc. Natl. Acad. Sci. 118, 1-3. https://doi.org/10.1073/pnas.2106567118

Couto, D., Zipfel, C., 2016. Regulation of pattern recognition receptor signalling in plants. Nat. Rev. Immunol. 16, 537–552. https://doi.org/10.1038/nri.2016.77

Delaux, P.M., Varala, K., Edger, P.P., Coruzzi, G.M., Pires, J.C., Ané, J.M., 2014. Comparative Phylogenomics Uncovers the Impact of Symbiotic Associations on Host Genome Evolution. PLoS Genet. 10. https://doi.org/10.1371/journal.pgen.1004487

Den Hartog, M., Musgrave, A., Munnik, T., 2001. Nod factor-induced phosphatidic acid and diacylglycerol pyrophosphate formation: A role for phospholipase C and D in root hair deformation. Plant J. 25, 55–65. https://doi.org/10.1046/j.1365-313X.2001.00931.x

Engstrom, E.M., Ehrhardt, D.W., Mitra, R.M., Long, S.R., 2002. Pharmacological analysis of Nod factor-induced calcium spiking in Medicago truncatula. Evidence for the requirement of type IIA calcium pumps and phosphoinositide signaling. Plant Physiol. 128, 1390–1401. https://doi.org/10.1104/pp.010691

Feng, F., Sun, J., Radhakrishnan, G. V., Lee, T., Bozsóki, Z., Fort, S., Gavrin, A., Gysel, K., Thygesen, M.B., Andersen, K.R., Radutoiu, S., Stougaard, J., Oldroyd, G.E.D., 2019. A combination of chitooligosaccharide and lipochitooligosaccharide recognition promotes arbuscular mycorrhizal associations in Medicago truncatula. Nat. Commun. 10, 1-12. https://doi.org/10.1038/s41467-019-12999-5

Fogg, V.C., Azpiazu, I., Linder, M.E., Smrcka, A., Scarlata, S., Gautam, N., 2001. Role of the γ Subunit Prenyl Moiety in G Protein βγ Complex Interaction with Phospholipase Cβ. J. Biol. Chem. 276, 41797–41802. https://doi.org/10.1074/jbc.M107661200

Gamas, P., Brault, M., Jardinaud, M.F., Frugier, F., 2017. Cytokinins in Symbiotic Nodulation: When, Where, What For? Trends Plant Sci. 22, 792–802. https://doi.org/10.1016/j.tplants.2017.06.012

Gleason, C., Chaudhuri, S., Yang, T., Munoz, A., Poovaiah, B.W., Oldroyd, G.E.D., 2006. Nodulation independent of rhizobia induced by a calcium-activated kinase lacking autoinhibition. Nature 441, 1149–1152.

Griesmann, M., Chang, Y., Liu, X., Song, Y., Haberer, G., Crook, M.B., Billault-Penneteau, B., Lauressergues, D., Keller, J., Imanishi, L., Roswanjaya, Y.P., Kohlen, W., Pujic, P., Battenberg, K., Alloisio, N., Liang, Y., Hilhorst, H., Salgado, M.G., Hocher, V., Gherbi, H., Svistoonoff, S., Doyle, J.J., He, S., Xu, Y., Xu, S., Qu, J., Gao, Q., Fang, X., Fu, Y., Normand, P., Berry, A.M., Wall, L.G., Ané, J.M., Pawlowski, K., Xu, X., Yang, H., Spannagl, M., Mayer, K.F.X., Wong, G.K.S., Parniske, M., Delaux, P.M., Cheng, S., 2018. Phylogenomics reveals multiple losses of nitrogen-fixing root nodule symbiosis. Science. 361, 1-11. https://doi.org/10.1126/science.aat1743

Jayaraman, D., Richards, A.L., Westphall, M.S., Coon, J.J., Ané, J.M., 2017. Identification of the phosphorylation targets of symbiotic receptor-like kinases using a high-throughput multiplexed assay for kinase specificity. Plant J. 90, 1196–1207. https://doi.org/10.1111/tpj.13529

Kevei, Z., Lougnon, G., Mergaert, P., Horváth, B., Kereszt, A., Jayaraman, D., Zaman, N., Marcel, F., Regulski, K., Kiss, G.B., Kondorosi, A., Endre, G., Kondorosi, E., Ané, J.-M., Horváth, G. V, Horvath, G. V, 2007. 3-hydroxy-3-methylglutaryl coenzyme A reductase1 interacts with NORK and is crucial for nodulation in

Medicago truncatula. Plant Cell 19, 3974–3989. https://doi.org/10.1105/tpc.107.053975
Krinke, O., Novotná, Z., Valentová, O., Martinec, J., 2007. Inositol trisphosphate receptor in higher plants: Is it real? J. Exp. Bot. 58, 361–376. https://doi.org/10.1093/jxb/erl220
Limpens, E., Mirabella, R., Fedorova, E.E., Franken, C., Franssen, H., Bisseling, T., Geurts, R., 2005. Formation of organelle-like N2-fixing symbiosomes in legume root nodules is controlled by DMI2. Proc Natl Acad Sci U S A 102, 10375–10380. https://doi.org/10.1073/pnas.0504284102
Muntz, K.H., Sternweis, P.C., Gilman, A.G., Mumby, S.M., 1992. Influence of γ subunit prenylation on association of guanine nucleotide-binding regulatory proteins with membranes. Mol. Biol. Cell 3, 49–61. https://doi.org/10.1091/mbc.3.1.49
Newman, M.A., Sundelin, T., Nielsen, J.T., Erbs, G., 2013. MAMP (microbe-associated molecular pattern) triggered immunity in plants. Front. Plant Sci. 4, 1–14. https://doi.org/10.3389/fpls.2013.00139
Oldroyd, G.E.D., 2013. Speak, friend, and enter: Signalling systems that promote beneficial symbiotic associations in plants. Nat. Rev. Microbiol. 11, 252–263. https://doi.org/10.1038/nrmicro2990
Pingret, J.L., Journet, E.P., Barker, D.G., 1998. Rhizobium Nod factor signaling. Evidence for a G protein-mediated transduction mechanism. Plant Cell 10, 659–672.
Rush, T.A., Puech-Pagès, V., Bascaules, A., Jargeat, P., Maillet, F., Haouy, A., Maës, A.Q.M., Carriel, C.C., Khokhani, D., Keller-Pearson, M., Tannous, J., Cope, K.R., Garcia, K., Maeda, J., Johnson, C., Kleven, B., Choudhury, Q.J., Labbé, J., Swift, C., O'Malley, M.A., Bok, J.W., Cottaz, S., Fort, S., Poinsot, V., Sussman, M.R., Lefort, C., Nett, J., Keller, N.P., Bécard, G., Ané, J.M., 2020. Lipo-chitooligosaccharides as regulatory signals of fungal growth and development. Nat. Commun. 11, 1-10. https://doi.org/10.1038/s41467-020-17615-5
Saha, S., Dutta, A., Bhattacharya, A., DasGupta, M., 2014. Intracellular catalytic domain of symbiosis receptor kinase hyperactivates spontaneous nodulation in absence of rhizobia. Plant Physiol. 166, 1699–1708. https://doi.org/10.1104/pp.114.250084
Shen, L., Tian, Q., Yang, L., Zhang, H., Shi, Y., Shen, Y., Zhou, Z., Wu, Q., Zhang, Q., Zhang, W., 2020. Phosphatidic acid directly binds with rice potassium channel OsAKT2 to inhibit its activity. Plant J. 102, 649–665. https://doi.org/10.1111/tpj.14731
Takeda, N., Maekawa, T., Hayashi, M., 2012. Nuclear-localized and deregulated calcium- and calmodulin-dependent protein kinase activates rhizobial and mycorrhizal responses in Lotus japonicus. Plant Cell 24, 810–822. https://doi.org/10.1105/tpc.111.091827
Taylor, C.W., Tovey, S.C., 2010. IP(3) receptors: toward understanding their activation. Cold Spring Harb. Perspect. Biol. 2, 1–22. https://doi.org/10.1101/cshperspect.a004010
Tirichine, L., Imaizumi-Anraku, H., Yoshida, S., Murakami, Y., Madsen, L.H., Miwa, H., Nakagawa, T., Sandal, N., Albrektsen, A.S., Kawaguchi, M., Downie, A., Sato, S., Tabata, S., Kouchi, H., Parniske, M., Kawasaki, S., Stougaard, J., 2006. Deregulation of a Ca2+/calmodulin-dependent kinase leads to spontaneous nodule

development. Nature 441, 1153–6. https://doi.org/10.1038/nature04862
Tominaga, A., Nagata, M., Futsuki, K., Abe, H., Uchiumi, T., Abe, M., Kucho, K., Hashiguchi, M., Akashi, R., Hirsch, A., Arima, S., Suzuki, A., 2010. Effect of abscisic acid on symbiotic nitrogen fixation activity in the root nodules of Lotus japonicus. Plant Signal. Behav. 5, 440–3.
Venkateshwaran, M., Jayaraman, D., Chabaud, M., Genre, A., Balloon, A.J., Maeda, J., Forshey, K.L., den Os, D., Kwiecien, N.W., Coon, J.J., Barker, D.G., Ané, J.-M., 2015. A role for the mevalonate pathway in early plant symbiotic signaling. Proc. Natl. Acad. Sci. 112, 9781-9786 https://doi.org/10.1073/pnas.1413762112
Zhang, C., He, J., Dai, H., Wang, G., Zhang, X., Wang, C., Shi, J., Chen, X., Wang, D., Wang, E., 2021. Discriminating symbiosis and immunity signals by receptor competition in rice. Proc. Natl. Acad. Sci. U. S. A. 118, 2–9. https://doi.org/10.1073/pnas.2023738118